Master Thesis

Epidemiological modeling with multiple virus variants

Marvin Schulte

Department of Mathematics
University of Kaiserslautern-Landau

Supervision

Prof. Dr. René Pinnau

April 14, 2023

Abstract

Epidemiological models have gained much interest during the COVID-19 pandemic. As the pandemic is now driven by newly emerging variants of SARS-CoV-2, the question arises how to model multiple virus variants in a single model.

In this thesis, we have extended an established model for COVID-19 forecasts to multiple virus variants. We analyzed the model mathematically and showed the global existence and uniqueness of the solution as well as important invariance properties for a meaningful model. The implementation into an existing framework which allows us to identify model parameters based on surveillance data is described briefly. When applying our model to actual transitions between SARS-CoV-2 variants, we found that forecasts would have been significantly improved by our model extension. In most cases, we were able to precisely predict peak dates and heights in case incidences of waves caused by newly emerging variants during early transition phases. More severe outcomes, like hospitalizations, are found to be harder to predict because of very limited observational data regarding these outcomes for newly emerging variants.

Contents

Chapter 1

Introduction

Beginning in late 2019, a significant increase in cases of severe pneumonia caused by an unknown pathogen happened in Wuhan, China [52]. Soon, scientists discovered a novel coronavirus, later called SARS-CoV-2, as the cause while the virus began to spread rapidly around the globe. On March 11, 2020, the World Health Organization declared COVID-19, the name of the disease caused by SARS-CoV-2, a pandemic [57]. Unprecedented measures affecting social life and economy have been applied to control the disease spread. At all times, the future trajectory of the pandemic and the effects of interventions have been urgent questions. To answer these questions, epidemiological models were applied and developed. Also at Fraunhofer ITWM, a model was developed [37] and established in the *European Covid-19 Forecast Hub* [48] and in advising decision-makers.

Later, beginning with the Alpha variant in late 2020 and cumulating in the Omicron variants in late 2021, the pandemic was mainly driven by newly emerging variants of SARS-CoV-2. They became dominant due to higher transmissibility and immune escape, resulting in only partial protection from previous infections or vaccination. The mentioned model showed difficulties to predict the trajectory of the pandemic during early transition phases between two predominant virus variants. The objective of this thesis is the extension of the current model to cover the effects of multiple virus variants that possess distinct transmissibilities and induce only partial immunity against each other.

To accomplish the objective, we will describe the newly developed model in Chapter 2. An ansatz to construct model parameters from available data is given at the end of the chapter, together with proofs that the ansatz fulfills the requirements on the parameters. The model is then analyzed mathematically in Chapter 3, regarding existence and uniqueness of a solution, invariance properties and equilibrium points. Chapter 4 briefly explains the numerical methods to solve the system and to fit model parameters to real data. Finally, the model is applied to actual transitions between SARS-CoV-2 variants in Chapter 5. Therefore, we create forecasts using the new model during early stages of such a transition and compare the results to the actual trajectory of the pandemic in the simulated weeks as well as to the predictions using the one-variant model.

Chapter 2

The model

In this chapter, we want to describe the epidemiological model we used. Mathematical epidemiology deals with the mathematical description of the spread of infectious diseases. Our model is based on the one described in [37]. This model computes new infections with an infectious disease (in this case COVID-19, but it could be applied to others as well) taking into account the effects of a latent period[1], vaccination and testing followed by an isolation of positively tested persons. However, it does not cover the effects of waning immunity and different virus variants which played a crucial role in the course of the COVID-19 pandemic [27] [32]. We developed extensions to the model to cover these effects. They will be described in Sections 2.6-2.8. The development of the existing model is also described briefly in Sections 2.2-2.5 such that the thesis is self-contained.

2.1   Model types

Nowadays, there are two main branches of epidemiological models, namely agent-based models and compartmental models [25]. An agent-based model is a type of computer simulation where so-called agents representing individuals can interact with each other and their environment according to a set of prescribed rules. These rules typically allow agents some choices of interactions and its behavior is then determined stochastically among these choices. In such a model, infections with a transmissible disease are modeled by the interaction of an infectious and a susceptible agent. One of its advantages is that heterogeneous behavior and social networks can be represented by the choice of rules agents act upon. However, agent-based models are computationally expensive and due to its stochastic nature require several runs for a robust result. Furthermore, numerous parameters in an agent-based model typically make it impossible to fit them to measured data so they must be set by other means. As one of the foci is to fit parameters to measurements from the past and use these parameters in a forward simulation, we will develop a compartmental

---

[1]The time interval between infection and infectiousness of a patient. Not to be confused with the incubation period which is the time interval between infection and the first symptoms of the disease, typically a bit longer than the latent period.

model. A lower number of parameters makes it possible to fit at least some of them to surveillance data.

One of the first approaches to epidemiological modeling by Kermack and McKendrick [28] was also a compartmental model. As suggested by the name, in a compartmental model the population is divided into compartments based on their state of infection and/or protection. A susceptible and an infectious compartment are usually the minimal ones for a compartmental model, often augmented by other compartments representing e.g. exposed (but not yet infectious), vaccinated and recovered individuals. These compartments can also be subdivided according to age or other relevant factors, but this increases the complexity of the model and the number of its parameters. Infections are then computed by the size of the respective compartments and an interaction coefficient describing their interactions. An assumption is that people in a compartment behave in a homogeneous way such that their interactions can be described by a single interaction coefficient. In its general form presented in the paper by Kermack and McKendrick, the transitions between these compartments are modeled by integro-differential equations (IDEs). But most popular models [10] are using ordinary differential equations (ODEs), mentioned as a special case in the original paper. We will also start with an IDE, but end up with delay differential equations (DDEs) under another assumption on the integral kernel, see Section 2.3. Many models, including ours, also consider the population to be constant, neglecting births and (non-disease-related) deaths, such that it should only be used for a restricted time frame.

2.2 The basic model

To start the development of our model in a very general form as described in [37], we can express the number of new infections as an integral over the number of previous infections, meaning that

$$\dot{n}(t) = \int_{-\infty}^{t} k(t,\tau)\dot{n}(\tau)d\tau. \tag{2.1}$$

Here, $n(t)$ denotes the total number of infections until time t relative to the total population and $k(t,\tau)$ is some integral kernel. Note that we will, in general, consider numbers relative to the total population, denoted by lower-case letters. Absolute numbers will be denoted by upper-case letters. The obvious relation between those numbers, in this case the numbers of total infections, is given by

$$N(t) = n(t) \cdot G,$$

where G denotes the total number of individuals in the model population. However, formulation (2.1) does not gather any insight into the spread of a communicable disease, despite the fact that the new infections at some time are correlated to the previous infections. It is crucial to specify the integral kernel $k(t,\tau)$ in order to clarify the relation between new and previous infections and hence be able to compute the disease spread over time.

We will assume that the integral kernel is a product of three factors which mainly influence the spread of the disease. These are the number of susceptibles $s(t)$, the critical contact rate $\kappa(t)$ and the infectiousness at time after infection $\omega(\tau)$, hence

$$k(t,\tau) = s(t)\kappa(t)\omega(t-\tau). \tag{2.2}$$

The susceptibles are assumed to be the complement of the infections $s(t) = 1 - n(t)$, meaning that no one is protected against infection due to vaccination or other reasons and reinfection is not possible. This also emphasizes the need to consider a restricted time frame because after a long period of time, even if the total population is constant, births and deaths will lead to a severe difference between the number of infections and the number of alive people in the population who have been infected. Thus, an underestimation of the susceptibles would occur.

The critical contact rate $\kappa(t)$ is the number of contacts a person has per day which would lead to infection if he were infectious and all contacts were susceptible. Hence, it depends not only on the number of his contacts, but also on their duration, their closeness, applied protective measures like wearing masks [7] and other factors. As behavior can change over time, it is dependent on t.

The choice of the model for the infectiousness at time after infection essentially influences the model structure. A variety of models can be obtained by choosing different functions for the infectiousness [9]. One classical assumption (however, in most cases not explicitly stated) is an exponential decline of the infectiousness as this leads to the classical SIR or SEIR model based on the publication of Kermack and McKendrick [28].

Inserting (2.2) into (2.1) the model up to this point is given by

$$\dot{n}(t) = (1-n(t))\kappa(t)\int_{-\infty}^{t}\omega(t-\tau)\dot{n}(\tau)d\tau. \tag{2.3}$$

2.3   From an IDE model to a DDE model

Studies show that the viral load of a patient infected with COVID-19 inclines rapidly up to a certain point after infection and will then decline naturally due to the immune system, but slower [26] [22]. For other transmissible diseases like influenza data for this is only available after symptom onset because of the lack of mass testing, i.e. lack of tests before symptom onset. Studies like [33] show at least similar behavior after symptom onset. We could model the infectiousness in our model by a function like this. Nevertheless, due to practical considerations like computability and identifiability of parameters and because infectiousness above a certain threshold of viral load will basically stay the same, we will consider a characteristic function for the infectiousness

$$\omega(t) = \chi_{[\tau^s,\tau^e]}(t) = \begin{cases} 1, & \text{if } 0 < \tau^s \le t \le \tau^e \\ 0, & \text{else} \end{cases}. \tag{2.4}$$

Wlog we can assume the height of this function to be normalized to 1 as any constant factor can also be included in $\kappa(t)$. The constants τ^s and τ^e represent the start and end of the infectious period, respectively.

With this choice for the infectiousness, our model simplifies to a delay-differential equation (DDE) as the integral is an evaluation of the infections at the boundary points of the characteristic function. Inserting (2.4) into (2.3) we obtain the DDE

$$\dot{n}(t) = (1 - n(t))\kappa(t)\big[n(t - \tau^s) - n(t - \tau^e)\big].$$

2.4 Inclusion of vaccination

Beginning in late 2020, COVID-19 vaccinations became available [17]. This had a major impact on the course of the pandemic [21]. Despite prevention of severe cases being the primary goal of the vaccinations, they also reduced the risk of infection significantly. First studies [38] found very high vaccine effectiveness of about 95 % against symptomatic infection, but as the virus mutated and protection against (symptomatic) infection waned over time, these numbers are considerably lower now, see also Section 2.6.2. Still, vaccination has a non-negligible effect on the COVID-19 pandemic and should be included in our model. For other widespread viral diseases like influenza vaccines are available as well and play an important role in the dynamics of disease spread [31].

For our model, we assumed so far that only those with a previous infection are protected against infection. This assumption has to be dropped in order to include vaccination. We introduce a new compartment, the people protected due to vaccination, $p(t)$. As we have seen, vaccines have an effectiveness below 1 which means that this quantity should be a product of vaccine effectiveness, number of vaccinations and the probability of vaccinating a person who has no protection yet, e.g. due to infection. We propose

$$\dot{p}(t) = \varepsilon \frac{1 - n(t)}{1 - d(t - \tau^p)} \dot{v}(t - \tau^p),$$
$$s(t) = 1 - n(t) - p(t).$$

Here, ε represents the vaccine effectiveness, $v(t)$ the relative number of vaccinations at time t and τ^p accounts for a time delay between vaccination and protection. Compared to [37] we drop the time-dependence of the vaccine effectiveness because of experiences with the one-variant model. It is also a preparation for the multi-variant case, where vaccine effectiveness will directly depend on the variant. The term for the probability of vaccinating an unprotected person is based on the assumption that no one is vaccinated more than once and people with known previous infection are not vaccinated (as they are assumed to be protected by the infection). The proportion of detected cases is denoted by $d(t)$ here. In Section 2.5, we will expand our model to compute this number also for future times.

A multi-dose vaccination schedule, like the primary immunization for COVID-19, is considered as one vaccination here. Such a multi-dose schedule could be represented as follows. One could consider all persons with non-complete vaccination

schedule as unvaccinated and let $v(t)$ represent the last doses of vaccinations. Many non-completed vaccine schedules could lead to an underestimation of the vaccine-protected compartment because of partial protection after non-completed schedules. To avoid this, one could let $v(t)$ represent the first dose and include the percentage of non-complete vaccinations and their respective effectiveness into ε and the time until the end of the vaccination schedule (or the "main dose") into τ^p.

Note that this formulation also means that no one will lose its protection due to vaccination once obtained. Especially seasonal vaccinations like those for influenza cannot be modeled with this approach if the simulation should cover multiple seasons. As we will include waning immunity in Subsection 2.6, we will also generalize the model to be able to include vaccinating persons more than once. In particular, booster and seasonal vaccinations can then be modeled.

We have now obtained a system of differential equations instead of a single DDE which is given by

$$\dot{n}(t) = s(t)\kappa(t)\big[n(t - \tau^s) - n(t - \tau^e)\big], \tag{2.5}$$

$$\dot{p}(t) = \varepsilon \frac{1 - n(t)}{1 - d(t - \tau^p)}\dot{v}(t - \tau^p), \tag{2.6}$$

$$s(t) = 1 - n(t) - p(t). \tag{2.7}$$

Note that one can substitute $s(t)$ in the differential equations by its algebraic expression based on $n(t)$ and $p(t)$, but we will not do this substitution here because of readability.

2.5   Inclusion of testing and isolation

Another important characteristic of the COVID-19 pandemic is widespread testing for the virus. This is not only done because of surveillance but also as a measure to reduce disease spread in form of isolation after positive testing. Its effect has been observed in mathematical modeling studies [23] as well as in the analysis of real data [6]. Therefore, we aim to include testing and subsequent isolation into our epidemiological model.

We introduce a new compartment into our model, the detected infections at time t. Clearly, not all infections can be detected, thus we need a detection rate $\lambda(t)$. The detection rate is dependent on time because it depends on the testing strategy applied at that time. Furthermore, infections will not be detected at time of infection, but with some delay when viral load is high enough and symptoms may have been developed. This delay, we call it τ^d, was also time-dependent in the original model because of its dependency on the testing strategy, but as a result of the experiences with the model we neglect the time-dependence here. Wlog we can assume

$$\tau^s \leq \tau^d \leq \tau^e,$$

because an earlier detection has the same influence on disease spread as a detection at the start of the infectious period and a later detection has none, just like a detection at the very end of the infectious period.

With these parameters we have obtained the following equation for the detected cases

$$\dot{d}(t) = \lambda(t)\dot{n}(t - \tau^d).$$

As a positive test resulted in mandatory isolation (§ 2 AbsonderungsVO), we can model this as the end of the infectious period for the positive tested patient.
With this assumption, we can write down the following equation for the infectious compartment $i(t)$ at time t

$$i(t) = n(t - \tau^s) - n(t - \tau^e) - \left[d(t) - d(t + \tau^d - \tau^e)\right].$$

Together with Equations (2.5)-(2.7) we have the model

$$\dot{n}(t) = s(t)\kappa(t)i(t), \tag{2.8}$$

$$\dot{p}(t) = \varepsilon \frac{1 - n(t)}{1 - d(t - \tau^p)}\dot{v}(t - \tau^p), \tag{2.9}$$

$$\dot{d}(t) = \lambda(t)\,\dot{n}(t - \tau^d), \tag{2.10}$$

$$s(t) = 1 - n(t) - p(t), \tag{2.11}$$

$$i(t) = n(t - \tau^s) - n(t - \tau^e) - d(t) + d(t + \tau^d - \tau^e). \tag{2.12}$$

Note that the algebraic equations can again be inserted into the differential ones in order to obtain a system of three differential equations.
In comparison with the complete model in [37], we neglected the external infections here. These are infections which are brought into a population from outside, e.g. by travellers. Its inclusion is particularly important if the disease spread is driven by such infections. Their inclusion is just a prescribed additive term for the new infections. However, we will not include them here because the focus of the thesis should be on the extensions added to the model, especially the effect of multiple virus variants.

2.6 Inclusion of waning immunity

Studies show that immunity against COVID-19 infection wanes over time, regardless of the way it was obtained, i.e. by infection [14] or vaccination [4] [5]. They also show that this effect was highly accelerated by the spread of the Omicron variant at the end of 2021, early 2022. Hence, we want to include the possibility of reinfection and waning immunity after vaccination into our model. Therefore, we have to drop the assumption that the number of infections is equal to the number of persons infected. Instead, we will redefine the compartment $p(t)$ now.

2.6.1 General model

Let $p(t)$ be the compartment of protected persons at time t, due to previous infection or vaccination. Then, the susceptibles (Equation (2.11)) are given as $1 - p(t)$ and hence we can rewrite Equation (2.8) as

$$\dot{n}(t) = (1 - p(t))\kappa(t)i(t). \tag{2.13}$$

Equations (2.10) and (2.12) will not be influenced by this redefinition and consequently stay the same. The possibility of reinfection leads to the effect that persons could be counted twice in the infectious compartment, if they are infected twice in a time period shorter than the infectious period. However, immunity typically lasts considerably longer than the infectious period, even for the Omicron variants. Hence, we will neglect this effect here due to its small size. It is our goal now to reformulate (2.9) such that it really models the immune compartment.

To model the immune proportion of the population we decompose the change of this proportion into the people who become immune due to infection $\dot{p}_{\mathrm{inf}}(t)$, due to vaccination $\dot{p}_{\mathrm{vac}}(t)$ and people who lose their immunity $\dot{p}_{\mathrm{wan}}(t)$. Therefore,

$$\dot{p}(t) = \dot{p}_{\mathrm{inf}}(t) + \dot{p}_{\mathrm{vac}}(t) + \dot{p}_{\mathrm{wan}}(t). \tag{2.14}$$

For the infection-induced immunity, we assume that every person is immune right after infection at least temporarily. Hence, $\dot{p}_{\mathrm{inf}}(t)$ equals the number of new infections:

$$\dot{p}_{\mathrm{inf}}(t) = \dot{n}(t).$$

For the vaccine-induced immunity, we assume that it is proportional to the vaccination rate at an earlier time given by $t - \tau^p$ as previously described in Section 2.4:

$$\dot{p}_{\mathrm{vac}}(t) = \varepsilon(1 - p(t))\dot{v}(t - \tau^p). \tag{2.15}$$

Note that in comparison to Section 2.4 we changed the factor which gives the probability of vaccinating a susceptible person. It is now given as the size of the susceptible compartment. This corresponds to a random distribution of the vaccination. We chose it this way due to the fact that the protection state of a person cannot be known any longer. This is caused by the possibility of becoming susceptible again and people receiving multiple vaccinations in order to "booster" their protection.

For the model of waning immunity, we first have to analyze data about the effect.

2.6.2   Data for waning immunity

In order to get a complete model we have to specify $\dot{p}_{\mathrm{wan}}(t)$. Therefore, we investigate data about vaccine effectiveness over time for different vaccines and virus variants as given in [4]. The data for protection caused by infection, e.g. in [14], was not really usable for an analysis over time because of many single data points for combinations of variants instead of time series. Hence, we assume that the effects leading to (waning) immunity are in principle the same for infection and vaccination. This leads to the assumption that $\dot{p}_{\mathrm{wan}}$ must not be split by the event which caused protection. We performed a curve fit for the data in [4] with an exponential function of the form

$$\mathrm{VE}(t; v_0, \alpha) = v_0 \mathrm{e}^{-\alpha t}. \tag{2.16}$$

As time for the data points we used the center of the given time intervals and continued the difference between them to the last interval (≥ 25 weeks). This led to the results displayed in Figure 2.1, where MSE stands for the mean squared error
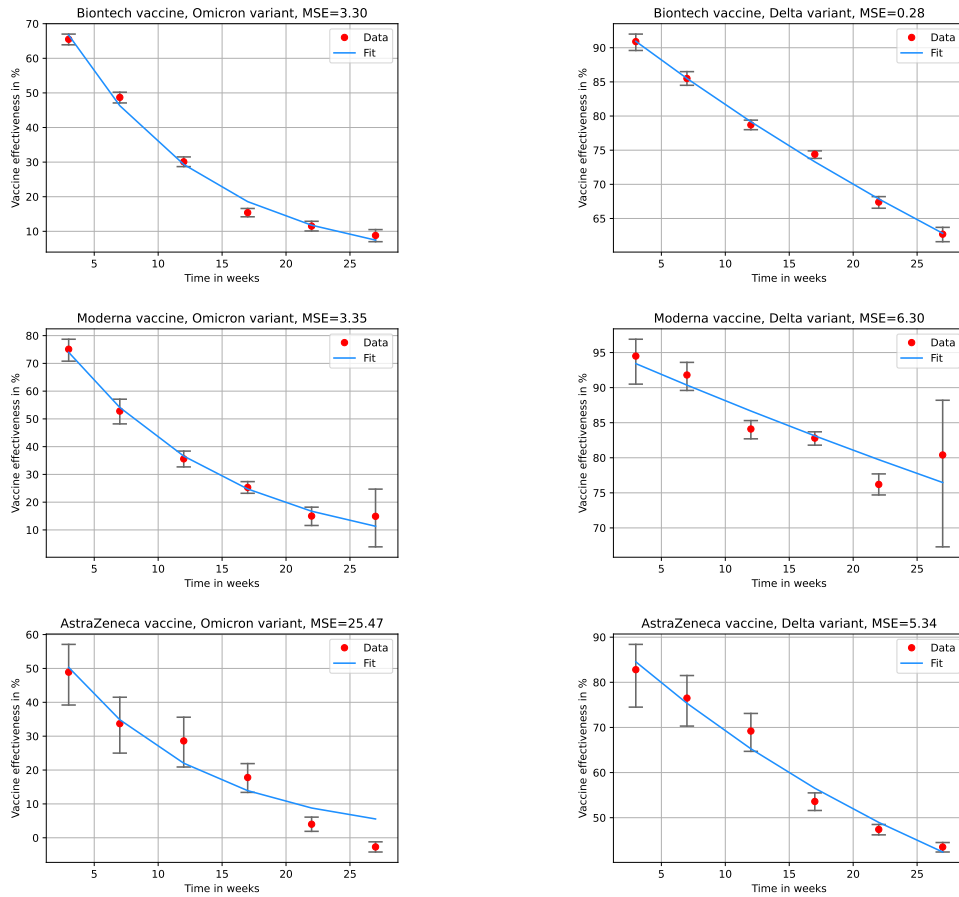
Figure 2.1: Exponential fits of vaccine effectiveness for different vaccines and variants

between the data points and the computed values with optimal parameters. One can see that the fitted curve is not in good accordance with the data points exactly for those combinations of vaccines and variants where the data is sparse and thus we observe a large confidence interval. The measurements for the Biontech vaccine, which has by far the smallest confidence intervals in the data set and is the most used vaccine in Germany (see e.g. [46]), can be fitted very well to the exponential decay. Thus, we conclude that Equation (2.16) can be a good approximation of the vaccine effectiveness over time.

The parameter v_0 in the ansatz is the vaccine effectiveness at time $t = 0$ by definition. Hence, v_0 is incorporated into the model via the factor ε in Equation (2.15).

2.6.3   Model for waning immunity

We now assume that immunity wanes over time independent of its type (infection- or vaccine-based) exponentially with the same parameter α. This type of decay is in accordance with our results in subsection 2.6.2. We choose the same parameter for infection- and vaccination-induced immunity because of lack of according data and to keep low the number of parameters in the model. In terms of differential

equations, an exponential decay can be modeled by

$$\dot{p}_{\text{wan}}(t) = -\alpha p(t).$$

Inserting this into Equation (2.14), we obtain the whole system together with Equations (2.13), (2.10) and (2.12) modeling vaccination, testing and isolation and waning immunity

$$\dot{n}(t) = (1 - p(t))\kappa(t)i(t), \tag{2.17}$$
$$\dot{p}(t) = \dot{n}(t) + \varepsilon(1 - p(t))\dot{v}(t - \tau^p) - \alpha p(t), \tag{2.18}$$
$$\dot{d}(t) = \lambda(t)\,\dot{n}(t - \tau^d), \tag{2.19}$$
$$i(t) = n(t - \tau^s) - n(t - \tau^e) - d(t) + d(t + \tau^d - \tau^e). \tag{2.20}$$

2.7   Extension to two virus variants

In later stages, the COVID-19 pandemic was highly driven by new virus variants with increased transmissibility and immune escape [53]. Especially during the transition phases, it was hard to predict the new infections based on our model described by Equations (2.17)-(2.20). For this reason, it is our goal to develop a model which differentiates between the infections of different variants. This can help to simulate the transition phase between or the co-existence of two predominant virus variants. One cannot just compute the infections of the different variants according to our one-variant model separately, mainly because infection with one variant induces partial immunity against infection with another variant [13] [36]. Additionally, the contact behavior of the persons stays the same such that the critical contact rates $\kappa(t)$ for the different variants are not independent of each other. However, different transmissibility means that they can be different for the variants but only by a time-independent factor.

2.7.1   Adaptations

The second point is easy to remedy. We just split the critical contact rate into a product of some contact rate $\kappa(t)$, which is the same for each variant, and a variant-inherent transmissibility factor ω_i. The first point, however, will lead to major changes in our model, especially the immune compartment will be subdivided. We will develop a model for two virus variants here, it can be generalized to more variants as described in Section 2.8. The focus on two variants in this subsection will hopefully help for a better understanding of the approach. In the following, the first variant will be referred to by index 0, the second one by index 1.

There are two main approaches for protected compartments, namely one where people in the compartment are fully protected but not all individuals move into the compartment after a protective event, e.g. vaccination. The other approach lets all individuals move into the compartment after a protective event, but they are only partially protected [11] [54]. As for vaccination in Section 2.4 we will follow the first approach here.

Modeling two virus variants, there are four different possible protection states. One could be protected against variant 0 or 1, against both or against neither. Thus, individuals will be split into four protection compartments corresponding to these four protection states. We will denote the protection compartments at time t by $p_j(t)$ with the index j indicating the variant(s) members of the compartment are protected against. As previously, the susceptibles (no protection against either variant) at time t will be denoted by $s(t)$, being the complement of $p_0(t)$, $p_1(t)$ and $p_{0,1}(t)$. We will also count the new infections and related quantities like infectious individuals and detected cases separately for each variant, indicated by the index 0 or 1. Their respective parameters for the start and end of the infectious period as well as the detection time, will be variant-dependent. This results in the representation

$$i_i(t) = n_i(t - \tau_i^s) - n_i(t - \tau_i^e) - \left[d_i(t) - d_i(t + \tau_i^d - \tau_i^e) \right],$$
$$\dot{d}_i(t) = \lambda_i(t)\dot{n}_i(t - \tau_i^d).$$

With the variant-inherent transmissibility factor ω_i, the new infections with variant i are given by

$$\dot{n}_i(t) = \kappa(t)\omega_i s_i(t) i_i(t), \tag{2.21}$$

where $s_i(t) = s(t) + p_{1-i}(t)$ are the susceptibles against variant i and $i_i(t)$ the infectious with variant i.

However, the key of the newly developed model will now be the transitions between the protection compartments.

2.7.2   Transitions between the protection compartments

Waning immunity

As described in Section 2.6, we will assume that immunity wanes over time. Still assuming an exponential decay, we have

$$\dot{p}_{j,\text{wan}}(t) = -\alpha_j p_j(t).$$

In particular, this means that waning immunity in protection group $p_{0,1}$ leads to the loss of immunity against both variants. This simplification is justified by the fact that, even for Omicron, immunity typically lasts considerably longer than the length of the transition phases we want to apply our model to. We also mention this in Section 5.3.3 when we model the transition between Delta and Omicron variants where immunity would actually wane faster for one variant than the other. In our numerical simulations, we even chose the same waning rate for all protection groups due to lack of differentiating measurements.

Infection-based transitions

We previously assumed that an infection leads to (temporal) immunity against the virus. This will only be valid for the respective variant in the two variant model. As mentioned before, infections with one variant lead only to partial immunity against

the other. Because we model compartments which are fully protected against the
indicated variants, only a part of the newly infected individuals will move into the
compartment with protection against both variants. The others will move into the
compartment with protection against their respective variant only. Hence, we intro-
duce the probability of obtaining cross-immunity π_i after infection with variant i.
Using Equation (2.21) and the definition of π_i we can model the transitions caused
by infections as follows

$$\dot{p}_{i,\mathrm{inf}}(t) = (1 - \pi_i)\big[\kappa(t)\omega_i s(t)i_i(t)\big] - \kappa(t)\omega_{1-i}p_i(t)i_{1-i}(t),$$
$$\dot{p}_{0,1,\mathrm{inf}}(t) = \pi_0\big[\kappa(t)\omega_0 s(t)i_0(t)\big] + \kappa(t)\omega_0 p_1(t)i_0(t)$$
$$+ \pi_1\big[\kappa(t)\omega_1 s(t)i_1(t)\big] + \kappa(t)\omega_1 p_0(t)i_1(t).$$

Figure 2.2 shows a flowchart representing the possible transitions caused by infec-
tions and their respective rates.
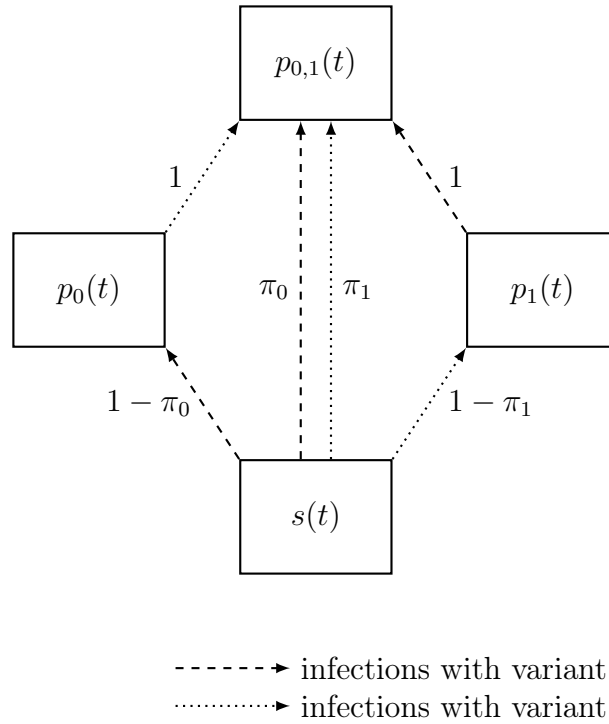
Figure 2.2: Infection-caused transitions between the protection groups with their
respective rates

Vaccination-based transitions

Also, vaccinations have an impact on the protection compartments. The vaccine
effectiveness depends on the variant [4] [5] [29]. Therefore, we introduce the proba-
bility of changing from protection group j to protection group k, $\varepsilon_{j,k}$. An ansatz to
construct this transition probabilities from the available data of vaccine effectiveness

against a certain variant will be presented in Section 2.8.2. The transitions between the compartments caused by vaccinations can then be written as

$$\dot{p}_{i,\text{vac}}(t) = \varepsilon_{s,i}s(t)\dot{v}(t - \tau^p) - \varepsilon_{i,01}p_i(t)\dot{v}(t - \tau^p),$$
$$\dot{p}_{0,1,\text{vac}}(t) = \varepsilon_{s,01}s(t)\dot{v}(t - \tau^p) + \varepsilon_{0,01}p_0(t)\dot{v}(t - \tau^p) + \varepsilon_{1,01}p_1(t)\dot{v}(t - \tau^p),$$

assuming random vaccinations among the protection groups again. The time delay of vaccinations is caused by immune response to the vaccine and hence not variant- or protection compartment-specific. Figure 2.3 shows a flowchart representing these transitions with their respective transition rate.
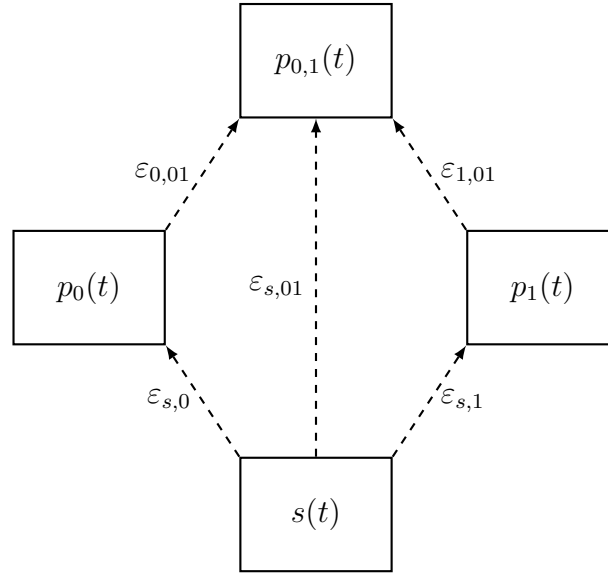
Figure 2.3: Vaccination-caused transitions between the protection groups with their respective rates

2.7.3   Complete two-variant model

If we write down all of the above equations and sum up the changes in the protection groups, we obtain the following system

$$\dot{n}_i(t) = \kappa(t)\big[\omega_i s_0(t)i_0(t)\big],$$

$$\begin{aligned}
\dot{p}_i(t) = &-\alpha_i p_i(t) \\
&+ (1 - \pi_i)\big[\kappa(t)\omega_i s(t)i_i(t)\big] - \kappa(t)\omega_{1-i}p_i(t)i_{1-i}(t) \\
&+ \varepsilon_{s,i}s(t)\dot{v}(t - \tau^p) - \varepsilon_{i,01}p_i(t)\dot{v}(t - \tau^p),
\end{aligned}$$

$$\begin{aligned}
\dot{p}_{0,1}(t) = &-\alpha_{0,1}p_{0,1}(t) \\
&+ \pi_0\big[\kappa(t)\omega_0 s(t)i_0(t)\big] + \kappa(t)\omega_0 p_1(t)i_0(t) \\
&+ \pi_1\big[\kappa(t)\omega_1 s(t)i_1(t)\big] + \kappa(t)\omega_1 p_0(t)i_1(t) \\
&+ \varepsilon_{s,01}s(t)\dot{v}(t - \tau^p) + \varepsilon_{0,01}p_0(t)\dot{v}(t - \tau^p) + \varepsilon_{1,01}p_1(t)\dot{v}(t - \tau^p),
\end{aligned}$$

$$i_i(t) = n_i(t - \tau_i^s) - n_i(t - \tau_i^e) - \left[d_i(t) - d_i(t + \tau_i^d - \tau_i^e) \right],$$
$$\dot{d}_i(t) = \lambda_i(t)\dot{n}_i(t - \tau_i^d),$$
$$s(t) = 1 - p_0(t) - p_1(t) - p_{0,1}(t),$$
$$s_i(t) = s(t) + p_{1-i}(t),$$

with $i \in \{0, 1\}$. Table 2.1 summarizes the interpretation of the variables and parameters used in the model. Their range with an epidemiologically meaningful interpretation is also given there.

Symbol	Interpretation	Range
$n_i(t)$	total infections with variant i until time t	$[0, \infty)$
$\kappa(t)$	critical contact rate at time t	$[0, \infty)$
ω_i	transmissibility of variant i	$(0, \infty)$
$s_i(t)$	susceptibles to variant i at time t	$[0, 1]$
$i_i(t)$	people infectious with variant i at time t	$[0, 1]$
$s(t)$	people susceptible to both variants at time t	$[0, 1]$
$p_i(t)$	people protected against variant i at time t	$[0, 1]$
$p_{0,1}(t)$	people protected against both variants at time t	$[0, 1]$
α_i	waning rate of protection against variant i	$[0, \infty)$
$\alpha_{0,1}$	waning rate of protection against both variants	$[0, \infty)$
π_i	probability of cross-immunity after infection with variant i	$[0, 1]$
$\varepsilon_{j,k}$	transition rate from protection group j to k by vaccination	$[0, 1]$
$v(t)$	total vaccinations until time t	$[0, \infty)$
τ^p	time after vaccination when protection starts	$[0, \infty)$
τ_i^s	start time of infectious period after infection with variant i	$(0, \tau_i^d]$
τ_i^e	end time of infectious period after infection with variant i	$[\tau_i^d, \infty)$
τ_i^d	detection time after infection with variant i	$[\tau_i^s, \tau_i^e]$
$d_i(t)$	total number of detected infections with variant i at time t	$[0, n_i(t - \tau_i^d)]$
$\lambda_i(t)$	detection rate of variant i at time t	$[0, 1]$

Table 2.1: Model variables, their interpretation and meaningful range

We set $\omega_0 = 1$ to avoid ambiguity of $\kappa(t)$, ω_0 and ω_1. In our numerical experiments, we furthermore assume that $\kappa(t)$ is a piecewise constant function whose constant intervals have the length of one week and the detection rates $\lambda_j(t)$ are piecewise constant with two detection rates per week, corresponding to weekdays and weekends.

2.8   Extension to more virus variants

2.8.1   The model

Now we want to extend the model to an arbitrary number of variants. Therefore, we introduce the set of all variants V and its power set $\mathcal{P}(\text{V})$. To model all possible combinations of protection states, we introduce a protection group $p_j(t)$ for each

$j \in \mathcal{P}(V)$. In this notation, people in group $p_j(t)$ are protected against all variants contained in j. Infections and other quantities counted for variants instead of combinations of them can easily be extended to more than two variants:

$$\dot{n}_i(t) = \kappa(t)\omega_i s_i(t) i_i(t), \qquad\qquad\qquad\qquad i \in V,$$
$$i_i(t) = n_i(t - \tau_i^s) - n_i(t - \tau_i^e) - \left[d_i(t) - d_i(t + \tau_i^d - \tau_i^e) \right], \qquad i \in V,$$
$$\dot{d}_i(t) = \lambda_i(t)\dot{n}_i(t - \tau_i^d), \qquad\qquad\qquad\qquad i \in V,$$
$$s_i(t) = \sum_{\substack{j \in \mathcal{P}(V) \\ i \notin j}} p_j(t), \qquad\qquad\qquad\qquad i \in V.$$

The adaptation of the transitions between the protection groups needs a bit more explanation. As before, we model waning immunity by an exponential decay from a protection group to the fully susceptible state:

$$\dot{p}_{j,\mathrm{wan}}(t) = -\alpha_j p_j(t), \quad j \in \mathcal{P}(V) \setminus \{\emptyset\}.$$

For the transitions caused by infection or vaccination we note that people can only change from a protection group $p_j(t)$ to another one $p_k(t)$ if $j \subset k$ because infection or vaccination does not lead to the loss of protection against a variant. Furthermore, if infection with variant i leads to a change of the protection state, then at least protection against i is obtained. Introducing, $\pi_{i,j,k}$ as the transition rate from $p_j(t)$ to $p_k(t)$ due to infection with variant i, we can write the transitions due to infection as

$$\dot{p}_{j,\mathrm{inf}}(t) = - \sum_{i \in V \setminus j} \kappa(t)\omega_i p_j(t) i_i(t)$$
$$+ \sum_{\substack{k \in \mathcal{P}(V) \\ k \subset j}} \sum_{i \in j \setminus k} \pi_{i,k,j}\kappa(t)\omega_i p_k(t) i_i(t), \quad j \in \mathcal{P}(V) \setminus \{\emptyset\}.$$

The first sum describes all infections in $p_j(t)$ with a variant this compartment is not protected against. They lead to a transition into a higher protection group[2]. The second term sums over all infections of lower protection groups $p_k(t)$ and variants i they are susceptible against. These infections lead to a transition into $p_j(t)$ with probability $\pi_{i,k,j}$. For consistency with the assumption that all people who get infected with a certain variant leave their protection group to a higher one, we have to require that for all $j \in \mathcal{P}(V) \setminus \{V\}$, $i \in V \setminus j$

$$1 \stackrel{!}{=} \sum_{\substack{k \in \mathcal{P}(V) \\ j \cup \{i\} \subseteq k}} \pi_{i,j,k}. \tag{2.22}$$

Analogously, we introduce $\varepsilon_{j,k}$ as the probability of transition from $p_j(t)$ to $p_k(t)$ by vaccination. Also for vaccination, transition from $p_j(t)$ to $p_k(t)$ is only possible if

---

[2]We call a protection group k a higher protection group than j if $j \subset k$

$j \subset k$. Hence, we have for the transitions due to vaccination the analogue description

$$\dot{p}_{j,\text{vac}}(t) = - \sum_{\substack{k \in \mathcal{P}(\text{V}) \\ j \subset k}} \varepsilon_{j,k} p_j(t) \dot{v}(t - \tau^p)$$

$$+ \sum_{\substack{k \in \mathcal{P}(\text{V}) \\ k \subset j}} \varepsilon_{k,j} p_k(t) \dot{v}(t - \tau^p), \quad j \in \mathcal{P}(\text{V}) \setminus \{\emptyset\}.$$

Here, we have to require that for all $j \in \mathcal{P}(\text{V})$

$$1 \stackrel{!}{\geq} \sum_{\substack{k \in \mathcal{P}(\text{V}) \\ j \subset k}} \varepsilon_{j,k}, \tag{2.23}$$

such that there are no more transitions than vaccinations. The sum could be smaller than 1 due to vaccination failure.

Altogether, we obtain the complete system for an arbitrary number of variants

$$\dot{n}_i(t) = \kappa(t)\omega_i s_i(t) i_i(t), \qquad\qquad i \in \text{V}, \tag{2.24}$$

$$\dot{p}_j(t) = -\alpha_j p_j(t) \tag{2.25}$$

$$- \sum_{i \in \text{V} \setminus j} \kappa(t)\omega_i p_j(t) i_i(t) + \sum_{\substack{k \in \mathcal{P}(\text{V}) \\ k \subset j}} \sum_{i \in j \setminus k} \pi_{i,k,j} \kappa(t)\omega_i p_k(t) i_i(t)$$

$$- \sum_{\substack{k \in \mathcal{P}(\text{V}) \\ j \subset k}} \varepsilon_{j,k} p_j(t) \dot{v}(t - \tau^p) + \sum_{\substack{k \in \mathcal{P}(\text{V}) \\ k \subset j}} \varepsilon_{k,j} p_k(t) \dot{v}(t - \tau^p), \qquad j \in \mathcal{P}(\text{V}) \setminus \{\emptyset\},$$

$$i_i(t) = n_i(t - \tau_i^s) - n_i(t - \tau_i^e) - \left[d_i(t) - d_i(t + \tau_i^d - \tau_i^e) \right], \qquad i \in \text{V}, \tag{2.26}$$

$$\dot{d}_i(t) = \lambda_i(t) \dot{n}_i(t - \tau_i^d), \qquad\qquad i \in \text{V}, \tag{2.27}$$

$$s(t) = 1 - \sum_{j \in \mathcal{P}(\text{V}) \setminus \{\emptyset\}} p_j(t), \tag{2.28}$$

$$s_i(t) = \sum_{\substack{j \in \mathcal{P}(\text{V}) \\ i \notin j}} p_j(t), \qquad\qquad i \in \text{V}. \tag{2.29}$$

The new variables and parameters compared to Table 2.1 can be found in Table 2.2

Symbol	Interpretation	Range
$p_j(t)$	people protected against all variants $i \in j$ at time t	$[0, 1]$
α_j	waning rate of protection group p_j	$[0, \infty)$
$\pi_{i,j,k}$	transition rate from p_j to p_k after infection with variant i	$[0, 1]$

Table 2.2: Model variables, their interpretation and meaningful range

2.8.2   Construction of the transition rates

Because data is not available in this form for $\pi_{i,j,k}$ and $\varepsilon_{j,k}$, we introduce $\pi_{i,l}$ as the probability of obtaining immunity against variant l by infection with variant i ($i \neq l$, $i, l \in V$) and ε_i of obtaining immunity against variant i by vaccination. For these variables, data is available (see e.g. [4] [5] [13] [29]), and we use a product ansatz to construct the variables for our model. For $j \in \mathcal{P}(V) \setminus \{V\}$, $k \in \mathcal{P}(V)$, $i \in V, i \notin j$, $j \cup \{i\} \subseteq k$ (this corresponds to a possible transition) we assume

$$\pi_{i,j,k} = \prod_{l \in k \setminus (j \cup \{i\})} \pi_{i,l} \cdot \prod_{l \in V \setminus k} (1 - \pi_{i,l}). \tag{2.30}$$

This is the product of the probabilities of obtaining immunity against the variants contained in k, but not in $j \cup \{i\}$ multiplied by the product of probabilities of not obtaining immunity against the variants which are not in k. Analogously, for $j \in \mathcal{P}(V) \setminus \{V\}$, $k \in \mathcal{P}(V)$, $j \subset k$ we assume

$$\varepsilon_{j,k} = \prod_{i \in k \setminus j} \varepsilon_i \cdot \prod_{i \in V \setminus k} (1 - \varepsilon_i), \tag{2.31}$$

with the same interpretation but for vaccine effectivenesses. This also reduces the number of independent parameters from

$$\sum_{i=1}^{n} \sum_{\substack{j \in \mathcal{P}(V) \\ i \notin j}} \sum_{\substack{k \in \mathcal{P}(V) \\ j \cup \{i\} \subseteq k}} 1 = \sum_{i=1}^{n} \sum_{\substack{j \in \mathcal{P}(V) \\ i \notin j}} 2^{n-1-|j|} = \sum_{i=1}^{n} \sum_{|j|=0}^{n-1} \binom{n-1}{|j|} 2^{n-1-|j|} = n3^{n-1}$$

to $n^2 - n$ for the infection-based immunity and from

$$\sum_{j \in \mathcal{P}(V)} \sum_{\substack{k \in \mathcal{P}(V) \\ j \subset k}} 1 = \sum_{j \in \mathcal{P}(V)} (2^{n-|j|} - 1) = \sum_{|j|=0}^{n} \binom{n}{|j|} (2^{n-|j|} - 1) = 3^n - 2^n$$

to n for vaccination-based immunity, where n is the number of variants in the model. Overall, the number of independent parameters can be reduced from exponential to quadratic size in n which would be especially beneficial if one wants to model a large number of variants.

We will now show that our product ansatz satisfies (2.22).

Theorem 1. *Let $j \in \mathcal{P}(V) \setminus \{V\}$, $i \in V \setminus j$. Choosing $\pi_{i,j,k}$ according to (2.30) for all $k \in \mathcal{P}(V)$, $j \cup \{i\} \subseteq k$, we have*

$$1 = \sum_{\substack{k \in \mathcal{P}(V) \\ j \cup \{i\} \subseteq k}} \pi_{i,j,k}.$$

Proof. We will prove the statement by induction over $q := |V| - (|j| + 1)$ for $0 \leq q \leq |V| - 1$. The variable q equals the number of variants that are in $V \setminus (j \cup \{i\})$, i.e. that appear in one of the products of the ansatz.

Base case. $q = 0$ implies that $j \cup \{i\} = \mathrm{V}$. Therefore,

$$\sum_{\substack{k \in \mathcal{P}(\mathrm{V}) \\ j \cup \{i\} \subseteq k}} \pi_{i,j,k} = \pi_{i,j,\mathrm{V}} = \prod_{l \in \mathrm{V} \setminus \mathrm{V}} \pi_{i,l} \cdot \prod_{l \in \mathrm{V} \setminus \mathrm{V}} (1 - \pi_{i,l}) = 1$$

as both products are empty.

Induction step. Let the statement be true for $q - 1$ and $m \in \mathrm{V} \setminus (j \cup \{i\})$. A variant m exists because $q > 0$. Using (2.30), we have that

$$\sum_{\substack{k \in \mathcal{P}(\mathrm{V}) \\ j \cup \{i\} \subseteq k}} \pi_{i,j,k} = \sum_{\substack{k \in \mathcal{P}(\mathrm{V}) \\ j \cup \{i\} \subseteq k}} \left(\prod_{l \in k \setminus (j \cup \{i\})} \pi_{i,l} \cdot \prod_{l \in \mathrm{V} \setminus k} (1 - \pi_{i,l}) \right)$$

$$= \pi_{i,m} \cdot \left(\sum_{\substack{k \in \mathcal{P}(\mathrm{V}) \\ j \cup \{i\} \cup \{m\} \subseteq k}} \prod_{l \in k \setminus (j \cup \{i\} \cup \{m\})} \pi_{i,l} \cdot \prod_{l \in \mathrm{V} \setminus k} (1 - \pi_{i,l}) \right)$$

$$+ (1 - \pi_{i,m}) \cdot \left(\sum_{\substack{k \in \mathcal{P}(\mathrm{V} \setminus \{m\}) \\ j \cup \{i\} \subseteq k}} \prod_{l \in k \setminus (j \cup \{i\})} \pi_{i,l} \cdot \prod_{l \in \mathrm{V} \setminus (k \cup \{m\})} (1 - \pi_{i,l}) \right)$$

$$= \pi_{i,m} \cdot \underbrace{\sum_{\substack{k \in \mathcal{P}(\mathrm{V}) \\ j \cup \{i\} \cup \{m\} \subseteq k}} \pi_{i,j \cup \{m\},k}}_{q' = |\mathrm{V}| - (|j| + 2) = q - 1} + (1 - \pi_{i,m}) \cdot \underbrace{\sum_{\substack{k \in \mathcal{P}(\mathrm{V} \setminus \{m\}) \\ j \cup \{i\} \subseteq k}} \pi_{i,j,k}}_{q' = (|\mathrm{V}| - 1) - (|j| + 1) = q - 1}$$

$$\stackrel{\text{I.H.}}{=} \pi_{i,m} + (1 - \pi_{i,m})$$

$$= 1.$$

$\square$

Similarly, one can prove that (2.23) is fulfilled by the product ansatz.

Theorem 2. *Let $j \in \mathcal{P}(\mathrm{V}) \setminus \{\mathrm{V}\}$. Choosing $\varepsilon_{j,k}$ according to (2.31), we have*

$$1 \geq \sum_{\substack{k \in \mathcal{P}(\mathrm{V}) \\ j \subset k}} \varepsilon_{j,k}.$$

Proof. In order to show the statement of the theorem we will show that

$$1 = \sum_{\substack{k \in \mathcal{P}(\mathrm{V}) \\ j \subset k}} \varepsilon_{j,k} + \prod_{i \in \mathrm{V} \setminus j} (1 - \varepsilon_i) \tag{2.32}$$

We will prove this statement by induction over $q := |\mathrm{V}| - |j|$ for $1 \leq q \leq |\mathrm{V}|$. Here, q equals the number of variants that are in $\mathrm{V} \setminus j$, i.e. that appear in one of the products in the ansatz.

Base case. $q = 1$ implies that $j \cup \{i\} = \mathrm{V}$ for some $i \in \mathrm{V}$. Therefore, we have

$$\sum_{\substack{k \in \mathcal{P}(\mathrm{V}) \\ j \subset k}} \varepsilon_{j,k} + \prod_{i \in \mathrm{V} \setminus j} (1 - \varepsilon_i) = \varepsilon_{j,V} + (1 - \varepsilon_i) = \varepsilon_i + (1 - \varepsilon_i) = 1.$$

Induction step. Let (2.32) be true for $q-1$ and $m \in V \setminus j$. Using (2.31), we have

$$
\sum_{\substack{k \in \mathcal{P}(V) \\ j \subset k}} \varepsilon_{j,k} + \prod_{i \in V \setminus j} (1 - \varepsilon_i) = \sum_{\substack{k \in \mathcal{P}(V) \\ j \subset k}} \left(\prod_{i \in k \setminus j} \varepsilon_i \cdot \prod_{i \in V \setminus k} (1 - \varepsilon_i) \right) + \prod_{i \in V \setminus j} (1 - \varepsilon_i)
$$

$$
= \varepsilon_m \cdot \left[\sum_{\substack{k \in \mathcal{P}(V) \\ j \cup \{m\} \subset k}} \left(\prod_{i \in k \setminus (j \cup \{m\})} \varepsilon_i \cdot \prod_{i \in V \setminus k} (1 - \varepsilon_i) \right) + \prod_{i \in V \setminus (j \cup \{m\})} (1 - \varepsilon_i) \right]
$$

$$
+ (1 - \varepsilon_m) \cdot \left[\sum_{\substack{k \in \mathcal{P}(V \setminus \{m\}) \\ j \subset k}} \left(\prod_{i \in k \setminus j} \varepsilon_i \cdot \prod_{i \in V \setminus (k \cup \{m\})} (1 - \varepsilon_i) \right) \right.
$$

$$
\left. + \prod_{i \in V \setminus (j \cup \{m\})} (1 - \varepsilon_i) \right]
$$

$$
= \varepsilon_m \cdot \underbrace{\left[\sum_{\substack{k \in \mathcal{P}(V) \\ j \cup \{m\} \subset k}} \varepsilon_{j \cup \{m\},k} + \prod_{i \in V \setminus (j \cup \{m\})} (1 - \varepsilon_i) \right]}_{q' = |V| - (|j| + 1) = q - 1}
$$

$$
+ (1 - \varepsilon_m) \cdot \underbrace{\left[\sum_{\substack{k \in \mathcal{P}(V \setminus \{m\}) \\ j \subset k}} \varepsilon_{j,k} + \prod_{i \in V \setminus (j \cup \{m\})} (1 - \varepsilon_i) \right]}_{q' = (|V| - 1) - |j| = q - 1}
$$

$$
\overset{\text{I.H.}}{=} \varepsilon_m + (1 - \varepsilon_m)
$$

$$
= 1.
$$

By showing (2.32) we have that

$$
\sum_{\substack{k \in \mathcal{P}(V) \\ j \subset k}} \varepsilon_{j,k} = 1 - \prod_{i \in V \setminus j} (1 - \varepsilon_i).
$$

As ε_i represent probabilities, it holds $\varepsilon_i \in [0, 1]$. Therefore, $\prod_{i \in V \setminus j} (1 - \varepsilon_i) \in [0, 1]$ and hence the statement of the theorem is shown. $\qquad\square$

Remark. The term $\prod_{i \in V \setminus j} (1 - \varepsilon_i)$ in Theorem 2 can be interpreted as the probability of a complete vaccination failure, meaning that the vaccination does not lead to a better protection.

Chapter 3

Analysis of the model

In this chapter, we will analyze the model given by Equations (2.24)-(2.28).

3.1 Assumptions

First, we will state general assumptions for the time-dependent functions in our model for the whole chapter.

For the critical contact rate $\kappa(t)$ and the detection rate $\lambda_i(t)$ we choose a piecewise constant function in our numerical simulations. In this chapter, however, we will first assume that $\kappa(t)$ is continuous, bounded and always positive (which especially includes positive constant functions) and $\lambda_i(t) = \lambda_i$ is a constant. In Section 3.7, we will treat the case of piecewise constant functions. For the function modeling the total number of vaccinations $v(t)$, we assume a continuously differentiable function with bounded and nonnegative $\dot{v}(t)$.

3.2 Elimination of the algebraic equations

With constant λ_i, Equation (2.26) can be simplified as

$$
\begin{aligned}
d_i(t) - d_i(t + \tau_i^d - \tau_i^e) &= \int_{t+\tau_i^d-\tau_i^e}^{t} \dot{d}_i(\tilde{t})\, d\tilde{t} \\
&= \lambda_i \int_{t+\tau_i^d-\tau_i^e}^{t} \dot{n}_i(\tilde{t} - \tau_i^d)d\tilde{t} \\
&= \lambda_i \left[n_i(t - \tau_i^d) - n_i(t - \tau_i^e) \right] \\
\Rightarrow \quad i_i(t) &= n_i(t - \tau_i^s) - n_i(t - \tau_i^e) - \left[d_i(t) - d_i(t + \tau_i^d - \tau_i^e) \right] \\
&= n_i(t - \tau_i^s) - n_i(t - \tau_i^e) - \lambda_i \left[n_i(t - \tau_i^d) - n_i(t - \tau_i^e) \right].
\end{aligned}
\tag{3.1}
$$

Additionally, we want to plug in the algebraic equations into the differential ones. Using Equations (2.28) and (2.29) we find for each $i \in V$

$$
\begin{aligned}
s_i(t) &= \sum_{\substack{j \in \mathcal{P}(V) \\ i \notin j}} p_j(t) \\
&= s(t) + \sum_{\substack{j \in \mathcal{P}(V) \setminus \{\emptyset\} \\ i \notin j}} p_j(t) \\
&= 1 - \sum_{j \in \mathcal{P}(V) \setminus \{\emptyset\}} p_j(t) + \sum_{\substack{j \in \mathcal{P}(V) \setminus \{\emptyset\} \\ i \notin j}} p_j(t) \\
&= 1 - \sum_{\substack{j \in \mathcal{P}(V) \setminus \{\emptyset\} \\ i \in j}} p_j(t) \\
&= 1 - \sum_{\substack{j \in \mathcal{P}(V) \\ i \in j}} p_j(t).
\end{aligned}
\tag{3.2}
$$

Plugging Equations (3.1) and (3.2) into (2.24) and (2.25), we obtain the differential equations

$$
\dot{n}_i(t) = \kappa(t)\omega_i \left(1 - \sum_{\substack{j \in \mathcal{P}(V) \\ i \in j}} p_j(t) \right)
\tag{3.3}
$$
$$
\cdot \left(n_i(t - \tau_i^s) - n_i(t - \tau_i^e) - \lambda_i \left[n_i(t - \tau_i^d) - n_i(t - \tau_i^e) \right] \right), \quad i \in V,
$$

$$
\dot{p}_j(t) = -\alpha_j p_j(t)
\tag{3.4}
$$
$$
- \sum_{i \in V \setminus j} \kappa(t)\omega_i p_j(t) \left(n_i(t - \tau_i^s) - n_i(t - \tau_i^e) - \lambda_i \left[n_i(t - \tau_i^d) - n_i(t - \tau_i^e) \right] \right)
$$
$$
+ \sum_{\substack{k \in \mathcal{P}(V) \setminus \{\emptyset\} \\ k \subset j}} \sum_{i \in j \setminus k} \pi_{i,k,j} \kappa(t)\omega_i p_k(t) \left(n_i(t - \tau_i^s) - n_i(t - \tau_i^e) - \lambda_i \left[n_i(t - \tau_i^d) - n_i(t - \tau_i^e) \right] \right)
$$
$$
+ \sum_{i \in j} \pi_{i,\emptyset,j} \kappa(t)\omega_i \left(1 - \sum_{k \in \mathcal{P}(V) \setminus \{\emptyset\}} p_k(t) \right)
$$
$$
\cdot \left(n_i(t - \tau_i^s) - n_i(t - \tau_i^e) - \lambda_i \left[n_i(t - \tau_i^d) - n_i(t - \tau_i^e) \right] \right)
$$
$$
- \sum_{\substack{k \in \mathcal{P}(V) \\ j \subset k}} \varepsilon_{j,k} p_j(t) \dot{v}(t - \tau^p) + \sum_{\substack{k \in \mathcal{P}(V) \setminus \{\emptyset\} \\ k \subset j}} \varepsilon_{k,j} p_k(t) \dot{v}(t - \tau^p)
$$
$$
+ \varepsilon_{\emptyset,j} \left(1 - \sum_{k \in \mathcal{P}(V) \setminus \{\emptyset\}} p_k(t) \right) \dot{v}(t - \tau^p), \quad j \in \mathcal{P}(V) \setminus \{\emptyset\}.
$$

This is the minimal representation of the system with all algebraic equations eliminated. However, it definitely lacks readability. Hence, we will still use the equivalent

system with the algebraic equations if it helps for the analysis.

3.3   Classification and notation

Classification

System (3.3)-(3.4) is a system of first order, nonlinear, nonautonomous delay differential equations with constant and hence bounded delay.

Notation

The theorems used in the following sections are mainly from [16]. Therefore, we will introduce notation now that will allow us to apply the theorems to our system.

Definition 1 ([16, Ch. 25]). Let $t \in \mathbb{R}$, $r > 0$ and χ be a function defined at least on $[t-r, t] \to \mathbb{R}^n$. We define a new function $\chi_t : [-r, 0] \to \mathbb{R}^n$ by

$$\chi_t(\sigma) = \chi(t + \sigma), \quad -r \le \sigma \le 0.$$

Remark ([16, Ch. 25]). χ_t is obtained by restricting χ to $[t-r, t]$ and then translating it to $[-r, 0]$.

Remark. The constant r is chosen to be the upper bound on the delay when analyzing delay differential equations.

Notation 1 ([16, Ch. 25]). For $A \subset \mathbb{R}^n$, we denote the set of all continuous functions from $[-r, 0]$ to A, $C([-r, 0], A)$, by $\mathcal{C}_A$.

For our model we will define the state vector

$$x(t) = \begin{pmatrix} \big(n_i(t)\big)_{i \in V} \\ \big(p_j(t)\big)_{j \in \mathcal{P}(V) \setminus \{\emptyset\}} \end{pmatrix}. \tag{3.5}$$

The state vector has dimension $m := |V| + (2^{|V|} - 1)$. We have seen in Section 3.2 that these variables suffice to describe the state of the system.

As the domain of interest, we define

$$D := (-\varepsilon, \infty)^{|V|} \times (-\varepsilon, 1 + \varepsilon)^{2^{|V|}-1} \tag{3.6}$$

for some $\varepsilon > 0$. The correction by ε is done to obtain an open set D.

For the right-hand side of our differential equation system, we define $F : [0, \infty) \times \mathcal{C}_D \to \mathbb{R}^m$ by

$$F(t, \psi) = \begin{pmatrix} \left(\kappa(t)\omega_i\big(1 - \sum_{\substack{j \in \mathcal{P}(V) \\ i \in j}} \psi_j(0)\big) \cdot \big(\psi_i(-\tau_i^s) - \psi_i(-\tau_i^e) - \lambda_i[\psi_i(-\tau_i^d) - \psi_i(-\tau_i^e)]\big) \right)_{i \in V} \\ \begin{pmatrix} -\alpha_j\psi_j(0) - \sum_{i \in V \setminus j} \kappa(t)\omega_i\psi_j(0)\big(\psi_i(-\tau_i^s) - \psi_i(-\tau_i^e) - \lambda_i[\psi_i(-\tau_i^d) - \psi_i(-\tau_i^e)]\big) \\ + \sum_{\substack{k \in \mathcal{P}(V) \setminus \{\emptyset\} \\ k \subset j}} \sum_{i \in j \setminus k} \pi_{i,k,j}\kappa(t)\omega_i\psi_k(0)\big(\psi_i(-\tau_i^s) - \psi_i(-\tau_i^e) - \lambda_i[\psi_i(-\tau_i^d) - \psi_i(-\tau_i^e)]\big) \\ + \sum_{i \in j} \pi_{i,\emptyset,j}\kappa(t)\omega_i\big(1 - \sum_{k \in \mathcal{P}(V) \setminus \{\emptyset\}} \psi_k(0)\big)\big(\psi_i(-\tau_i^s) - \psi_i(-\tau_i^e) - \lambda_i[\psi_i(-\tau_i^d) - \psi_i(-\tau_i^e)]\big) \\ - \sum_{\substack{k \in \mathcal{P}(V) \\ j \subset k}} \varepsilon_{j,k}\psi_j(0)\dot{v}(t - \tau^p) + \sum_{\substack{k \in \mathcal{P}(V) \setminus \{\emptyset\} \\ k \subset j}} \varepsilon_{k,j}\psi_k(0)\dot{v}(t - \tau^p) \\ + \varepsilon_{\emptyset,j}\big(1 - \sum_{k \in \mathcal{P}(V) \setminus \{\emptyset\}} \psi_k(0)\big)\dot{v}(t - \tau^p) \end{pmatrix}_{j \in \mathcal{P}(V) \setminus \{\emptyset\}} \end{pmatrix} \tag{3.7}$$

Here, $\psi_i(t)$ with $i \in V$ represents the i-th component of $\psi(t)$ (this component represents $n_i(t)$ in our state vector) and $\psi_j(t)$ with $j \in \mathcal{P}(V) \setminus \{\emptyset\}$ represents the component of $\psi(t)$ which corresponds to the component of $p_j(t)$ in our state vector. With this definition together with Definition 1, our system can be represented by

$$\dot{x}(t) = F(t, x_t).$$

Initial conditions

Additional to the differential equations, we must specify some initial conditions. In contrast to ordinary differential equations, delay differential equations do not only need an initial value, but an initial history. This is because not only the present value has to be evaluated, but also past ones. In particular, one would need to specify the history of a component back to the maximal delay which appears for this component. In our system, the protection groups $p_j(t)$ just need an initial value, while the infections $n_i(t)$ need to be specified back to $t_0 - \tau_i^e$. Wlog we set $t_0 = 0$ because we can shift the time-dependent input functions $\kappa(t)$ and $\dot{v}(t - \tau^p)$ by t_0.

In agreement with the usual definition of initial conditions in [16] and other literature regarding DDEs, we will, however, specify the initial history on the same time interval for all components. Therefore, we define

$$\tau_{\max}^e := \max_{i \in V} \tau_i^e.$$

This is the upper bound for all delays because for each $i \in V$ we have

$$\tau_{\max}^e \geq \tau_i^e \geq \tau_i^d \geq \tau_i^s > 0.$$

We will therefore require

$$x(t) = \theta(t), \quad -\tau_{\max}^e \leq t \leq 0,$$

for some initial history $\theta : [-\tau_{\max}^e, 0] \to D$. Comparing with the previous notation, we also set $r := \tau_{\max}^e$ for our model.

Note that, although we specify longer initial histories than needed for some components, this will not influence the solution for $t \geq 0$ because these values of the initial history will never be evaluated in the differential equations.

3.4 Uniqueness and local existence of a solution

In this section, we want to examine the uniqueness and local existence of a solution to our system given an initial history. First, we have to define what a solution to a delay differential system is.

Definition 2 ([16, Ch. 23])**.** A *solution* of

$$\dot{x}(t) = F(t, x_t), \qquad\qquad\qquad t_0 \leq t \leq \beta, \qquad\qquad (3.8)$$
$$x(t) = \theta(t), \qquad\qquad\qquad t_0 - r \leq t \leq t_0, \qquad\qquad (3.9)$$

is a continuous function $x : [t_0 - r, \beta_1) \to D$, for some $\beta_1 \in (t_0, \beta]$, such that

$$x(t) = \theta(t), \qquad\qquad\qquad t_0 - r \leq t \leq t_0,$$
$$\dot{x}(t) = F(t, x_t), \qquad\qquad\qquad t_0 \leq t < \beta_1.$$

The solution is said to be *unique* if every two solutions agree with each other as far as both are defined.

Remark. In our case, $F(t, x_t)$ is (assumed to be) defined for each $t \geq 0$. Therefore, we set $\beta := \infty$. With $t_0 = 0$ and $r = \tau_{\max}^e$, we are searching for a solution to the system

$$\dot{x}(t) = F(t, x_t), \qquad\qquad\qquad 0 \leq t < \infty, \qquad\qquad (3.10)$$
$$x(t) = \theta(t), \qquad\qquad\qquad -\tau_{\max}^e \leq t \leq 0, \qquad\qquad (3.11)$$

with F given by Equation (3.7).

The theorems in [16] also require a certain continuity condition which is given here.

Definition 3 ([16, Ch. 25]). *Continuity Condition (C) is satisfied if* $F(t, \chi_t)$ *is continuous with respect to* t *in* $[t_0, \beta)$ *for each given continuous function* $\chi : [t_0 - r, \beta) \to D$.

We can show that this condition holds for our problem.

Lemma 1. *Continuity Condition (C) is satisfied by our choice of* F *(see Equation (3.7)).*

Proof. Under the assumptions that $\kappa(t)$, $\dot{v}(t - \tau^p)$ and χ are continuous in t, $F(t, \chi_t)$ is a composition of continuous functions in t and hence also continuous in t. This is Continuity Condition (C). $\qquad\qquad\square$

We furthermore need the notion of (local) Lipschitz continuity for functionals like F.

Definition 4 ([16, Ch. 25]). Let $J \subseteq \mathbb{R}$, $F : J \times \mathcal{C}_D \to \mathbb{R}^n$ and let $\mathcal{C}$ be a subset of $J \times \mathcal{C}_D$. If for some $K \geq 0$,

$$\|F(t, \psi) - F(t, \tilde{\psi})\| \leq K\|\psi - \tilde{\psi}\|_r$$

whenever (t, ψ) and $(t, \tilde{\psi}) \in \mathcal{C}$, we say F satisfies a *Lipschitz condition* (or F is *Lipschitzian*) on $\mathcal{C}$ with Lipschitz constant K.

Remark. More precisely, the Lipschitz condition in [16] is a Lipschitz condition in the function space, not in time.

Here, we used the definition that

$$\|\psi\|_r = \sup_{-r \leq \sigma \leq 0} \|\psi(\sigma)\|,$$

which defines a norm on $\mathcal{C}_{\mathbb{R}^n}$ [16].

In order to prove that our system fulfills a local Lipschitz condition, we will use the following lemma about sums and products of Lipschitz functionals.

Lemma 2. *Let* $J \subseteq \mathbb{R}$, F, G : $J \times \mathcal{C}_D \to \mathbb{R}^n$, $\mathcal{C}$ *be a subset of* $J \times \mathcal{C}_D$ *and* F, G *satisfy a Lipschitz condition on* $\mathcal{C}$. *Then,* F + G *also satisfies a Lipschitz condition on* $\mathcal{C}$. *If furthermore* $n = 1$ *and* F, G *are bounded on* $\mathcal{C}$, *then* F $\cdot$ G *satisfies a Lipschitz condition on* $\mathcal{C}$ *as well.*

Proof. Let F, G : $J \times \mathcal{C}_D \to \mathbb{R}^n$ satisfy a Lipschitz condition on $\mathcal{C} \subseteq J \times \mathcal{C}_D$ with Lipschitz constant K, L, respectively. Now, let (t, ψ), $(t, \tilde{\psi}) \in \mathcal{C}$. Then,

$$
\begin{aligned}
\|(\mathrm{F} + \mathrm{G})(t, \psi) - (\mathrm{F} + \mathrm{G})(t, \tilde{\psi})\| &= \|\mathrm{F}(t, \psi) + \mathrm{G}(t, \psi) - \mathrm{F}(t, \tilde{\psi}) - \mathrm{G}(t, \tilde{\psi})\| \\
&\leq \|\mathrm{F}(t, \psi) - \mathrm{F}(t, \tilde{\psi})\| + \|\mathrm{G}(t, \psi) - \mathrm{G}(t, \tilde{\psi})\| \\
&\leq \mathrm{K}\|\psi - \tilde{\psi}\|_r + \mathrm{L}\|\psi - \tilde{\psi}\|_r \\
&= (\mathrm{K} + \mathrm{L})\|\psi - \tilde{\psi}\|_r.
\end{aligned}
$$

Therefore, F + G satisfies a Lipschitz condition on $\mathcal{C}$ with Lipschitz constant K + L. Now, assume that F, G are bounded on $\mathcal{C}$ with upper bounds M, N, respectively. Let (t, ψ), $(t, \tilde{\psi}) \in \mathcal{C}$. Then,

$$
\begin{aligned}
&\|(\mathrm{F} \cdot \mathrm{G})(t, \psi) - (\mathrm{F} \cdot \mathrm{G})(t, \tilde{\psi})\| \\
={}& \|\mathrm{F}(t, \psi) \cdot \mathrm{G}(t, \psi) - \mathrm{F}(t, \tilde{\psi}) \cdot \mathrm{G}(t, \tilde{\psi})\| \\
={}& \|\mathrm{F}(t, \psi) \cdot \mathrm{G}(t, \psi) - \mathrm{F}(t, \psi) \cdot \mathrm{G}(t, \tilde{\psi}) + \mathrm{F}(t, \psi) \cdot \mathrm{G}(t, \tilde{\psi}) - \mathrm{F}(t, \tilde{\psi}) \cdot \mathrm{G}(t, \tilde{\psi})\| \\
\leq{}& \|\mathrm{F}(t, \psi)\| \cdot \|\mathrm{G}(t, \psi) - \mathrm{G}(t, \tilde{\psi})\| + \|\mathrm{G}(t, \tilde{\psi})\| \cdot \|\mathrm{F}(t, \psi) - \mathrm{F}(t, \tilde{\psi})\| \\
\leq{}& \mathrm{MK}\|\psi - \tilde{\psi}\|_r + \mathrm{NL}\|\psi - \tilde{\psi}\|_r \\
={}& (\mathrm{MK} + \mathrm{NL})\|\psi - \tilde{\psi}\|_r.
\end{aligned}
$$

Therefore, F$\cdot$G satisfies a Lipschitz condition on $\mathcal{C}$ with Lipschitz constant MK+NL.
$\qquad\square$

Definition 5 ([16, Ch. 25]). The functional F : $J \times \mathcal{C}_D \to \mathbb{R}^n$ is said to be *locally Lipschitzian* if for each given $(\bar{t}, \overline{\psi}) \in J \times \mathcal{C}_D$ there exist numbers $a > 0$ and $b > 0$ such that
$$
\mathcal{C} = ([\bar{t} - a, \bar{t} + a] \cap J) \times \{\psi \in \mathcal{C}_{\mathbb{R}^n} : \|\psi - \overline{\psi}\|_r \leq b\}
$$
is a subset of $J \times \mathcal{C}_D$ and F is Lipschitzian on $\mathcal{C}$.

We will now show that our F satisfies a local Lipschitz condition.

Lemma 3. F *defined by* (3.7) *satisfies a local Lipschitz condition on* $[0, \infty) \times \mathcal{C}_D$.

Proof. Let $(\bar{t}, \overline{\psi}) \in \mathbb{R}_{\geq 0} \times \mathcal{C}_D$. Because $[-\tau^e_{\max}, 0]$ is compact and D is open we can find b such that $\{\psi \in \mathcal{C}_{\mathbb{R}^n} : \|\psi - \overline{\psi}\|_{\tau^e_{\max}} \leq b\} \subseteq \mathcal{C}_D$. Choose $a > 0$ arbitrary and let $\mathcal{C}$ be defined as in Definition 5 with $J = \mathbb{R}_{\geq 0}$.
Now let (t, ψ), $(t, \tilde{\psi}) \in \mathcal{C}$. Especially, we have $\|\psi - \overline{\psi}\|_{\tau^e_{\max}} \leq b$ which implies that $\|\psi(\tau)\| \leq \|\overline{\psi}(\tau)\| + b \leq \|\overline{\psi}\|_{\tau^e_{\max}} + b =: \mathrm{M}$ for each $\tau \in [-\tau^e_{\max}, 0]$. This also holds for $\tilde{\psi}$.

For $i \in V$, we have

$$\mathrm{F}(t,\psi)_i = \kappa(t)\omega_i\big(1 - \sum_{\substack{j\in\mathcal{P}(\mathrm{V})\\ i\in j}} \psi_j(0)\big) \cdot \big(\psi_i(-\tau_i^s) - \psi_i(-\tau_i^e) - \lambda_i[\psi_i(-\tau_i^d) - \psi_i(-\tau_i^e)]\big).$$

Clearly, $f(t,\psi) = \psi_q(\tau)$ is Lipschitzian with constant 1 for arbitrary $\tau \in [-\tau_{\max}^e, 0]$ and $q \in \mathrm{V} \cup \mathcal{P}(\mathrm{V}) \setminus \{\emptyset\}$. $\kappa(t)$ is bounded by our assumptions stated in Section 3.1. On $\mathcal{C}$, ψ_j is bounded by M and hence also $\big(1 - \sum_{\substack{j\in\mathcal{P}(\mathrm{V})\\ i\in j}} \psi_j(0)\big)$ and $\big(\psi_i(-\tau_i^s) - \psi_i(-\tau_i^e) - \lambda_i[\psi_i(-\tau_i^d) - \psi_i(-\tau_i^e)]\big)$ are bounded on $\mathcal{C}$. Therefore, $\mathrm{F}(t,\psi)_i$ is a sum and product of bounded Lipschitz functionals on $\mathcal{C}$ and we can apply Lemma 2 to show that $\mathrm{F}(t,\psi)_i$ is also Lipschitzian on $\mathcal{C}$.

For $j \in \mathcal{P}(\mathrm{V}) \setminus \{\emptyset\}$, we have

$$
\begin{aligned}
\mathrm{F}(t,\psi)_j = &- \alpha_j\psi_j(0) - \sum_{i\in\mathrm{V}\setminus j} \kappa(t)\omega_i\psi_j(0)\big(\psi_i(-\tau_i^s) - \psi_i(-\tau_i^e) - \lambda_i[\psi_i(-\tau_i^d) - \psi_i(-\tau_i^e)]\big) \\
&+ \sum_{\substack{k\in\mathcal{P}(\mathrm{V})\setminus\{\emptyset\}\\ k\subset j}} \sum_{i\in j\setminus k} \pi_{i,k,j}\kappa(t)\omega_i\psi_k(0)\big(\psi_i(-\tau_i^s) - \psi_i(-\tau_i^e) - \lambda_i[\psi_i(-\tau_i^d) - \psi_i(-\tau_i^e)]\big) \\
&+ \sum_{i\in j} \pi_{i,\emptyset,j}\kappa(t)\omega_i\big(1 - \sum_{k\in\mathcal{P}(\mathrm{V})\setminus\{\emptyset\}} \psi_k(0)\big)\big(\psi_i(-\tau_i^s) - \psi_i(-\tau_i^e) - \lambda_i[\psi_i(-\tau_i^d) - \psi_i(-\tau_i^e)]\big) \\
&- \sum_{\substack{k\in\mathcal{P}(\mathrm{V})\\ j\subset k}} \varepsilon_{j,k}\psi_j(0)\dot{v}(t - \tau^p) + \sum_{\substack{k\in\mathcal{P}(\mathrm{V})\\ k\subset j}} \varepsilon_{k,j}\psi_k(0)\dot{v}(t - \tau^p) \\
&+ \varepsilon_{\emptyset,j}\big(1 - \sum_{k\in\mathcal{P}(\mathrm{V})\setminus\{\emptyset\}} \psi_k(0)\big)\dot{v}(t - \tau^p).
\end{aligned}
$$

We also assumed boundedness of $\dot{v}$ in our general assumptions in Subsection 3.1. As for the i components we can apply Lemma 2 to show that $\mathrm{F}(t,\psi)_j$ is Lipschitzian on $\mathcal{C}$ as a sum and product of Lipschitz functionals on $\mathcal{C}$.

Finally, we can apply the Lipschitz continuity for the single components to get

$$
\begin{aligned}
\|\mathrm{F}(t,\psi) - \mathrm{F}(t,\tilde\psi)\| &\leq \sum_{i\in\mathrm{V}} |\mathrm{F}(t,\psi)_i - \mathrm{F}(t,\tilde\psi)_i| + \sum_{j\in\mathcal{P}(\mathrm{V})\setminus\{\emptyset\}} |\mathrm{F}(t,\psi)_j - \mathrm{F}(t,\tilde\psi)_j| \\
&\leq \mathrm{K}\|\psi - \tilde\psi\|_{\tau_{\max}^e}
\end{aligned}
$$

for some $\mathrm{K} > 0$. This shows that F is Lipschitzian on $\mathcal{C}$ and, as $(\bar{t},\overline{\psi}) \in \mathbb{R}_{\geq 0} \times \mathcal{C}_\mathrm{D}$ was arbitrary, that F is locally Lipschitzian.

$\square$

With the continuity condition and the local Lipschitz condition shown, we would now be able to apply theorems about uniqueness and local existence of a solution. However, there is also a theorem for the extended existence of a solution which we can apply to our system. After establishing some properties in Sections 3.5 and 3.6, we will be able to use this theorem to show global existence of a solution to our system. The following definitions are needed for the theorem.

Definition 6 ([16, Ch. 26]). Let x on $[t_0 - r, \beta_1)$ and γ on $[t_0 - r, \beta_2)$ both be solutions of Equations (3.8) and (3.9). If they agree with each other on $[t_0 - r, \beta_1)$ and $\beta_2 > \beta_1$, we say γ is a *continuation* of x, or x can be *continued* to $[t_0 - r, \beta_2)$. A solution x of Equations (3.8) and (3.9) is *noncontinuable* if it has no continuation.

Definition 7 ([16, Ch. 26]). The functional $F : [t_0, \beta) \times \mathcal{C}_D \to \mathbb{R}^n$ is said to be *quasi-bounded* if F is bounded on every set of the form $[t_0, \beta_1] \times \mathcal{C}_A$ where $t_0 < \beta_1 < \beta$ and A is a closed bounded subset of D.

Lemma 4. F *defined as in* (3.7) *is quasi-bounded.*

Proof. Let $\beta_1 > 0$ and A be a closed bounded subset of D which is defined by Equation (3.6). For $\psi \in \mathcal{C}_A$, in particular ψ_i and ψ_j are bounded. Together with the boundedness of κ and $\dot{v}$ (see Section 3.1), we see that every component of F is a composition of bounded functions and hence F is bounded on $[t_0, \beta_1] \times \mathcal{C}_A$. As β_1 and A were arbitrary, we conclude that F is quasi-bounded. $\square$

We can now state the extended existence theorem and apply it to our system.

Theorem 3 ([16, Thm. 26-C]). *Let* $F : [t_0, \beta) \times \mathcal{C}_D \to \mathbb{R}^n$ *satisfy Continuity Condition (C), and let it be locally Lipschitzian and quasi-bounded. Then for each* $\theta \in \mathcal{C}_D$, *Equations* (3.8) *and* (3.9) *have a unique noncontinuable solution x on* $[t_0 - r, \beta_1)$; *and if* $\beta_1 < \beta$, *then, for every closed bounded set* $A \subset D$,

$$x(t) \notin A \text{ for some } t \text{ in } (t_0, \beta_1).$$

This theorem can be applied to our system as we have proven all the conditions on F before.

Theorem 4. *For each* $\theta \in \mathcal{C}_D$, *Equations* (3.10) *and* (3.11) *have a unique noncontinuable solution x on* $[-\tau_{max}^e, \beta_1)$; *and if* $\beta_1 < \infty$, *then, for every closed bounded set* $A \subset D$,

$$x(t) \notin A \text{ for some } t \text{ in } (0, \beta_1).$$

Proof. We have shown in Lemmas 1, 3 and 4 that F fulfills the assumptions of Theorem 3 which we can apply to prove this theorem. $\square$

3.5 Invariance properties

In order to have a meaningful model, we must also establish some invariance properties of the solution which will be stated and proven in this section. They will also be used to show global existence.

Definition 8. Let $x(t)$ be the state vector defined in (3.5). We call $x_t \in \mathcal{C}_D$ *feasible* if it fulfills $\dot{n}_i(\tau) \geq 0$ for all $\tau \in [t - \tau_i^e, t - \tau_i^s]$ and $i \in V$, $p_j(t) \geq 0$ for all $j \in \mathcal{P}(V) \setminus \{\emptyset\}$ and $\sum_{j \in \mathcal{P}(V) \setminus \{\emptyset\}} p_j(t) \leq 1$.
We call an initial history $\theta \in \mathcal{C}_D$ *feasible* if it is a feasible function with $t = 0$ and additionally $\dot{n}_i(\tau) \geq 0$ for $\tau \in [-\tau_i^s, 0]$ and $n_i(-\tau_i^e) \geq 0$.

Remark. We chose $\dot{n}_i(\tau) \geq 0$ only for $\tau \in [t - \tau_i^e, t - \tau_i^s]$ and not until t because this condition already allows us to prove $i_i(t) \geq 0$, as it will be done in the proof of Lemma 5.

Hence, feasibility means that the protection groups really form a partition of the population and the number of infectious individuals is nonnegative.

We will now show three lemmas which will be used to show that provided a feasible initial history, the solution to Equations (3.10) and (3.11) will be feasible for all times it exists.

Lemma 5. *Let $i \in V$, $t \geq 0$ and x_t be feasible. Then*

$$\dot{n}_i(t) \geq 0.$$

Proof. Assume that x_t is feasible. Then, we have

$$i_i(t) = n_i(t - \tau_i^s) - n_i(t - \tau_i^e) - \lambda_i \big[n_i(t - \tau_i^d) - n_i(t - \tau_i^e) \big]$$

$$= \int_{t-\tau_i^e}^{t-\tau_i^s} \dot{n}_i(\tau) d\tau - \lambda_i \int_{t-\tau_i^e}^{t-\tau_i^d} \dot{n}_i(\tau) d\tau$$

$$\geq 0$$

because $\tau_i^s \leq \tau_i^d \leq \tau_i^e$ and $\lambda_i \in [0,1]$. With this we can compute that

$$\dot{n}_i(t) = \underbrace{\kappa(t)\omega_i}_{\substack{>0 \\ \text{by general assumption}}} \underbrace{\Big(1 - \sum_{\substack{j \in \mathcal{P}(V) \\ i \in j}} p_j(t)\Big)}_{\substack{\geq 1 - \sum_{j \in \mathcal{P}(V) \setminus \{\emptyset\}} p_j(t) \geq 0 \\ \text{by assumption}}} \underbrace{i_i(t)}_{\substack{\geq 0 \\ \text{as shown previously}}} \geq 0.$$

$\square$

Lemma 6. *Let $j \in \mathcal{P}(V) \setminus \{\emptyset\}$, $t \geq 0$ and x_t be feasible. If $p_j(t) = 0$, we have*

$$\dot{p}_j(t) \geq 0.$$

Proof. Let $p_j(t) = 0$. Because of the assumption on $\dot{n}_i(\tau)$ we have, as in the proof of Lemma 5, that $i_i(t) \geq 0$. Also, $s(t) = p_\emptyset(t) = 1 - \sum_{j \in \mathcal{P}(V) \setminus \{\emptyset\}} p_j(t) \geq 0$.
We can then compute that[1]

$$\dot{p}_j(t) = -\alpha_j \underbrace{p_j(t)}_{=0}$$

$$- \sum_{i \in V \setminus j} \kappa(t)\omega_i \underbrace{p_j(t)}_{=0} i_i(t) + \sum_{\substack{k \in \mathcal{P}(V) \\ k \subset j}} \sum_{i \in j \setminus k} \pi_{i,k,j} \kappa(t)\omega_i p_k(t) i_i(t)$$

$$- \sum_{\substack{k \in \mathcal{P}(V) \\ j \subset k}} \varepsilon_{j,k} \underbrace{p_j(t)}_{=0} \dot{v}(t - \tau^p) + \sum_{\substack{k \in \mathcal{P}(V) \\ k \subset j}} \varepsilon_{k,j} p_k(t) \dot{v}(t - \tau^p)$$

---

[1]We use the formulation with $s(t)$ here.

$$= \sum_{\substack{k\in\mathcal{P}(\mathrm{V})\\k\subset j}} \sum_{i\in j\setminus k} \pi_{i,k,j}\kappa(t)\omega_i p_k(t)i_i(t) + \sum_{\substack{k\in\mathcal{P}(\mathrm{V})\\k\subset j}} \varepsilon_{k,j}p_k(t)\dot{v}(t-\tau^p)$$

$$\geq 0,$$

because all factors are nonnegative. $\qquad\qquad\qquad\qquad\qquad\qquad\qquad\qquad\square$

Lemma 7. *Let $t \geq 0$ and x_t be feasible. If $\sum_{j\in\mathcal{P}(\mathrm{V})\setminus\{\emptyset\}} p_j(t) = 1$, we have*

$$\sum_{j\in\mathcal{P}(\mathrm{V})\setminus\{\emptyset\}} \dot{p}_j(t) \leq 0.$$

This is equivalent to the statement that if $s(t) = 0$, then

$$\dot{s}(t) \geq 0.$$

Proof. The equivalency of the statements can be seen by the definition of $s(t) = p_\emptyset(t)$ $= 1 - \sum_{j\in\mathcal{P}(\mathrm{V})\setminus\{\emptyset\}} p_j(t)$. Hence, $\dot{s}(t) = -\sum_{j\in\mathcal{P}(\mathrm{V})\setminus\{\emptyset\}} \dot{p}_j(t)$. Therefore, the following equivalences hold

$$\sum_{j\in\mathcal{P}(\mathrm{V})\setminus\{\emptyset\}} p_j(t) = 1 \quad \Leftrightarrow \quad s(t) = 0,$$

$$\sum_{j\in\mathcal{P}(\mathrm{V})\setminus\{\emptyset\}} \dot{p}_j(t) \leq 0 \quad \Leftrightarrow \quad \dot{s}(t) \geq 0,$$

proving the equivalence of the statements.
Now assume x_t is feasible and $\sum_{j\in\mathcal{P}(\mathrm{V})\setminus\{\emptyset\}} p_j(t) = 1$. Because we require (see Equation (2.22)) that $\sum_{\substack{k\in\mathcal{P}(\mathrm{V})\\j\cup\{i\}\subseteq k}} \pi_{i,j,k} = 1$ for all $j \in \mathcal{P}(\mathrm{V}) \setminus \{\mathrm{V}\}$, $i \in \mathrm{V} \setminus j$ we have that

$$\sum_{\substack{k\in\mathcal{P}(\mathrm{V})\\j\cup\{i\}\subseteq k}} \pi_{i,j,k}\kappa(t)\omega_i p_j(t)i_i(t) = \kappa(t)\omega_i p_j(t)i_i(t). \qquad (3.12)$$

In order to compute $\sum_{j\in\mathcal{P}(\mathrm{V})\setminus\{\emptyset\}} \dot{p}_j(t)$ we will now compute two terms which appear in the sum. Using Equation (3.12) ($\star$), reordering the sums ($\#$) and swapping indices (Δ) we can compute that[2]

$$\sum_{j\in\mathcal{P}(\mathrm{V})\setminus\{\emptyset\}} \Big[- \sum_{i\in\mathrm{V}\setminus j} \kappa(t)\omega_i p_j(t)i_i(t) + \sum_{\substack{k\in\mathcal{P}(\mathrm{V})\\k\subset j}} \sum_{i\in j\setminus k} \pi_{i,k,j}\kappa(t)\omega_i p_k(t)i_i(t) \Big]$$

$$\stackrel{(\#)}{=} \sum_{i\in\mathrm{V}} \Big[- \sum_{\substack{j\in\mathcal{P}(\mathrm{V})\setminus\{\emptyset\}\\i\notin j}} \kappa(t)\omega_i p_j(t)i_i(t) + \sum_{\substack{j\in\mathcal{P}(\mathrm{V})\setminus\{\emptyset\}\\i\in j}} \sum_{\substack{k\in\mathcal{P}(\mathrm{V})\\i\notin k\\k\subset j}} \pi_{i,k,j}\kappa(t)\omega_i p_k(t)i_i(t) \Big]$$

$$\stackrel{(\Delta)}{=} \sum_{i\in\mathrm{V}} \Big[- \sum_{\substack{j\in\mathcal{P}(\mathrm{V})\setminus\{\emptyset\}\\i\notin j}} \kappa(t)\omega_i p_j(t)i_i(t) + \sum_{\substack{k\in\mathcal{P}(\mathrm{V})\setminus\{\emptyset\}\\i\in k}} \sum_{\substack{j\in\mathcal{P}(\mathrm{V})\\i\notin j\\j\subset k}} \pi_{i,j,k}\kappa(t)\omega_i p_j(t)i_i(t) \Big]$$

---

[2]Again using the formulation with $s(t)$.

$$\stackrel{(\#)}{=} \sum_{i\in V} \Big[- \sum_{\substack{j\in\mathcal{P}(V)\setminus\{\emptyset\} \\ i\notin j}} \kappa(t)\omega_i p_j(t)i_i(t) + \sum_{\substack{j\in\mathcal{P}(V) \\ i\notin j}} \sum_{\substack{k\in\mathcal{P}(V) \\ j\cup\{i\}\subseteq k}} \pi_{i,j,k}\kappa(t)\omega_i p_j(t)i_i(t) \Big]$$

$$\stackrel{(\star)}{=} \sum_{i\in V} \Big[- \sum_{\substack{j\in\mathcal{P}(V)\setminus\{\emptyset\} \\ i\notin j}} \kappa(t)\omega_i p_j(t)i_i(t) + \sum_{\substack{j\in\mathcal{P}(V) \\ i\notin j}} \kappa(t)\omega_i p_j(t)i_i(t) \Big]$$

$$= \sum_{i\in V} \kappa(t)\omega_i p_\emptyset(t)i_i(t).$$

Furthermore, we can compute that

$$\sum_{j\in\mathcal{P}(V)\setminus\{\emptyset\}} \Big[- \sum_{\substack{k\in\mathcal{P}(V) \\ j\subset k}} \varepsilon_{j,k}p_j(t)\dot{v}(t-\tau^p) + \sum_{\substack{k\in\mathcal{P}(V) \\ k\subset j}} \varepsilon_{k,j}p_k(t)\dot{v}(t-\tau^p) \Big]$$

$$\stackrel{(\#)}{=} - \sum_{j\in\mathcal{P}(V)\setminus\{\emptyset\}} \sum_{\substack{k\in\mathcal{P}(V) \\ j\subset k}} \varepsilon_{j,k}p_j(t)\dot{v}(t-\tau^p) + \sum_{k\in\mathcal{P}(V)} \sum_{\substack{j\in\mathcal{P}(V)\setminus\{\emptyset\} \\ k\subset j}} \varepsilon_{k,j}p_k(t)\dot{v}(t-\tau^p)$$

$$\stackrel{(\Delta)}{=} - \sum_{j\in\mathcal{P}(V)\setminus\{\emptyset\}} \sum_{\substack{k\in\mathcal{P}(V) \\ j\subset k}} \varepsilon_{j,k}p_j(t)\dot{v}(t-\tau^p) + \sum_{j\in\mathcal{P}(V)} \sum_{\substack{k\in\mathcal{P}(V)\setminus\{\emptyset\} \\ j\subset k}} \varepsilon_{j,k}p_j(t)\dot{v}(t-\tau^p)$$

$$= \sum_{k\in\mathcal{P}(V)\setminus\{\emptyset\}} \varepsilon_{\emptyset,k}p_\emptyset(t)\dot{v}(t-\tau^p).$$

Using these equations and the assumption that $s(t)=0$, we can then compute

$$\sum_{j\in\mathcal{P}(V)\setminus\{\emptyset\}} \dot{p}_j(t) = \sum_{j\in\mathcal{P}(V)\setminus\{\emptyset\}} -\alpha_j p_j(t)$$

$$+ \sum_{j\in\mathcal{P}(V)\setminus\{\emptyset\}} \Big[- \sum_{i\in V\setminus j} \kappa(t)\omega_i p_j(t)i_i(t) + \sum_{\substack{k\in\mathcal{P}(V) \\ k\subset j}} \sum_{i\in j\setminus k} \pi_{i,k,j}\kappa(t)\omega_i p_k(t)i_i(t) \Big]$$

$$+ \sum_{j\in\mathcal{P}(V)\setminus\{\emptyset\}} \Big[- \sum_{\substack{k\in\mathcal{P}(V) \\ j\subset k}} \varepsilon_{j,k}p_j(t)\dot{v}(t-\tau^p) + \sum_{\substack{k\in\mathcal{P}(V) \\ k\subset j}} \varepsilon_{k,j}p_k(t)\dot{v}(t-\tau^p) \Big]$$

$$= \sum_{j\in\mathcal{P}(V)\setminus\{\emptyset\}} -\alpha_j p_j(t) + \sum_{i\in V} \kappa(t)\omega_i \underbrace{p_\emptyset(t)}_{=s(t)=0} i_i(t) + \sum_{k\in\mathcal{P}(V)\setminus\{\emptyset\}} \varepsilon_{\emptyset,k} \underbrace{p_\emptyset(t)}_{=s(t)=0} \dot{v}(t-\tau^p)$$

$$= \sum_{j\in\mathcal{P}(V)\setminus\{\emptyset\}} -\alpha_j p_j(t)$$

$$\leq 0,$$

which is the statement we wanted to show. $\square$

Now, we are ready to show that any solution with a feasible initial history remains feasible as long as it exists.

Theorem 5. *Let* $x = \begin{pmatrix} (n_i)_{i \in V} \\ (p_j)_{j \in \mathcal{P}(V) \setminus \{\emptyset\}} \end{pmatrix}$ *be the unique noncontinuable solution to Equations* (3.10) *and* (3.11) *which exists on* $[-\tau_{max}^e, \beta_1)$ *for some* $\beta_1 > 0$. *If the initial history is feasible, then the solution is feasible for each* $t \in [0, \beta_1)$.

Proof. First, note that by definition of a solution (see Definition 2) x is continuous. Especially, the components of x are continuous. Now, define

$$\beta_{\max} := \inf\{t \in [0, \beta_1) : \dot{n}_i(t) < 0, \, p_j(t) < 0 \text{ or } \sum_{j \in \mathcal{P}(V) \setminus \{\emptyset\}} p_j(t) > 1$$

$$\text{for some } i \in V \text{ or } j \in \mathcal{P}(V) \setminus \{\emptyset\}\}.$$

$\beta_{\max}$ is not necessarily the first point in time where the solution is not feasible anymore because we only required $\dot{n}_i(\tau) \geq 0$ for $\tau \in [t - \tau_i^e, t - \tau_i^s]$, not until t.
We will show the statement by showing that $\beta_{\max} = \infty$. Assume $\beta_{\max} < \infty$. By definition we must have $\beta_{\max} \in [0, \beta_1)$ and $\dot{n}_i(t) \geq 0$, $p_j(t) \geq 0$, $\sum_{j \in \mathcal{P}(V) \setminus \{\emptyset\}} p_j(t) \leq 1$ for all $t \in [-\tau_i^e, \beta_{\max})$, $i \in V$ and $j \in \mathcal{P}(V) \setminus \{\emptyset\}$. By continuity of these functions, we also have $p_j(\beta_{\max}) \geq 0$ and $\sum_{j \in \mathcal{P}(V) \setminus \{\emptyset\}} p_j(\beta_{\max}) \leq 1$ for all $j \in \mathcal{P}(V) \setminus \{\emptyset\}$.

If $p_j(\beta_{\max}) = 0$ for some $j \in \mathcal{P}(V) \setminus \{\emptyset\}$, we can apply Lemma 6 to show that $\dot{p}_j(\beta_{\max}) \geq 0$ and hence $p_j(t) \geq 0$ also in $[\beta_{\max}, \beta_{\max} + \beta_j]$ for some $\beta_j > 0$. Otherwise such a β_j exists by continuity.

If $\sum_{j \in \mathcal{P}(V) \setminus \{\emptyset\}} p_j(\beta_{\max}) = 1$, we can apply Lemma 7 to show that $\sum_{j \in \mathcal{P}(V) \setminus \{\emptyset\}} \dot{p}_j(\beta_{\max}) \leq 0$ and hence $\sum_{j \in \mathcal{P}(V) \setminus \{\emptyset\}} p_j(t) \leq 1$ also in $[\beta_{\max}, \beta_{\max} + \beta_0]$ for some $\beta_0 > 0$. Otherwise such a β_0 exists by continuity.

Let $0 < \varepsilon < \min\{\min_{i \in V}\{\tau_i^s\}, \min_{j \in \mathcal{P}(V) \setminus \{\emptyset\}}\{\beta_j\}, \beta_0\}$. Such ε exists because all elements, over which the minimum is taken, are positive. We can then apply Lemma 5 for all $t \in [\beta_{\max}, \beta_{\max} + \varepsilon]$ to show that $\dot{n}_i(t) \geq 0$ also in $t \in [\beta_{\max}, \beta_{\max} + \varepsilon]$.

Therefore, we have shown that $\dot{n}_i(t) \geq 0$, $p_j(t) \geq 0$, $\sum_{j \in \mathcal{P}(V) \setminus \{\emptyset\}} p_j(t) \leq 1$ for all $i \in V$ and $j \in \mathcal{P}(V) \setminus \{\emptyset\}$ in $t \in [\beta_{\max}, \beta_{\max} + \varepsilon]$, contradicting its definition. Hence, we conclude that $\beta_{\max} = \infty$. $\qquad\square$

With this theorem, we have established that for all times where a solution exists, it is feasible given a feasible initial history. This means that the number of new infections is nonnegative and the protection groups form a feasible partition of the population if its initial history fulfills these requirements.

3.6   Global existence of a solution

In Section 3.5 we have shown that the solution to Equations (3.10) and (3.11) remains in a reasonable region for all times it exists. To show that the solution exists even globally we have to establish an upper bound on the total number of

new infections depending on the initial history and the time t. We will do this by using Gronwalls inequality.

Theorem 6 (Generalized Gronwalls inequality [51, Lemma 2.7]). *Suppose $\psi(t)$ satisfies*

$$\psi(t) \leq \alpha(t) + \int_0^t \beta(s)\psi(s)ds, \quad t \in [0, \mathrm{T}],$$

with $\alpha(t) \in \mathbb{R}$ and $\beta(t) \geq 0$ and all these functions are continuous. Then,

$$\psi(t) \leq \alpha(t) + \int_0^t \alpha(s)\beta(s)\exp\left(\int_s^t \beta(r)dr\right)ds, \quad t \in [0, \mathrm{T}].$$

Moreover, if in addition $\alpha(s) \leq \alpha(t)$ for $s \leq t$, then

$$\psi(t) \leq \alpha(t)\exp\left(\int_0^t \beta(s)ds\right), \quad t \in [0, \mathrm{T}].$$

Lemma 8. *Let $x = \begin{pmatrix} (n_i)_{i \in \mathrm{V}} \\ (p_j)_{j \in \mathcal{P}(\mathrm{V})\setminus\{\emptyset\}} \end{pmatrix}$ be the unique noncontinuable solution to Equations (3.10) and (3.11) which exists on $[-\tau_{max}^e, \beta_1)$ for some $\beta_1 > 0$. If the initial history is feasible, then*

$$n_i(t) \leq n_i(0)\exp\left(\int_0^t \kappa(s)\omega_i ds\right)$$

for all $t \in [0, \beta_1)$ and $i \in \mathrm{V}$.

Proof. Let $i \in \mathrm{V}$. By Theorem 5, we know that the solution is also feasible. Because $0 < \tau_i^s \leq \tau_i^d \leq \tau_i^e$, $\lambda_i \in [0, 1]$ and $n_i(t), \dot{n}_i(t) \geq 0$ for all $t \in [-t_i^e, \beta_1 - \tau_i^s)$ we know that

$$0 \leq i_i(t) = \underbrace{n_i(t - \tau_i^s)}_{\leq n_i(t)} - \underbrace{n_i(t - \tau_i^e)}_{\geq 0} - \underbrace{\lambda_i\big(n_i(t - \tau_i^d) - n_i(t - \tau_i^e)\big)}_{\geq 0} \leq n_i(t). \quad (3.13)$$

Furthermore, a feasible solution implies that for all $s \in [0, \beta_1)$

$$1 - \sum_{\substack{j \in \mathcal{P}(\mathrm{V})\setminus\{\emptyset\} \\ i \in j}} p_j(s) \in [0, 1]. \quad (3.14)$$

Now, let $\mathrm{T} \in [0, \beta_1)$. Using Equation (3.13) and (3.14), we find that for all $t \in [0, \mathrm{T}]$

$$n_i(t) = n_i(0) + \int_0^t \dot{n}_i(s)ds$$

$$= n_i(0) + \int_0^t \kappa(s)\omega_i\big(1 - \sum_{\substack{j \in \mathcal{P}(\mathrm{V})\setminus\{\emptyset\} \\ i \in j}} p_j(s)\big)i_i(s)ds$$

$$\leq n_i(0) + \int_0^t \kappa(s)\omega_i n_i(s)ds.$$

As $\kappa(s)\omega_i \geq 0$ and κ, n_i are continuous, we can apply Gronwalls inequality to get

$$n_i(t) \leq n_i(0) \exp\left(\int_0^t \kappa(s)\omega_i ds\right)$$

for all $t \in [0, \mathrm{T}]$. As $\mathrm{T} \in [0, \beta_1)$ was arbitrary, this even holds for all $t \in [0, \beta_1)$. $\square$

This allows us to prove global existence of a solution to our system.

Theorem 7. *For each feasible initial history $\theta \in \mathcal{C}_{\mathrm{D}}$, Equations (3.10) and (3.11) have a unique solution x on $[-\tau_{max}^e, \infty)$.*

Proof. By Theorem 3, we know that such a solution x exists on $[-\tau_{\max}^e, \beta_1)$ for some $\beta_1 > 0$ and if $\beta_1 < \infty$ for every closed bounded subset $\mathrm{A} \subset \mathrm{D}$,

$$x(t) \notin \mathrm{A} \text{ for some } t \text{ in } (0, \beta_1). \tag{3.15}$$

Assume $\beta_1 < \infty$. We know by our assumptions in Section 3.1 that κ is bounded. Let K be such that $\kappa(t) \leq \mathrm{K}$ for all $t \in [0, \infty)$. Define $\omega := \max_{i \in \mathrm{V}}\{\omega_i\}$. For a given feasible initial history $\theta \in \mathcal{C}_{\mathrm{D}}$, we define $n_0 := \max_{i \in \mathrm{V}}\{n_i(0)\}$ and

$$\mathrm{A} := [0, n_0 \exp(\mathrm{K}\omega\beta_1)]^{|\mathrm{V}|} \times [0, 1]^{2^{|\mathrm{V}|}-1}.$$

A is a closed bounded subset of D. By Theorem 5, $p_j(t) \in [0, 1]$ for all $j \in \mathcal{P}(\mathrm{V}) \backslash \{\emptyset\}$ and $t \in [0, \beta_1)$. By Lemma 8, we also have

$$n_i(t) \leq n_i(0) \exp\left(\int_0^t \kappa(s)\omega_i ds\right) \leq n_0 \exp(\mathrm{K}\omega\beta_1)$$

for all $i \in \mathrm{V}$ and $t \in [0, \beta_1)$. Therefore, $x(t) \in \mathrm{A}$ for all $t \in (0, \beta_1)$, contradicting Equation 3.15. Hence, we must have $\beta_1 = \infty$. $\square$

3.7   Extension to piecewise constant functions

As mentioned in Section 3.1, we actually use piecewise constant functions for κ and λ_i. We will now give the ideas how we can extend the theory to these cases.

Since only the present value of $\kappa(t)$ appears in the differential equations, we can just solve the problem until the discontinuity of κ and then use this solution as the initial history for the problem with the value of κ after the discontinuity. We can use the previous theory on these sections to show that we still obtain a global solution which is continuous, but with discontinuities in the derivatives.

For the discontinuities of λ_i we cannot do this because we have to evaluate λ_i over some time interval for the differential equations. Assume λ_i has a discontinuity at $\bar{t} \in [t + \tau_i^d - \tau_i^e, t]$ for some $t > 0$ with $\lambda_i(t) = \lambda_i^0$ for $t < \bar{t}$ and $\lambda_i(t) = \lambda_i^1$ for $t \geq \bar{t}$.

Then, we can compute

$$
\begin{aligned}
d_i(t) - d_i(t + \tau_i^d - \tau_i^e) &= \int_{t+\tau_i^d-\tau_i^e}^{t} \dot{d}_i(\tilde{t})\, d\tilde{t} \\
&= \int_{t+\tau_i^d-\tau_i^e}^{t} \lambda_i(\tilde{t})\dot{n}_i(\tilde{t} - \tau_i^d)\mathrm{d}\tilde{t} \\
&= \int_{t+\tau_i^d-\tau_i^e}^{\bar{t}} \lambda_i^0 \dot{n}_i(\tilde{t} - \tau_i^d)d\tilde{t} + \int_{\bar{t}}^{t} \lambda_i^1 \dot{n}_i(\tilde{t} - \tau_i^d)d\tilde{t} \\
&= \lambda_i^0 \big[n_i(\bar{t} - \tau_i^d) - n_i(t - \tau_i^e) \big] + \lambda_i^1 \big[n_i(t - \tau_i^d) - n_i(\bar{t} - \tau_i^d) \big] \\
\Rightarrow \quad i_i(t) &= n_i(t - \tau_i^s) - n_i(t - \tau_i^e) - \big[d_i(t) - d_i(t + \tau_i^d - \tau_i^e) \big] \\
&= n_i(t - \tau_i^s) - n_i(t - \tau_i^e) - \lambda_i^0 \big[n_i(\bar{t} - \tau_i^d) - n_i(t - \tau_i^e) \big] \\
&\quad - \lambda_i^1 \big[n_i(t - \tau_i^d) - n_i(\bar{t} - \tau_i^d) \big].
\end{aligned}
$$

The delay is still bounded because we only need to evaluate $\bar{t} - \tau_i^d$ if $t \in [\bar{t}, \bar{t} + \tau_i^e - \tau_i^d]$. By plugging in the boundary cases, we also see that $i_i(t)$ still depends continuously on t if n_i is continuous. Therefore, we can also establish all the above theorems for piecewise constant detection rates λ_i.

3.8   Equilibrium points

In this section, we want to determine the equilibrium points of the system. The goal is to understand the long-term behavior of the model. Therefore, we set further assumptions, namely $\dot{v}(t) = 0$, $\kappa(t) = \kappa$ and $\lambda(t) = 0$ for all $t \geq 0$. This means that there is no vaccination nor testing and isolation strategy applied and the contact behavior is constant. Also assume that immunity actually wanes, i.e. $\alpha > 0$. We will start with the one-variant model because the fixed point investigation has also not been done for this model and we are able to determine all equilibria algebraically. This is not possible anymore for the two-variant model.
Note that by our assumptions the system has become autonomous, i.e. we can represent the differential equation by

$$
\dot{x} = \mathrm{F}(x_t).
$$

3.8.1   One-variant model

By definition of an equilibrium point [47, Ch. 12], we are searching for constant $\overline{x}(t) = \overline{x}$ for which

$$
0 = \mathrm{F}(\overline{x}_t).
$$

As the total number of infections $n(t)$ is one of our state variables, we will only be able to encounter an equilibrium with no new infections. In classical SEIR models this equilibrium is called disease-free equilibrium (DFE) [11, Ch. 2]. But, there is another equilibrium called the endemic equilibrium (EE) with a constant number of

new infections in classical models. To calculate this, which corresponds to constant $\dot{n}(t)$ in our model, we reformulate the equation for $n(t)$ in terms of the infectious compartment[3] $i(t)$. We have[4]

$$i(t) = n(t - \tau^s) - n(t - \tau^e) \tag{3.16}$$

$$\Rightarrow \quad i'(t) = n'(t - \tau^s) - n'(t - \tau^e) \tag{3.17}$$

$$= \kappa(1 - p(t - \tau^s))i(t - \tau^s) - \kappa(1 - p(t - \tau^e))i(t - \tau^e). \tag{3.18}$$

Hence, we are now searching for equilibria of the system

$$i'(t) = \kappa(1 - p(t - \tau^s))i(t - \tau^s) - \kappa(1 - p(t - \tau^e))i(t - \tau^e), \tag{3.19}$$

$$p'(t) = -\alpha p(t) + \kappa(1 - p(t))i(t), \tag{3.20}$$

which fulfill

$$i(t) = \int_{t-\tau^e}^{t-\tau^s} \dot{n}(\tilde{t})d\tilde{t} = \int_{t-\tau^e}^{t-\tau^s} \kappa\big(1 - p(\tilde{t})\big)i(\tilde{t})d\tilde{t}. \tag{3.21}$$

By deriving the expression for $i(t)$ in (3.18) we lose this information for the initial history.

Disease-free equilibrium (DFE)

One equilibrium of the Equations (3.19)-(3.20) is the DFE with $i(t) = 0$. Because of the waning factor $\alpha > 0$, we can then see that we must have $p(t) = 0$. Hence, the DFE is given by

$$(i(t), p(t)) = (0, 0). \tag{3.22}$$

Endemic equilibrium (EE)

Now, we are searching for an equilibrium $(i(t), p(t)) = (i^*, p^*)$ with $i^* > 0$. As the right-hand side of $i'(t)$ always equals 0 for such constant solutions, we evaluate

$$i^* = i(t) = \int_{t-\tau^e}^{t-\tau^s} \kappa(1 - p(\tilde{t}))i(\tilde{t})d\tilde{t}$$

$$= (\tau^e - \tau^s)\kappa(1 - p^*)i^* \tag{3.23}$$

$$\overset{i^* \gtrless 0}{\Rightarrow} \quad 1 - p^* = \frac{1}{(\tau^e - \tau^s)\kappa}$$

$$\Rightarrow \quad p^* = 1 - \frac{1}{(\tau^e - \tau^s)\kappa}.$$

---

[3]Note that (in contrast to classical models) the infectious are not a compartment in our model in the strict sense because they are not part of a partition of the population and could mathematically even be slightly greater than 1 because of waning immunity.

[4]Using $x'(t)$ instead of $\dot{x}(t)$ for the time-derivative because of readibility for $i(t)$.

Plugging this into Equation (3.20) with $p'(t) = 0$ we find that

$$0 = -\alpha\left(1 - \frac{1}{(\tau^e - \tau^s)\kappa}\right) + \kappa\frac{1}{(\tau^e - \tau^s)\kappa}i^*$$

$$\Rightarrow \quad i^* = \alpha\left(1 - \frac{1}{(\tau^e - \tau^s)\kappa}\right) \cdot (\tau^e - \tau^s).$$

Based on the terms appearing in the computation, we define the basic reproduction number in our model as follows:

Definition 9. The basic reproduction number R^0 of system (3.19)-(3.20) is given by

$$R^0 := (\tau^e - \tau^s)\kappa.$$

Remark. Our definition corresponds to the usual definition of a basic reproduction number as the number of primary cases an infectious individual causes in a fully susceptible population. This is the case because our R^0 is the product of the length of the infectious period and the critical contacts a person has per time.

Now, the question arises when the EE is in the feasible region and distinct from the DFE, i.e. $i^* > 0$ and $p^* \in [0, 1]$. By observation of the computed value for p^* we see that this is the case if $R^0 > 1$. Hence, we can state:

Theorem 8. *The endemic equilibrium of system* (3.19)-(3.20) *given by*

$$\big(i(t), p(t)\big) = \big(i^*, p^*\big) = \left(\alpha p^*(\tau^e - \tau^s), 1 - \frac{1}{R^0}\right)$$

is in the feasible region and distinct from the DFE if and only if $R^0 > 1$.

Stability

Now, we want to characterize the stability of the equilibria by linearization. Around the DFE, the linearization is

$$\begin{pmatrix} i(t) \\ p(t) \end{pmatrix}' = \begin{pmatrix} 0 & 0 \\ \kappa & -\alpha \end{pmatrix}\begin{pmatrix} i(t) \\ p(t) \end{pmatrix} + \begin{pmatrix} \kappa & 0 \\ 0 & 0 \end{pmatrix}\begin{pmatrix} i(t - \tau^s) \\ p(t - \tau^s) \end{pmatrix} + \begin{pmatrix} -\kappa & 0 \\ 0 & 0 \end{pmatrix}\begin{pmatrix} i(t - \tau^e) \\ p(t - \tau^e) \end{pmatrix}.$$

We know that the trivial solution of a linear delay differential equation system

$$x'(t) = \sum_{j=1}^{m} A_j x(t - r_j)$$

is asymptotically stable if and only if all roots of the characteristic equation

$$\det\left(\lambda I - \sum_{j=1}^{m} A_j \exp(-\lambda r_j)\right) = 0$$

have negative real parts [16] [8, Ch. 4]. Computing the characteristic equation of
the linearized system

$$0 = \det\left(\lambda\mathrm{I} - \begin{pmatrix} 0 & 0 \\ \kappa & -\alpha \end{pmatrix} - \begin{pmatrix} \kappa\exp(-\lambda\tau^s) & 0 \\ 0 & 0 \end{pmatrix} - \begin{pmatrix} -\kappa\exp(-\lambda\tau^e) & 0 \\ 0 & 0 \end{pmatrix}\right)$$

$$\Leftrightarrow \quad 0 = \det\left(\begin{pmatrix} \lambda - \kappa\exp(-\lambda\tau^s) + \kappa\exp(-\lambda\tau^e) & 0 \\ -\kappa & \lambda + \alpha \end{pmatrix}\right)$$

$$\Leftrightarrow \quad 0 = \big(\lambda - \kappa\exp(-\lambda\tau^s) + \kappa\exp(-\lambda\tau^e)\big) \cdot \big(\lambda + \alpha\big),$$

we see that $\lambda = -\alpha < 0$ is a root. The other roots are the roots of

$$f(\lambda) := \lambda + \kappa\big(\exp(-\lambda\tau^e) - \exp(-\lambda\tau^s)\big).$$

Clearly, 0 is a root of f. By examining f in more detail, we can show that all roots
of the characteristic equation except 0 have negative real part if $R^0 < 1$.
First, we investigate the real roots of f. We have

$$f'(\lambda) = 1 - \kappa\tau^e\exp(-\lambda\tau^e) + \kappa\tau^s\exp(-\lambda\tau^s)$$

$$\Rightarrow \quad f'(0) = 1 - \kappa(\tau^e - \tau^s) = 1 - R^0$$

$$f''(\lambda) = \kappa(\tau^e)^2\exp(-\lambda\tau^e) - \kappa(\tau^s)^2\exp(-\lambda\tau^s).$$

We see that f'' has a zero if and only if

$$\frac{(\tau^e)^2}{(\tau^s)^2} = \exp(\lambda(\tau^e - \tau^s)),$$

i.e. by monotonicity of the exponential function it has exactly one zero. Using
Rolle's theorem [18, Kap. 16, Satz 2], we conclude that f' has at most two real
roots (counted with its multiplicity). But as $f'(\lambda) \xrightarrow{\lambda\to-\infty} -\infty$ and $f'(\lambda) \xrightarrow{\lambda\to\infty} 1$,
we conclude that the number of roots (counted with its multiplicity) of f' must be
odd and hence f' has exactly one root. Again, we can use Rolle to conclude that f
has at most two roots. Furthermore, we observe that $f(\lambda) \xrightarrow{\lambda\to-\infty} \infty$, $f(\lambda) \xrightarrow{\lambda\to\infty} \infty$
and 0 is a root of f. Therefore, we can determine the sign of the other real root
by examining $f'(0)$. We find that the other root of f has negative sign iff $R^0 < 1$
and positive sign iff $R^0 > 1$. In particular, we can already conclude that the DFE
is unstable if $R^0 > 1$.
Now we want to examine the imaginary roots of f. We set $\lambda = \mu + i\omega$. As both,
the real and the imaginary part of f, have to be 0, we obtain the system

$$0 = \mu + \kappa\exp(-\mu\tau^e)\cos(-\omega\tau^e) - \kappa\exp(-\mu\tau^s)\cos(-\omega\tau^s), \qquad (3.24)$$

$$0 = \omega + \kappa\exp(-\mu\tau^e)\sin(-\omega\tau^e) - \kappa\exp(-\mu\tau^s)\sin(-\omega\tau^s). \qquad (3.25)$$

Clearly, if $R^0 = 0$, i.e. $\tau^e = \tau^s$, only 0 is a solution to the system. Now, we want
to show that no imaginary solution crosses the imaginary axis while $R^0 < 1$. First,
we show that there are no imaginary solutions with $\mu = 0$, $\omega \neq 0$. Assume such a
solution exists. By setting $\mu = 0$ in (3.24) and (3.25), we obtain

$$0 = \kappa\cos(-\omega\tau^e) - \kappa\cos(-\omega\tau^s), \qquad (3.26)$$

$$0 = \omega + \kappa\sin(-\omega\tau^e) - \kappa\sin(-\omega\tau^s). \qquad (3.27)$$

Solutions of (3.26) are given by

$$-\omega\tau^e = \pm\omega\tau^s - 2\pi n, \quad n \in \mathbb{Z} \tag{3.28}$$

$$\Rightarrow \quad \omega_\pm = \frac{2\pi n}{\tau^e \pm \tau^s}, \qquad n \in \mathbb{Z}. \tag{3.29}$$

For ω_- one can see that

$$\sin\left(-\omega_-\tau^e\right) = \sin\left(-\omega_-(\tau^s + (\tau^e - \tau^s))\right) = \sin\left(-\omega_-\tau^s - 2\pi n\right) = \sin\left(-\omega_-\tau^s\right).$$

Plugging this into (3.27) one gets that $\omega_- = 0$ is the only possible solution in this case.

For ω_+ one observes that a solution of (3.27) corresponds to an intersection of the line $h(y) = \frac{2\pi y}{\tau^e+\tau^s}$ and

$$g(y) := -\kappa \sin\left(-\frac{2\pi y}{\tau^e + \tau^s}\tau^e\right) + \kappa \sin\left(-\frac{2\pi y}{\tau^e + \tau^s}\tau^s\right)$$

with $y \in \mathbb{Z}$. By visualization of the sine function, we know that there exists an intersection distinct from 0, with $y \in \mathbb{R}$, only if $g'(0) > h'(0) = \frac{2\pi}{\tau^e+\tau^s}$. But we have

$$g'(y) = \kappa\frac{2\pi}{\tau^e + \tau^s}\tau^e \cos\left(-\frac{2\pi y}{\tau^e + \tau^s}\tau^e\right) - \kappa\frac{2\pi}{\tau^e + \tau^s}\tau^s \cos\left(-\frac{2\pi y}{\tau^e + \tau^s}\tau^s\right)$$

$$\Rightarrow \quad g'(0) = \frac{2\pi}{\tau^e + \tau^s}\kappa(\tau^e - \tau^s) = \frac{2\pi}{\tau^e + \tau^s}R^0 < \frac{2\pi}{\tau^e + \tau^s},$$

if $R^0 < 1$. Therefore, no pair of complex conjugate eigenvalues can cross the imaginary axis while $R^0 < 1$, except through the origin.

By expanding (3.25) we find that

$$\begin{aligned}0 &= \omega + \kappa \exp(-\mu\tau^e)\sin(-\omega\tau^e) - \kappa\exp(-\lambda\tau^s)\sin(-\omega\tau^s) \\ &= \omega - \kappa\exp(-\mu\tau^e)\omega\tau^e + \kappa\exp(-\lambda\tau^s)\omega\tau^s + \mathcal{O}(\omega^2) \\ &= \omega\big(1 - \kappa\exp(-\mu\tau^e)\tau^e + \kappa\exp(-\lambda\tau^s)\tau^s + \mathcal{O}(\omega)\big) \\ &= \omega\big(1 - R^0 + \mathcal{O}(\mu) + \mathcal{O}(\omega)\big).\end{aligned}$$

Hence, if $R^0 < 1$, the only solution close to the origin is $\omega = 0$. This corresponds to a real root of f. However, we ruled out the possibility that a real root crosses the imaginary axis while $R^0 < 1$. Hence, all roots of the characteristic except 0 have negative real part if $R^0 < 1$.

Now, we want to determine the eigenspace N corresponding to 0, called *center eigenspace* [12]. We can compute it by solving

$$\begin{pmatrix}0\\0\end{pmatrix} = \begin{pmatrix}0 & 0\\\kappa & -\alpha\end{pmatrix}\begin{pmatrix}i(t)\\p(t)\end{pmatrix} + \begin{pmatrix}\kappa & 0\\0 & 0\end{pmatrix}\begin{pmatrix}i(t-\tau^s)\\p(t-\tau^s)\end{pmatrix} + \begin{pmatrix}-\kappa & 0\\0 & 0\end{pmatrix}\begin{pmatrix}i(t-\tau^e)\\p(t-\tau^e)\end{pmatrix}.$$

Thus, it is given by

$$N = \{(\frac{\alpha}{\kappa}p, p) \in \mathcal{C}_\mathrm{D} : p \in [0,1]\}.$$

However, the only function in N fulfilling (3.21) is the DFE. If $R^0 < 1$, this also holds for the corresponding *center manifold M* [12], which we can explicitly compute by solving

$$0 = \kappa(1 - p(t - \tau^s))i(t - \tau^s) - \kappa(1 - p(t - \tau^e))i(t - \tau^e), \qquad (3.30)$$

$$0 = -\alpha p(t) + \kappa(1 - p(t))i(t). \qquad (3.31)$$

We find

$$M = \{(\frac{\alpha p}{\kappa(1 - p)}, p) \in \mathcal{C}_D : p \in [0, 1]\}.$$

But the only other solution to (3.30) and (3.31) fulfilling (3.21) is the EE, which is not in the feasible region for $R^0 < 1$.

Therefore, for $R^0 < 1$, all feasible solutions fulfilling (3.21) apart from the DFE correspond to eigenvalues of the linearized system with negative real part. We conclude that the DFE is asymptotically stable for $R^0 < 1$. It is unstable for $R^0 > 1$ as we have a positive real root. Thus, $R^0 = 1$ is a bifurcation point. We expect a transcritical bifurcation [50] because a real root passes the imaginary axis and the EE passes through the DFE (and enters the feasible region) for $R^0 = 1$.

The linearization around the EE is

$$\begin{pmatrix} i(t) \\ p(t) \end{pmatrix}' = \begin{pmatrix} 0 & 0 \\ \kappa(1 - p^*) & -\alpha \end{pmatrix} \begin{pmatrix} i(t) - i^* \\ p(t) - p^* \end{pmatrix}$$
$$+ \begin{pmatrix} \kappa(1 - p^*) & -\kappa i^* \\ 0 & 0 \end{pmatrix} \begin{pmatrix} i(t - \tau^s) - i^* \\ p(t - \tau^s) - p^* \end{pmatrix}$$
$$+ \begin{pmatrix} -\kappa(1 - p^*) & \kappa i^* \\ 0 & 0 \end{pmatrix} \begin{pmatrix} i(t - \tau^e) - i^* \\ p(t - \tau^e) - p^* \end{pmatrix}$$

with the characteristic equation

$$0 = \left(\lambda - \kappa(1 - p^*)\exp(-\lambda\tau^s) + \kappa(1 - p^*)\exp(-\lambda\tau^e)\right) \cdot \left(\lambda + \alpha\right)$$
$$- \left(\kappa i^*\exp(-\lambda\tau^s) - \kappa i^*\exp(-\lambda\tau^e)\kappa(1 - p^*)\right).$$

As this is not factorized, an analysis of the roots would be even more involved than for the DFE. We skip it here and note that we expect asymptotic stability of the EE if $R^0 > 1$ because of the above mentioned transcritical bifurcation occurring at $R^0 = 1$.

3.8.2 Two-variant model

By transforming the two-variant model to a system in $i_i(t)$ and $p_j(t)$ like in (3.18) we obtain

$$i_0'(t) = \kappa s_0(t)i_0(t - \tau^s) - \kappa s_0(t)i_0(t - \tau^e),$$
$$i_1'(t) = \kappa\omega_1 s_1(t)i_1(t - \tau^s) - \kappa\omega_1 s_1(t)i_1(t - \tau^e),$$
$$p_0'(t) = -\alpha_0 p_0(t) + \kappa(1 - \pi_0)s(t)i_0(t) - \kappa\omega_1 p_0(t)i_1(t),$$
$$p_1'(t) = -\alpha_1 p_1(t) + \kappa\omega_1(1 - \pi_1)s(t)i_1(t) - \kappa p_1(t)i_0(t),$$
$$p_{0,1}'(t) = -\alpha_{0,1}p_{0,1}(t) + \kappa\pi_0 s(t)i_0(t) + \kappa\omega_1\pi_1 s(t)i_1(t) + \kappa p_1(t)i_0(t) + \kappa\omega_1 p_0(t)i_1(t),$$

with $s(t) = 1 - p_0(t) - p_1(t) - p_{0,1}(t)$ and $s_i(t) = 1 - p_i(t) - p_{0,1}(t)$. Again, we see that the right-hand side of $i'_i(t)$ is 0 for any constant solution. Using the same computation as in (3.23), we are searching for a solution to the system

$$i_0^* = (\tau_0^e - \tau_0^s)\kappa(1 - p_0^* - p_{0,1}^*)i_0^*, \tag{3.32}$$

$$i_1^* = (\tau_1^e - \tau_1^s)\kappa\omega_1(1 - p_1^* - p_{0,1}^*)i_1^*, \tag{3.33}$$

$$0 = -\alpha_0 p_0^* + (1 - \pi_0)\kappa(1 - p_0^* - p_1^* - p_{0,1}^*)i_0^* - \kappa\omega_1 p_0^* i_1^*, \tag{3.34}$$

$$0 = -\alpha_1 p_1^* + (1 - \pi_1)\kappa\omega_1(1 - p_0^* - p_1^* - p_{0,1}^*)i_1^* - \kappa p_1^* i_0^*, \tag{3.35}$$

$$0 = -\alpha_{0,1} p_{0,1}^* + \pi_0\kappa(1 - p_0^* - p_1^* - p_{0,1}^*)i_0^* + \pi_1\kappa\omega_1(1 - p_0^* - p_1^* - p_{0,1}^*)i_1^* \tag{3.36}$$

$$+ \kappa\omega_1 p_0^* i_1^* + \kappa p_1^* i_0^*.$$

Based on Equations (3.32) and (3.33), we can distinguish four cases.

Disease-free equilibrium

One solution is given by $(i_0, i_1, p_0, p_1, p_{0,1}) = (0, 0, 0, 0, 0)$. This is the disease-free equilibrium.

Endemic equilibria

As for the one-variant model we define the basic reproduction of variant i as follows.

Definition 10. The basic reproduction number R^0 of variant i is given by

$$R_i^0 := (\tau^e - \tau^s)\kappa\omega_i.$$

As usual, we set $\omega_0 = 1$.

Case 1 ($i_0^* = 0$, $i_1^* > 0$): Another solution of (3.32) and (3.33) is given by $i_0^* = 0$, $i_1^* > 0$. Then, we must have $1 - p_1^* - p_{0,1}^* = \frac{1}{R_1^0}$. Using this, we can compute that

$$i_1^* = \left(\frac{1}{\alpha_1}(1 - \pi_{1,s})\frac{1}{\tau_1^e - \tau_1^s} + \frac{1}{\alpha_{0,1}}\pi_{1,s}\frac{1}{\tau_1^e - \tau_1^s}\right)^{-1}\left(1 - \frac{1}{R_1^0}\right),$$

$$p_1^* = \frac{1}{\alpha_1}(1 - \pi_{1,s})\frac{1}{\tau_1^e - \tau_1^s}i_1^*,$$

$$p_{0,1}^* = \frac{1}{\alpha_{0,1}}\pi_{1,s}\frac{1}{\tau_1^e - \tau_1^s}i_1^*,$$

which equals the one-variant case if $\alpha_0 = \alpha_{0,1}$ as stated in Section 3.9. As for one variant, we see that this endemic equilibrium is in the feasible region and distinct from the DFE if and only if $R_1^0 > 1$.

Case 2 ($i_0^* > 0$, $i_1^* = 0$): Because of symmetry we have the same results as for Case 1, swapping the indices 0 and 1. Especially this endemic equilibrium is in the feasible region and distinct from the DFE if and only if $R_0^0 > 1$.

Case 3 $(i_0^* > 0,\ i_1^* > 0)$**:** In this case we have

$$1 - p_0^* - p_{0,1}^* = \frac{1}{R_0^0},$$

$$1 - p_1^* - p_{0,1}^* = \frac{1}{R_1^0}.$$

We see that $R_0^0 > 1$ and $R_1^0 > 1$ are necessary for this equilibrium to be in the feasible region and distinct from the DFE. However, an algebraic expression for i_i^* and p_j^* could not be found, neither by computations by hand nor using symbolic math tools like SymPy [35]. For given parameter values, the system (3.32)-(3.36) can be solved numerically. An example is given in Section 3.8.4.

We omit a stability analysis here. However, we note that we expect the same behavior as for the one-variant model, meaning that transcritical bifurcations occur at $R_i^0 = 1$.

3.8.3 Multi-variant model

We can extend the procedure to determine the equilibria of the system to an arbitrary number of variants $n = |V|$. In this case, we must distinguish 2^n cases, because for each $i \in V$, $i_i^* = 0$ and $i_i^* > 0$ are possible solutions to the equation for i_i^* in the feasible region. Again, we find that $i_i^* > 0$ can only lead to a feasible solution distinct from other equilibria if $R_i^0 > 0$. Hence, defining $V' := \{i \in V : R_i^0 > 1\}$, we expect $2^{|V'|}$ distinct, feasible equilibria for our model.[5]

3.8.4 Numerical examples

In this section, we want to give numerical examples for the long-term behavior of the system. Therefore, we set the parameters to some values such that the value of R^0 is below or above 1. We solved the system using a Python package called *ddeint* [59] which solves delay differential equations using SciPy [55] methods. The plots show the numerical solutions and the constant solutions (i^*, p^*) of the endemic equilibria. Clearly, $\dot{n}(t)$ is also constant if $i(t)$ and $p(t)$ are constant and the constant can be computed by the differential equation for $\dot{n}(t)$, see Equation (2.24). For the obtained value $\dot{n}^*$, we also plotted the function $n^*(t) = \dot{n}^* \cdot t$ for the endemic equilibria and expect the solution for the total number of infections to converge towards a line parallel to the function n^*.
As the initial history we set a linear function for the total number of infections from 0 at $-\tau^e$ to n^0 at 0. For the protected, only the value of $p(t)$ appears in the differential equations for $p(t)$ and $n(t)$, so that only $p(0)$ of the initial history affects the solution. Hence, we just use a constant function with $p(0) = p^0$ as the initial history. For all depicted cases we set $\alpha = 0.02$, $\kappa = 0.4$, $\tau_i^s = 3$ and $p_j^0 = 0$. $n_i^0 = 0.001$ is set in all but one case.

---

[5]In special cases, like two actually identical variants as discussed in Section 3.9, this number might be smaller.

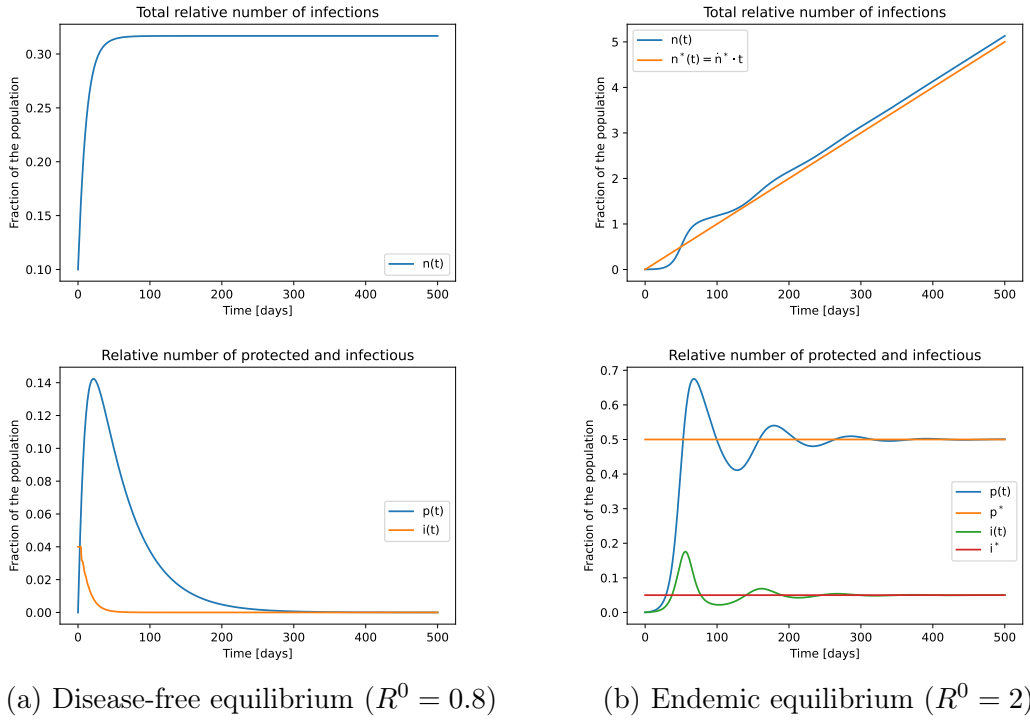(a) Disease-free equilibrium ($R^0 = 0.8$)   (b) Endemic equilibrium ($R^0 = 2$)

Figure 3.1: Numerical solutions of the one-variant model

In the one-variant model, we set $\tau^e = 5$ and $\tau^e = 8$ such that $R^0 = 0.8$ and $R^0 = 2$, respectively. We expect the solutions to converge towards the DFE and the EE in the respective cases. To see an initial outbreak of observable size, we set $n^0 = 0.1$ in case of the DFE. The numerical solutions are shown in Figure 3.1 and exhibit the expected behavior. The first plot depicts the total number of infections for both cases, while the second one displays the protected and infectious compartment converging towards the respective equilibrium point.

For the two-variant model, we set $\pi_{0,s} = \pi_{1,s} = 0.7$. The DFE is obtained with $\tau_0^e = \tau_1^e = 5$ and $\omega_1 = 1.125$ such that $R_0^0 = 0.8$, $R_1^0 = 0.9$. For the endemic equilibrium with one endemic variant, we set $\tau_1^e = 8$ and $\omega_1 = 1.5$ in contrast to the previous values, such that $R_1^0 = 3$. Setting additionally $\tau_0^e = 8$ to obtain $R_0^0 = 2$, we observe the endemic equilibrium with two endemic variants. Since an expression for $(i_0^*, i_1^*, p_0^*, p_1^*, p_{0,1}^*)$ could not be computed algebraically, we solved system (3.32)-(3.36) numerically. The results for the DFE are shown in Figure 3.2 and those for the EE in Figure 3.3. Again, the first plot depicts the total number of infections, the second one depicts only the protection compartments here, while the third one depicts the infectious compartments. All converge towards the equilibrium solutions we added to the plot.

It is interesting to see that cross-immunity leads to a slightly lower infectious equilibrium for variant 1 compared to the case with one endemic variant. We also observe an effect on the protection groups, i.e. $p_{0,1}^*$ is bigger and p_1^* smaller. This is the result of a second endemic variant whose infections cause partial immunity against
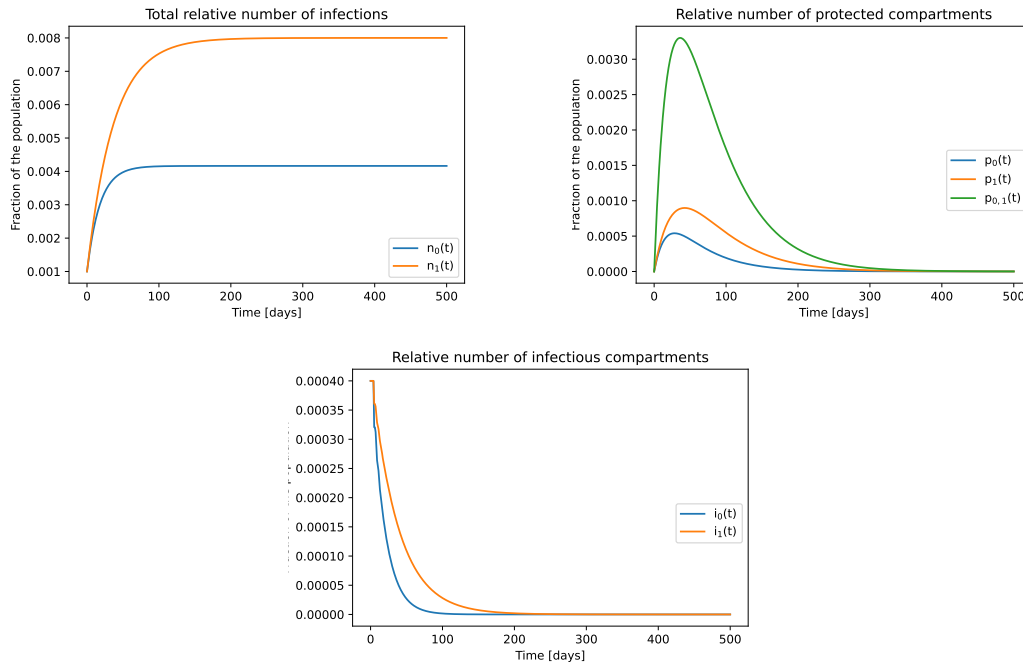
Figure 3.2: Numerical solutions of the two-variant model with DFE ($R_0^0 = 0.8$, $R_1^0 = 0.9$)

variant 1.

Another interesting area of research would be to examine the influence of the parameters on the actual solution, both algebraically and numerically. For example, it is clear that the period of the visible oscillations varies with α. As α denotes the waning rate, it determines how fast the protection groups shrink and therefore the period of the oscillations, but the exact relation and other influences on the oscillation periods are a possible subject of further investigation. The motivation of the thesis being the actual application to SARS-CoV-2 transitions, we omit this investigation here.

(a) EE (Case 1)
$(R_0^0 = 0.8, R_1^0 = 3)$

(b) EE (Case 3)
$(R_0^0 = 2, R_1^0 = 3)$
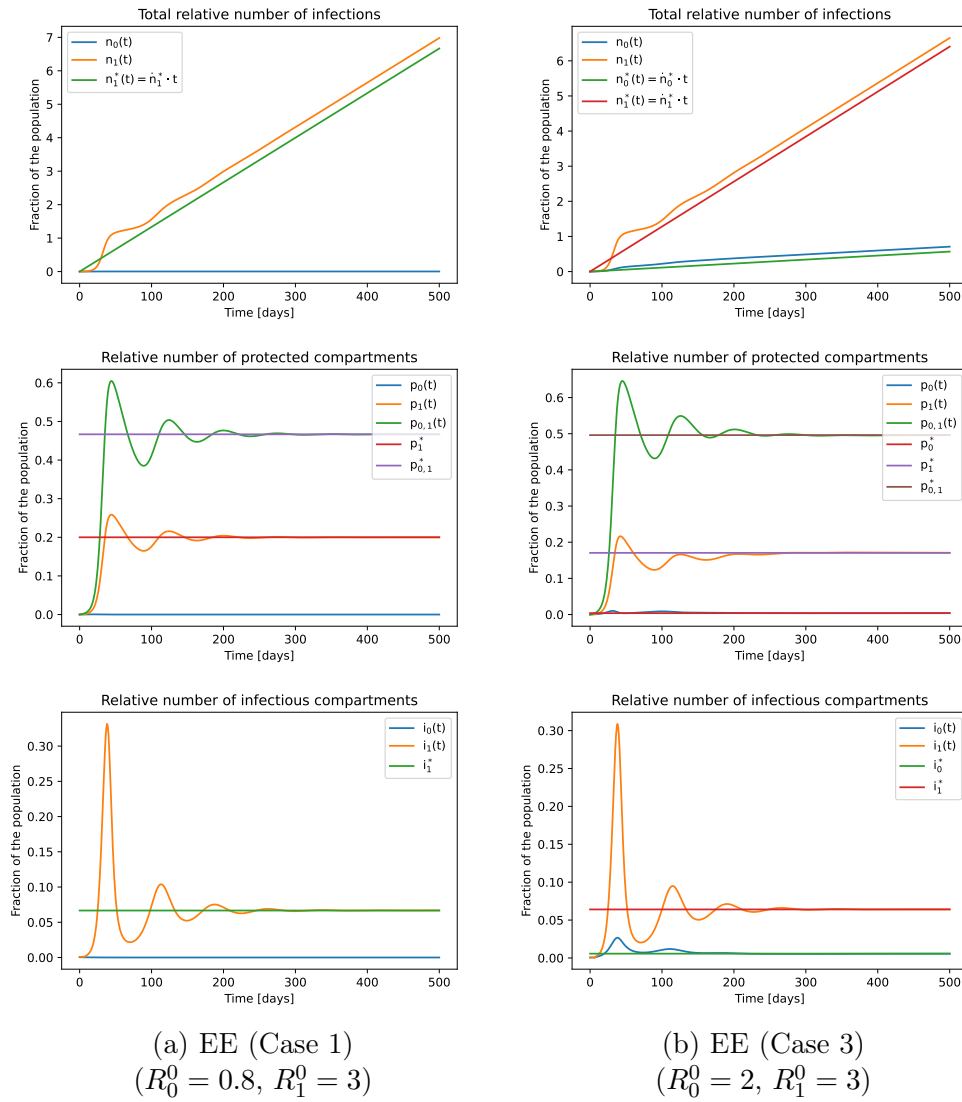
Figure 3.3: Numerical solutions of the two-variant model with endemic equilibria

3.9   Consistency with the one variant model

As the last part of the analysis, we want to show that our multi-variant model is consistent with the one-variant model in the following cases:

1. $V = \{0\}$.

2. One (of two) variants in the model has no new infections, i.e. $\dot{n}_1(t) = 0$ for all $t \geq 0$.

3. The two simulated variants in our model are actually the same, especially cross-immunity is always obtained.

We will now compute briefly that we have consistency for all three cases, focusing on the differential equations because the algebraic ones carry over naturally. Note that we required $\omega_0 = 1$ in order to avoid ambiguity of ω_0 and $\kappa(t)$.

1. If $V = \{0\}$ we have $s_0(t) = s(t)$ and hence

$$\dot{n}_0(t) = \kappa(t)s(t)i_0(t),$$
$$\dot{p}_0(t) = -\alpha_0 p_0(t) + \kappa(t)s(t)i_0(t) + \varepsilon_{s,0}s(t)\dot{v}(t - \tau^p),$$

   which equals the one-variant model with waning immunity.

2. Now let $V = \{0, 1\}$ and $i_1(t) = 0$ for all $t \geq 0$. By the consistency requirement in Equation (2.22) we have $\pi_{0,s,0} + \pi_{0,s,01} = 1$ and $\pi_{0,1,01} = 1$. Using the product ansatz in Equation (2.31) we also have $\varepsilon_{s,0} + \varepsilon_{s,01} = \varepsilon_0 = \varepsilon_{1,01}$. Hence, we obtain

$$\dot{n}_0(t) = \kappa(t)s_0(t)i_0(t),$$
$$\begin{aligned} \dot{p}_0(t) + \dot{p}_{01}(t) = & -\alpha_0 p_0(t) - \alpha_{01} p_{01}(t) \\ & + \pi_{0,s,0}\kappa(t)s(t)i_0(t) + \pi_{0,s,01}\kappa(t)s(t)i_0(t) + \pi_{0,1,01}\kappa(t)p_1(t)i_0(t) \\ & + \varepsilon_{s,0}s(t)\dot{v}(t - \tau^p) + \varepsilon_{s,01}s(t)\dot{v}(t - \tau^p) + \varepsilon_{1,01}p_1(t)\dot{v}(t - \tau^p) \\ = & -\alpha_0 p_0(t) - \alpha_{01} p_{01}(t) + \kappa(t)s_0(t)i_0(t) + \varepsilon_0 s_0(t)\dot{v}(t - \tau^p), \end{aligned}$$

   which equals the one-variant model for $n(t) := n_0(t)$ and $p(t) := p_0(t) + p_{01}(t)$ under the condition that $\alpha_0 = \alpha_{01}$.

3. Let $V = \{0, 1\}$. If the two variants are actually the same we must have $\tau_0^s = \tau_1^s$, $\tau_0^e = \tau_1^e$, $\lambda_0(t) = \lambda_1(t)$, $\omega_0 = \omega_1$, $\pi_{0,s,01} = \pi_{1,s,01} = 1$, $\varepsilon_{s,01} = \varepsilon_0 = \varepsilon_1$ [6] and $p_0(0) = p_1(0) = 0$. We can then see that $\dot{p}_0(t) = \dot{p}_1(t) = 0$ for all $t \geq 0$. Thus, $s_0(t) = s_1(t) = s(t)$ and we find that

$$\dot{n}_0(t) + \dot{n}_1(t) = \kappa(t)s(t)i_0(t) + \kappa(t)s(t)i_1(t),$$
$$\dot{p}_{01}(t) = -\alpha_{01} p_{01}(t) + \kappa(t)s(t)i_0(t) + \kappa(t)s(t)i_1(t) + \varepsilon_{s,01}s(t)\dot{v}(t - \tau^p),$$

   which equals the one-variant model for $d(t) := d_0(t) + d_1(t)$, $i(t) := i_0(t) + i_1(t)$, $n(t) := n_0(t) + n_1(t)$ and $p(t) := p_{01}(t)$.

---

[6]Note that this condition violates the product ansatz (2.31) in case $\varepsilon_0 < 1$. This is clear because the product ansatz uses the assumption that immunity against the different variants is obtained independently of each other.

Chapter 4

Numerical implementation

As mentioned in the Introduction, we want to apply our model to transitions between dominant virus variants during the COVID-19 pandemic. Therefore, we will have to solve the model numerically and estimate the parameters used in the model based on available data. In this chapter, we will describe the methods applied for solving and fitting as well as the databases used.

4.1 Numerical solution method of the DDE system

In this section, we want to describe how we solved the delay differential equation system with given parameters numerically. We actually extended the existing program, which was developed at Fraunhofer ITWM and used e.g. in [37] and for the *European Covid-19 Forecast Hub* [48], to the multi-variant case. The computations are performed in a C++ program, and the interface for loading and preparing data is written in Python. The main part of our work was the preparation of the C++ program for multiple variants and the implementation of a numerical solution method to the differential equation system for the protection groups (instead of a single equation) which we will focus on in this chapter. The following definitions are from [37] with adapted notation:

$$\Delta t > 0 \quad \text{(constant timestep)},$$
$$t_l = l\Delta t,$$
$$\sigma_i(t) = \kappa(t)\omega_i i_i(t).$$

If we assume that our time discretization is small enough, in particular we require $2\Delta t < \min_{i \in V} \tau_i^s$, we can compute the infectious compartments just by past values. This allows us to formulate the differential equation for $p = (p_j)_{j \in \mathcal{P}(V) \setminus \{\emptyset\}}$ as

$$\dot{p}(t) = A(t)p(t) + b(t)$$

with $A(t) = (a_{j,k}(t))_{j,k \in \mathcal{P}(V) \setminus \{\emptyset\}}$ and $b(t) = (b_j(t))_{j \in \mathcal{P}(V) \setminus \{\emptyset\}}$. The components are

given by

$$a_{j,j}(t) = -\alpha_j - \sum_{i\in V\backslash j} \sigma_i(t) - \sum_{\substack{k\in\mathcal{P}(V)\\ j\subset k}} \varepsilon_{j,k}\dot{v}(t-\tau^p) - \sum_{i\in j}\pi_{i,\emptyset,j}\sigma_i(t) - \varepsilon_{\emptyset,j}\dot{v}(t-\tau^p),$$

$$a_{j,k}(t) = \sum_{i\in j\backslash k}\pi_{i,k,j}\sigma_i(t) - \sum_{i\in j}\pi_{i,\emptyset,j}\sigma_i(t) + \varepsilon_{k,j}\dot{v}(t-\tau^p) - \varepsilon_{\emptyset,j}\dot{v}(t-\tau^p), \qquad k\subset j,$$

$$a_{j,k}(t) = -\sum_{i\in j}\pi_{i,\emptyset,j}\sigma_i(t) - \varepsilon_{\emptyset,j}\dot{v}(t-\tau^p), \qquad\qquad\qquad\qquad k\not\subseteq j,$$

$$b_j(t) = \sum_{i\in j}\pi_{i,\emptyset,j}\sigma_i(t) + \varepsilon_{\emptyset,j}\dot{v}(t-\tau^p).$$

As the discretization, we then use

$$\frac{p(t_{l+1}) - p(t_l)}{\Delta t} = A(t_{l+\frac{1}{2}})\frac{p(t_{l+1}) + p(t_l)}{2} + b(t_{l+\frac{1}{2}}) \tag{4.1}$$

$$\Rightarrow (I - \frac{\Delta t}{2}A(t_{l+\frac{1}{2}}))p(t_{l+1}) = (I + \frac{\Delta t}{2}A(t_{l+\frac{1}{2}}))p(t_l) + \Delta t b(t_{l+\frac{1}{2}}) \tag{4.2}$$

$$\Rightarrow \quad p(t_{l+1}) = (I - \frac{\Delta t}{2}A(t_{l+\frac{1}{2}}))^{-1}\big[(I + \frac{\Delta t}{2}A(t_{l+\frac{1}{2}}))p(t_l) + \Delta t b(t_{l+\frac{1}{2}})\big]. \tag{4.3}$$

By Neumann series [56, Satz II.1.12], we know that $I - \frac{\Delta t}{2}A(t_{l+\frac{1}{2}})$ is invertible if Δt is small enough.

For the new infections we use the discretization

$$\frac{n_i(t_{l+1}) - n_i(t_l)}{\Delta t} = \frac{s_i(t_{l+1}) + s_i(t_l)}{2}\sigma_i(t_{l+\frac{1}{2}})$$

$$\Rightarrow \quad n_i(t_{l+1}) = n_i(t_l) + \Delta t\frac{s_i(t_{l+1}) + s_i(t_l)}{2}\sigma_i(t_{l+\frac{1}{2}}).$$

$s_i(t)$ is obtained from $p(t)$ as stated in the model (2.29). Past values of $n_i(t)$ for t between the discrete timepoints t_l are obtained by quadratic interpolation.

For V we set $V = \{0, \ldots, n-1\}$ and for $\mathcal{P}(V)$ we use the canonical binary representation and the order of p is done in this way in our implementation. With this representation we can also easily check if variant i is in j or some set j is a proper subset of another set k by bitwise operations. If $\phi(j)$ is the binary representation of j interpreted as an integer and & is the bitwise AND-operator, we have

$$j\subset k \quad\Leftrightarrow\quad \big((\phi(j)\,\&\,\phi(k)) = \phi(j)\big)\wedge\big(\phi(j)\neq\phi(k)\big),$$

$$i\in j \quad\Leftrightarrow\quad \frac{\phi(j)}{2^i} = 1 \mod 2.$$

We implemented these checks, which are heavily used in the multi-variant model, in this way.

4.2   Databases and distribution of accumulated data to variants

Despite the undoubted topicality of the COVID-19 pandemic, there is another reason to use this pandemic as the real world application of our epidemiological model: Surveillance has never been so good as for this pandemic and many of the data are publicly available. In our simulations, we will focus on Rhineland-Palatinate as the state of residence of both, university and institute. The main German research institute for public health is the Robert-Koch-Institut (RKI). Most importantly for us, RKI gathers surveillance data regarding COVID-19, e.g. all positive PCR tests in Germany have to be reported to RKI via the corresponding local health departments (§ 6 and § 11 IfSG). Parts of the data are available via a RKI Github, including case [44], hospitalization [41], intensive-care units [43], death [42], vaccination [46] and sequencing data [45]. In this thesis, we focus on case and hospitalization data. The computation of hospitalized patients, which uses the infections computed by our model, is explained in Chapter 5.

For the cases we will use the data provided on the RKI Github, hospitalization data is also provided to us by the *Landesuntersuchungsamt Rheinland-Pfalz* in a more user-friendly way, hence we use this data. As these are not split by the virus variant, we have to assign the cases to the respective variants ourselves. Therefore, we use the distribution of virus variants among a representative sample of positive cases in Germany. We assume that this also represents the distribution in Rhineland-Palatinate. This data is available on the RKI web page [40], the Github only provides all individual sequencing data regardless of the cause of sequencing. Because only the weekly distribution is specified, we have to specify how to split daily data.

Therefore, we assume a logistic behavior during the transition period between two variants. If $vf_1(t)$ is the fraction of variant 1 among the cases, then the proposed formula is given by

$$vf_1(t) = \frac{1}{1 + a \exp(\lambda t)}$$

for some $a > 0$, $\lambda \in \mathbb{R}$. This was indicated by Figure 4.1 which displays the variant fractions of some variants of concern (VOC) over time in Germany. The only exception of this visual observation is the re-rise of the Omicron BA.2 variant in late 2022 due to the rise of a new sublineage of this variant. This sublineage is also a part of the recombinant XBB variant [58] whose rise occurs at a similar time. In our model, the sublineage should probably be seen as another variant than previous Omicron BA.2 sublineages, but the transitions we are actually investigating are earlier ones because of better surveillance at that time.

It has also been shown that such a logistic growth can be used to model the early growth of COVID-19 [39]. Plots of the fits for the actual transitions we are modeling can be found in Chapter 5.

If parameters used in our model are based on measured values by retrospective case-studies, these will be mentioned in Section 5 when their findings are used for our computations.
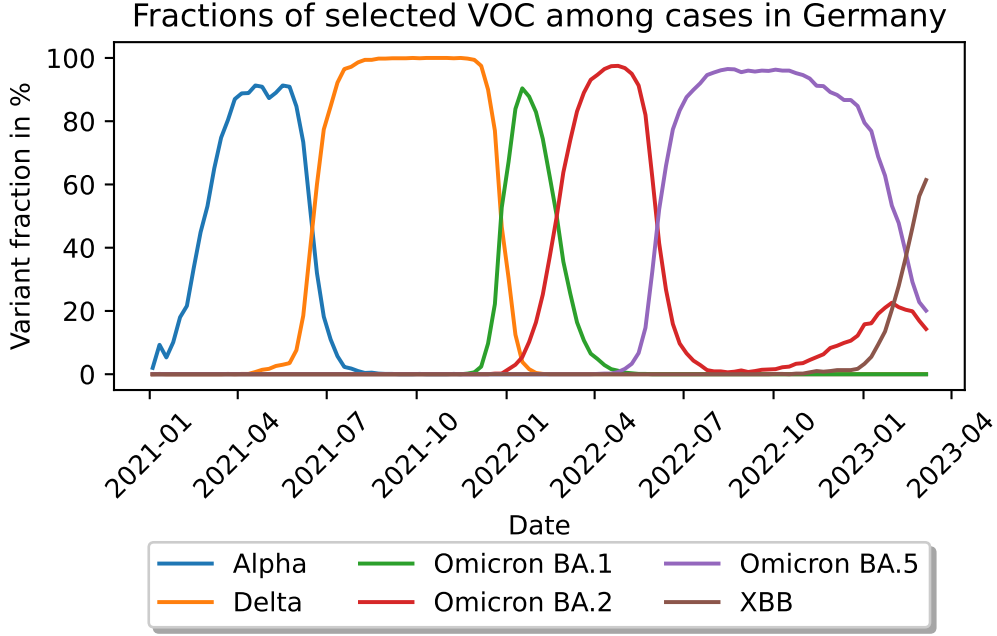
Figure 4.1: Fractions of selected VOC in a representative sample of COVID-19 cases in Germany

4.3 Parameter fitting

In order to determine parameters like the critical contact rate for a certain week, we want to fit them to measured data. Therefore, the procedure already implemented and described in [37] is used. For completeness, we will briefly sketch it here.

We are looking for a maximum-likelihood estimate for our parameters. Let $y \in \mathbb{R}^p$ be the parameter vector, $\hat{m}$ the vector of measured values for days $1, \ldots, q$ and $m(y)$ the related quantity in our model. Assuming that the measurement errors are independent and identically distributed with a normal distribution and standard deviation σ_m, the maximum-likelihood estimate is given by solving

$$\min_{y \in \mathbb{R}^p} \sum_{i=1}^{q} \left(\frac{m_i(y) - \hat{m}_i}{\sigma_m} \right)^2.$$

If additional measurements are taken into account, we add them up in the function to be minimized. We estimate the standard deviation by

$$\sigma_m = \sqrt{\frac{1}{q} \sum_{i=1}^{q} (m_i(y) - \hat{m}_i)^2}.$$

This is done in an outer loop of the parameter fitting until the value converges. To solve the least-squares problem we use a gradient-based method. Hence, we need

$D_q m$ in our computation. Therefore, automatic differentiation (AD) [20] is used. As an addition to the existing procedure, we had to implement a solver for a linear system with AD variables as such appears in the update step (4.2) of the protection groups. To describe this, let a linear system be given by

$$A(q)x = b(q) \tag{4.4}$$

with $A(q)$ invertible. By implicit function theorem [19, Kap. 8, Satz 2] we can compute

$$D_q x = -(A(q))^{-1}\big(D_q A(x) - D_q b\big) \tag{4.5}$$

for a solution to the system. As $D_q A$ and $D_q b$ are known by automatic differentiation, we can first solve the system (4.4) and with the obtained x compute (4.5). As both times the inverse of $A(q)$ appears, we can even use the same decomposition of $A(q)$ for both steps, in our implementation a LU decomposition.

As in [37], we also use automatic differentiation to get an estimate on the standard deviation of the parameters, because

$$C = \mathrm{cov}(q) = \sigma_m^2\big((D_q m)^t (D_q m)\big)^{-1}.$$

The estimates for the standard deviation allow us to give confidence intervals. These are also shown in the plots of Section 5.

Chapter 5

Application to SARS-CoV-2 variant transitions

This chapter is dedicated to present the application of our model to actual transitions between predominant SARS-CoV-2 variants. Therefore, we determined three dates at which a new variant began to spread. At these dates, we performed a simulation with the one-variant and the two-variant model. A simulation consists of fitting the parameters to previous data and a forward simulation with the obtained parameters. This is the usual procedure to compute forecasts. Our implementation fits the parameters and computes the solution automatically as briefly described in Chapter 4. To validate our model, we compare the data of our simulated forecast at the transition dates with the actual measured data afterwards.

The transitions we modeled are those between Omicron BA.2 and Omicron BA.5, Omicron BA.1 and Omicron BA.2 and Delta and Omicron (BA.1). Corresponding dates during the transition phase are May 30, 2022, February 28, 2022 and January 10, 2022.

For the simulations, we used detected cases and hospitalized patients as given data up to the simulation start date. Then, we ran the program with the one-variant model once. Afterwards, we split the input data to the variants according to our ansatz in Section 4.2 which form the input data for the two-variant model. A run of the two-variant program is done with initial values from the one-variant run.

As we were not able to fit detection rates for two variants separately, we used the detection rates from the one-variant simulation as fixed ones for both variants. The reason for this is that the detection rates can be determined because underreporting for severe outcomes like hospitalizations is negligible compared to detected cases. But for the newly emerging variant, there are barely any severe outcomes yet (for some times in the fit period even reported cases) because these numbers just start to rise at our simulation start.

Contact rates are changed weekly, while detection rates are changed twice a week, corresponding to one detection rate during weekdays and another one on the weekends. For the prediction, the last fitted values around one week before simulation start are continued to the simulation.

New hospitalizations (and other quantities not discussed here like deaths) are com-

puted from our model as a fraction, called hospitalization rate β, of new infections at an earlier time. Patients leave the hospital also after a fixed time, like the infectious compartment. These delays are fitted in the one-variant runs and assumed to be fixed for the two-variant case. The hospitalization rate will be fitted for the variants. When splitting the hospitalization data to the variants, the time delays and rates have to be taken into account.

All figures show total quantities in blue and variant-specific quantities in orange and green. Lines depict simulated values with a 99 % confidence interval around them, computed according to Section 4.3, and dots measured data. Transparent dots have not been provided to the simulation, they are depicted for comparison.

In this chapter we always assume that 0 denotes the other variants (especially the previously predominant variant) and 1 the newly emerging variant. Also, in accordance with the regular forecasts created with the one-variant model, we set $\tau_0^s = \tau_1^s = 4.67$ and $\tau_0^e = \tau_1^e = 9.67$.

5.1   Omicron BA.2/BA.5 transition

The transition from Omicron BA.2 to Omicron BA.5 as the dominant variant in Germany occurred in May/June 2022. We used May 30, 2022 as the starting date of our forecast.

5.1.1   Results with the one-variant model

Using the one-variant model, we see that we could not predict the BA.5 wave on May 30, 2022 yet. Figure 5.1 shows the forecast of the case incidence on this day. We note the severe difference between the prediction and the actual values after simulation start. For the hospitalized patients (Figure 5.2 [1]) we see the same underestimation using this model.

Looking at Figure 5.3 depicting the contact rates using the one-variant model, we also see that a strong increase of the critical contact rate is used to explain the values prior to the simulation start. While some increase can be expected by the easing of COVID restrictions at that time, such a big increase looks unreasonable. It should, however, not be overinterpreted, because the confidence interval also grows significantly, showing that the values are very uncertain.

Overall, we can say that the one-variant model does not provide satisfactory results at May 30, 2022 which would lead to wrong conclusions about the future course of the pandemic.

5.1.2   Results with the two-variant model

For the two-variant model, we split the cases according to our logistic ansatz. The results of the fit for this transition can be seen in Figure 5.4. It seems to be a

---

[1]Values of 0 mean that data has not been provided for this day and hence these values are neglected in the fit.
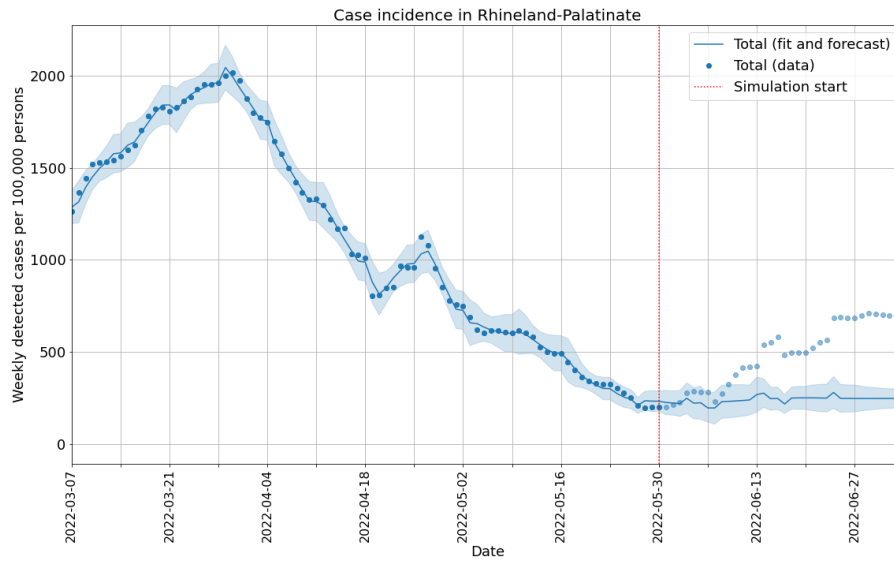
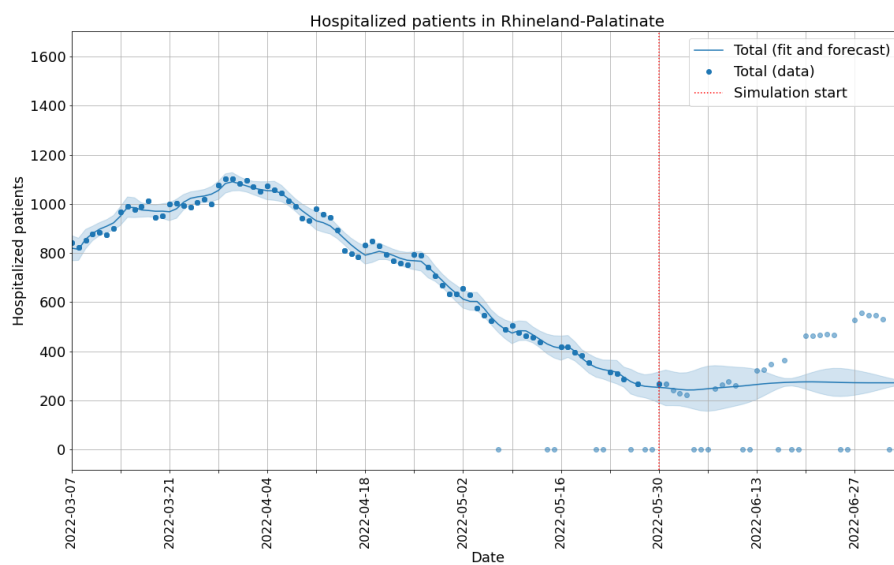Figure 5.1: Forecast of the case incidence using the one-variant model

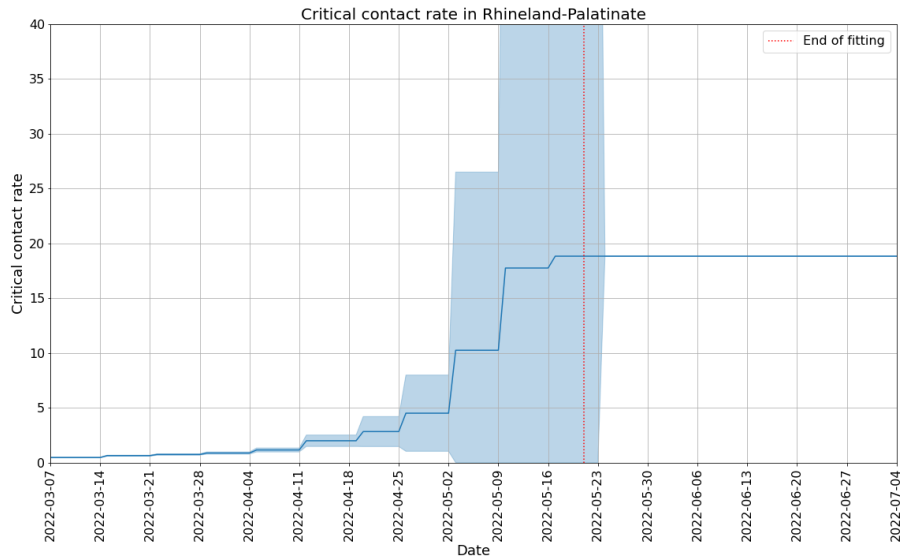Figure 5.2: Forecast of the hospitalized patients using the one-variant model

Figure 5.3: Critical contact rate using the one-variant model

Parameter	Initial value	Optimal value	standard deviation
ω_1	1	0.97	0.020
β_0	0.0023	0.0023	5.2e-06
β_1	0.0023	0.00070	0.00040
π_0	0.8 [2]	-	-
π_1	0.8	-	-
ε_0	0.7 [29]	-	-
ε_1	0.7 [30]	-	-

Table 5.1: Initial and optimal values of two-variant model parameters

reasonable ansatz to split the cases according to this function. Note that we also did not use the last datapoint before the simulation starts because the data is always published with a time delay. As an estimation, the weekly distribution has been set to the Thursday of the corresponding week.

Initial values for the parameters and the optimal ones rounded to two significant digits as well as their standard deviations are shown in Table 5.1. The protection groups are initialized in accordance with the initialization of the one-variant model. Therefore, if $p(0) = p_0$ in the one-variant case, we set $p_{0,1}(0) = 0.8 \cdot p_0$ and $p_0(0) = 0.2 \cdot p_0$ in accordance with the choice of π_0. Furthermore, we assume $p_1(0) = 0.1 \cdot p_0$. People can be in this compartment e.g. by vaccination failure against Omicron BA.2, but not BA.5. That now slightly more people are protected against at least one variant is justified by the fact that a part of them is only partially protected.

For the figures presenting the results of our simulation, special attention should be given to the blue quantities as these represent the total numbers which are actually measured. For the variant data, we have to assign them ourselves given limited information. Hence, their values are also dependent on the ansatz for distribution
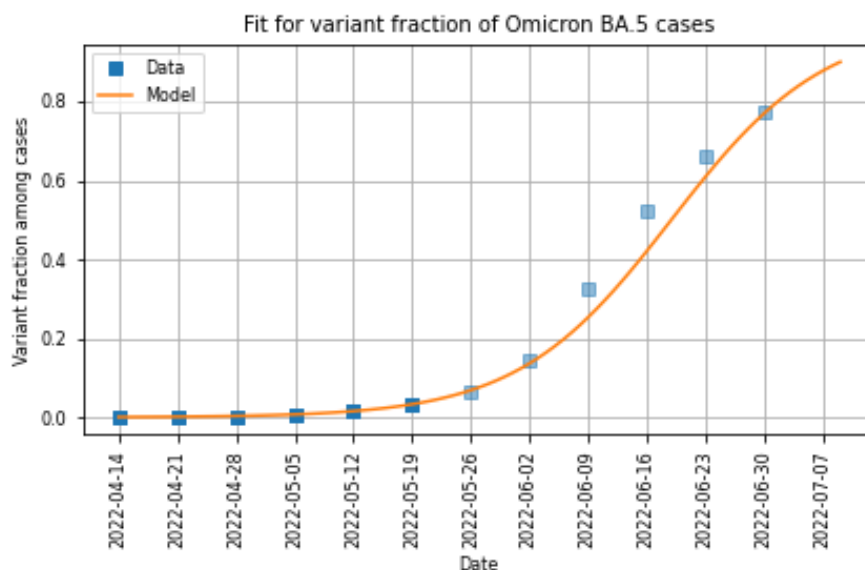
Figure 5.4: Fit of variant fraction among cases

we used. Figure 5.5 shows that we are now able to predict the peak date and height of the BA.5 wave very precisely, while providing good estimates for the total number of infections in general. This is especially remarkable because this peak occurs four weeks after the simulation starts. For many forecasts, e.g. the *European Covid-19 Forecast Hub* [48], this is the maximal forecast time. The variant incidences are, however, not well represented by the model. But, as explained, the dots do not represent real data here, the data was assigned to the variants by us. Therefore, they are also error-prone. An example that the variant data points could be slightly wrong is the re-rise of other variant cases in the second week of June which (special effects like holidays can be excluded) does not look like a natural epidemic curve.

Figure 5.6 shows the hospitalized patients in Rhineland-Palatinate. While the total values are in the range of the confidence interval, they are far off from the actual prediction and the confidence interval is quite big. This can be explained by the fact that at the start of a new variant rising, only individual, if not none, patients are hospitalized with the new variant yet. Hence, the hospitalization rate is not well known (see Table 5.1) and thus a prediction of the hospitalized patients is hardly possible at this point in time.

Looking at the critical contact rates in Figure 5.7, we also see that they are in a more reasonable range than for the one-variant model while still increasing, possibly by loosened restrictions. Examining Table 5.1, we furthermore recognize that Omicron BA.5 became the dominant variant in our model not by higher transmissibility itself, but only by immune escape. Another observation is that β_0 is close to its initial value obtained from the one-variant model because nearly all hospitalizations are still caused by other variants than BA.5.

All in all, using the two-variant model would have improved the forecast on May 30, 2022 significantly, in particular for the case incidence.
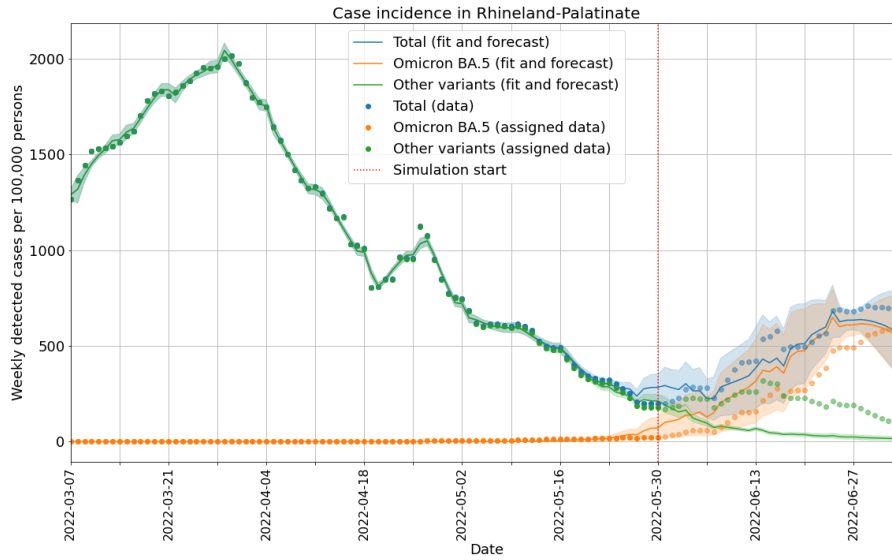
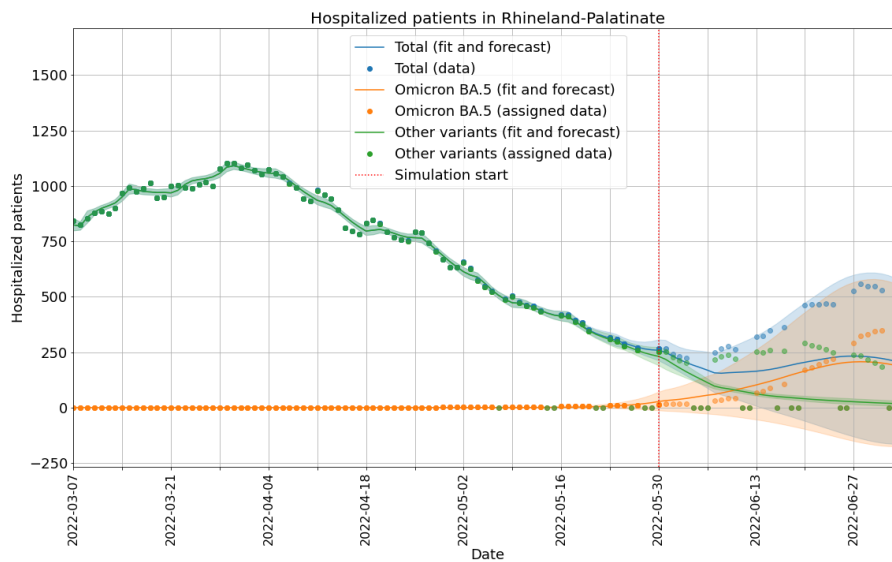Figure 5.5: Forecast of the case incidence using the two-variant model

Figure 5.6: Forecast of the hospitalized patients using the two-variant model
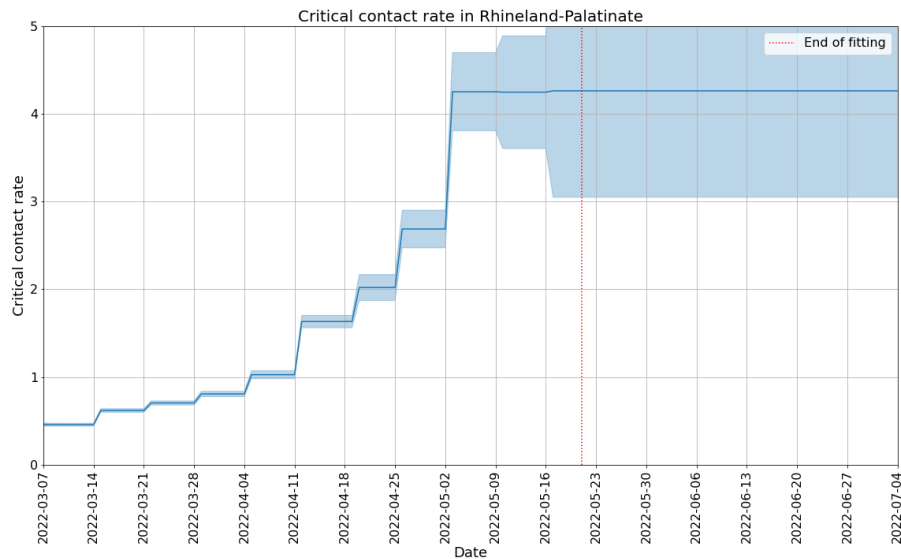
Figure 5.7: Critical contact rate using the two-variant model

5.2   Omicron BA.1/BA.2 transition

The transition from Omicron BA.1 to Omicron BA.2 occurred in February/March 2022 in Germany, just after Omicron BA.1 became the dominant variant. As the forecast start for this transition we selected February 28, 2022.

5.2.1   Results with the one-variant model

The results for this transition are similar to those found in Section 5.1.1. Figure 5.8 shows that we have an underestimation of the detected cases again, this time the difference is even higher. Contact rates (see Figure 5.9) also increase without sufficient explanation.

5.2.2   Results with the two-variant model

Using the same procedure and splitting of the initially protected, we find that the logistic approach (see Figure 5.10) delivers good results and the forecast for the case incidences (Figure 5.11) is very good for the next week. Afterwards, there is a significant difference, but the general trend is still in good accordance with the actual course of disease spread. Examining the week before the forecast starts in more detail, we observe a quite unnatural epidemic curve for the Omicron BA.2 cases. Namely, it drops notably between two growth phases, to be able to reproduce the assigned data. This is caused by a huge decline of the critical contact rate the week before. Both lack the explanation of implemented measures. Therefore, we questioned the assumption that the variant fraction of BA.2 in Germany represents the one in Rhineland-Palatinate accordingly. If BA.2 spread later in Rhineland-Palatinate than in Germany, we could shift the German data to obtain the right
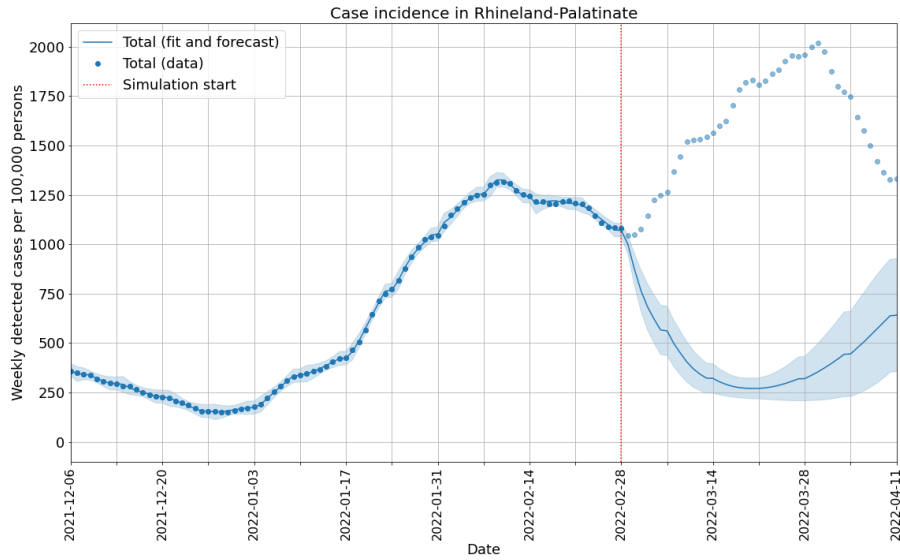
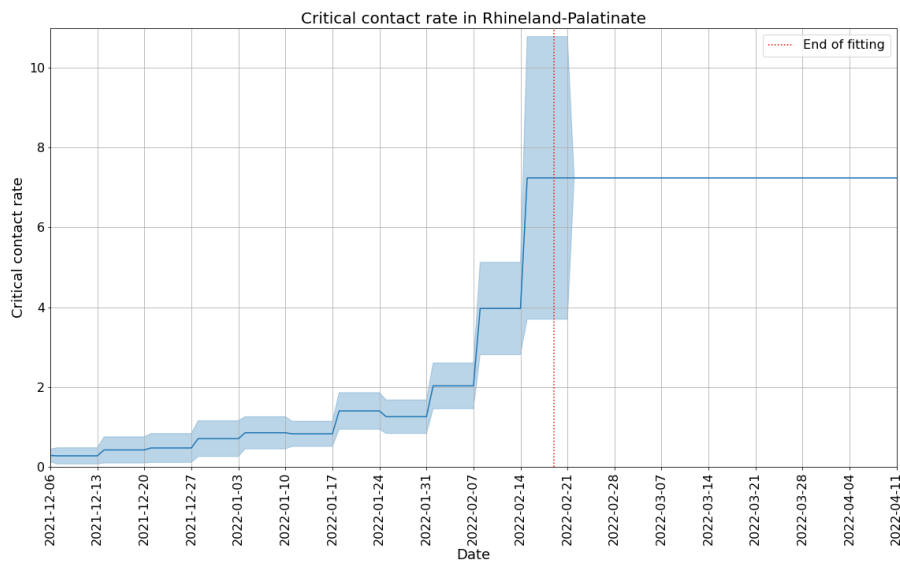Figure 5.8: Forecast of the case incidence using the one-variant model

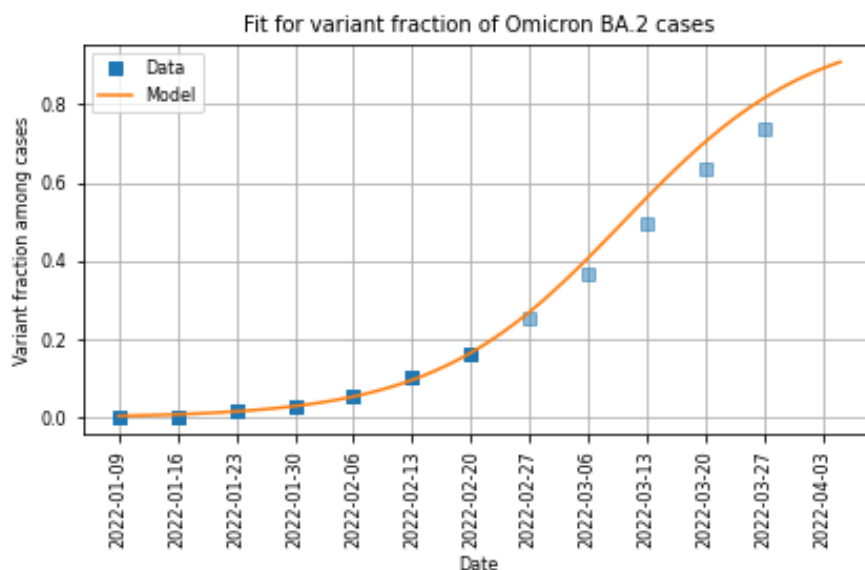Figure 5.9: Critical contact rate using the one-variant model

Figure 5.10: Fit of variant fraction among cases

data for Rhineland-Palatinate.

Using such a time shift of 10 days, we were able to eliminate the non-explicable behavior of the model. The parameter values for this case are presented in Table 5.2, while the case incidences, hospitalized patients and contact rates are portrayed in Figures 5.13, 5.14 and 5.15, respectively.

We notice that the fit and forecast of the case incidences now describe a much more natural epidemic curve for the variants and the contact rate does not have a hard decline. As in Section 5.1.2, we see that our model improves the forecast quality massively. We are able to precisely predict the peak height and up to a few days the peak date of the BA.2 wave, compared to predicting a strong decline in cases with the one-variant model. For the total number of cases as the main focus (see the discussion in Section 5.1.2), we even see very good accordance with the actual data for all six forecast weeks. Hospitalized patients are, however, still hard to predict because of the reasons discussed in the same section.

The optimal values show that BA.2 did not only become the predominant SARS-CoV-2 variant because of immune escape, but also because of a inherent higher transmissibility. This finding is even quantitatively in accordance with a case study in Denmark [34] for unvaccinated household contacts.

---

[2]The difference to the model parameter in case of BA.2/BA.5 transition can be explained by a much longer hospital period (fitted in the one-variant model) here.
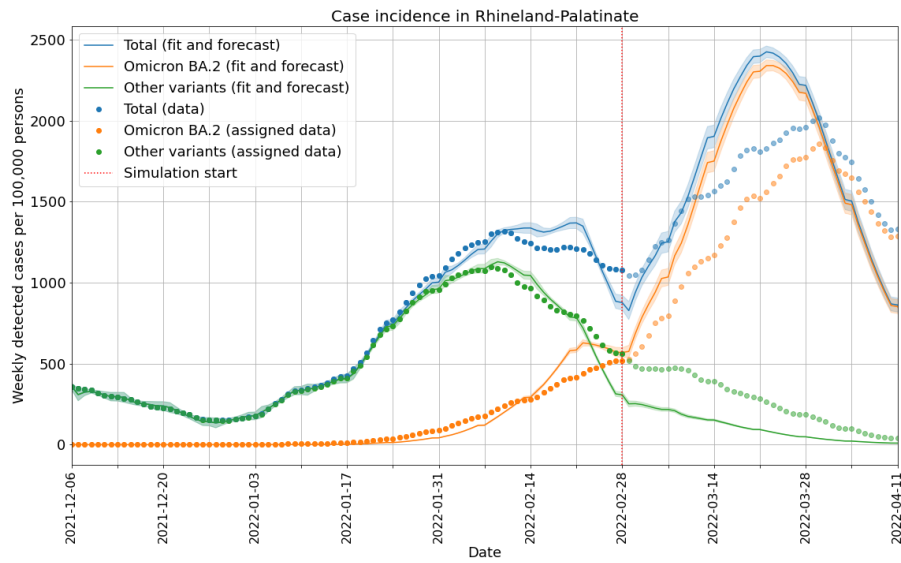
Figure 5.11: Forecast of the case incidence using the two-variant model without time shift
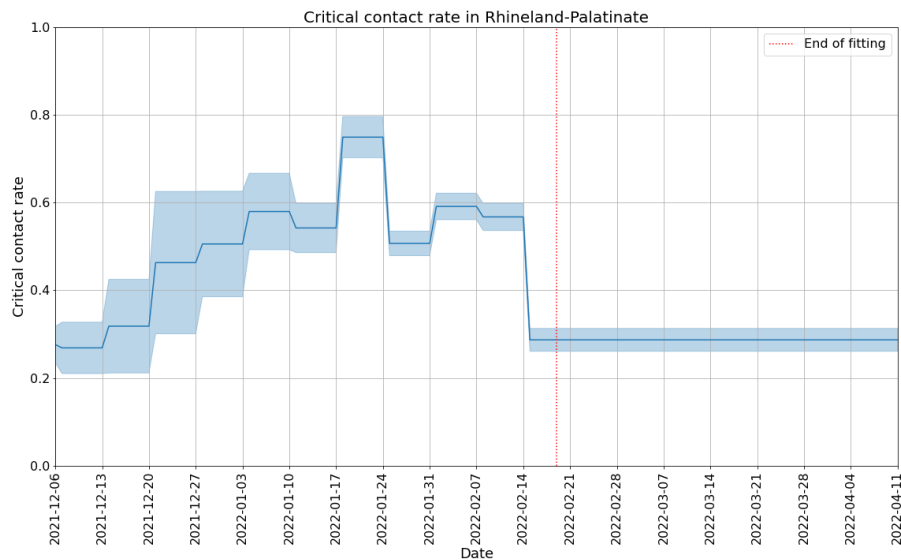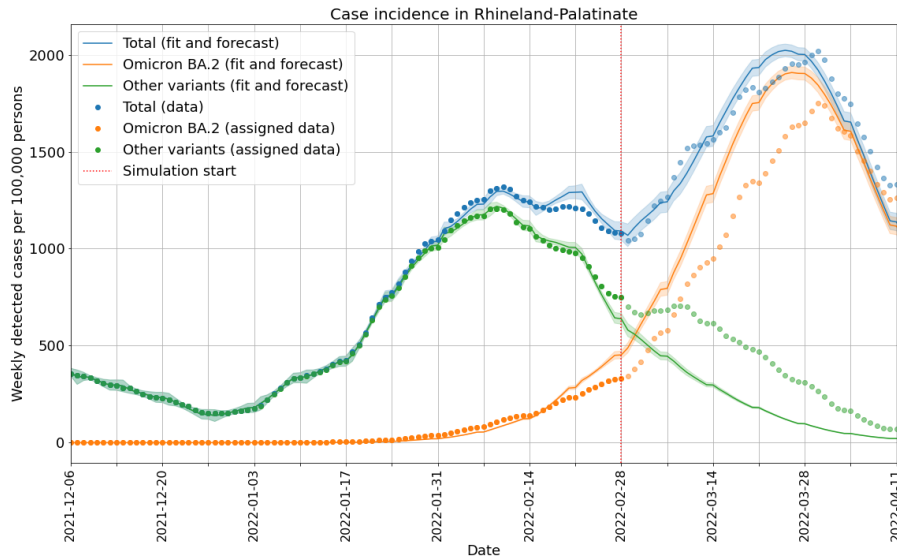

Figure 5.12: Critical contact rate using the two-variant model without time shift

Parameter	Initial value	Optimal value	standard deviation
ω_1	1	1.92	0.0030
β_0	0.00072^2	0.00073	4.4e-06
β_1	0.00072	0.00032	8.6e-05
π_0	0.8 [13]	-	-
π_1	0.94 [13]	-	-
ε_0	0.7 [4]	-	-
ε_1	0.7 [29]	-	-

Table 5.2: Initial and optimal values of two-variant model parameters

Figure 5.13: Forecast of the case incidence using the two-variant model with time shift
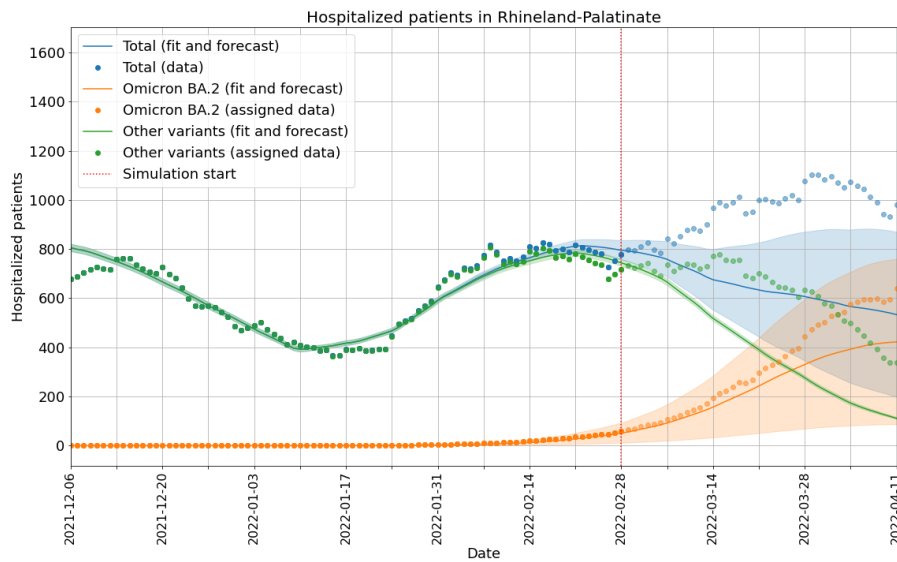

Figure 5.14: Forecast of the hospitalized patients using the two-variant model with time shift
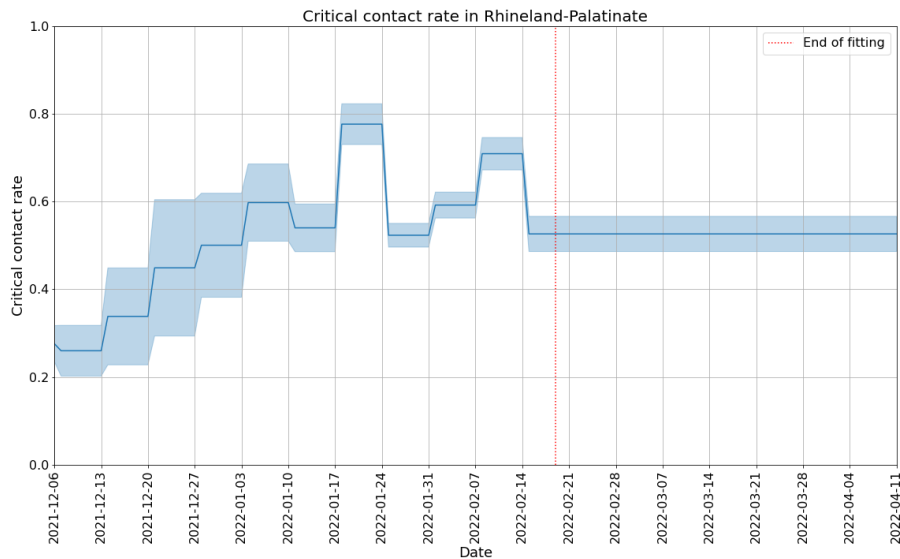
Figure 5.15: Critical contact rate using the two-variant model with time shift

5.3   Delta/Omicron BA.1 transition

The transition between Delta and Omicron (BA.1) occurred in December 2021/January 2022 in Germany. It was maybe the most serious transition because virus characteristics changed massively [49]. We used January 10, 2022 as the starting point for our forecasts. This section will also show some aspects which have to be handled with caution when computing forecasts with the two-variant model.

5.3.1   Results with the one-variant model

In this case, the one-variant model gives reasonable predictions for the case incidences, seen in Figure 5.16. This is because we chose a date for the forecast, where we already see the total number of cases rising. It leads to a jump in the critical contact rate, illustrated in Figure 5.18, caused by the higher transmissibility of the Omicron variant compared to the Delta variant. However, as just one hospitalization rate is used and is fitted to data of the Delta wave, we see a severe overestimation of the hospitalized patients in Figure 5.17.

5.3.2   Results with the two-variant model

We use the usual procedure with the values of the one-variant model as initial values for the two-variant model, but splitting the initially protected more evenly across $p_{0,1}(0)$ and $p_0(0)$ because of lower protection and faster waning immunity from previous infections against Omicron [3]. Keep in mind that we used the detection rates of the one-variant model as fixed detection rates for both variants in this procedure. In contrast to our previous results, we would have been able to locate the peak of the case incidence four weeks in advance, but we would have completely
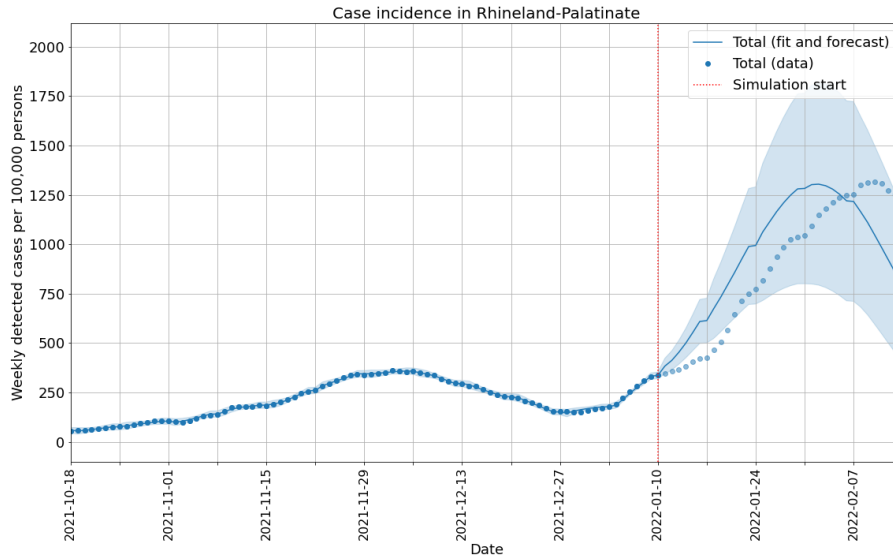
Figure 5.16: Forecast of the case incidence using the one-variant model
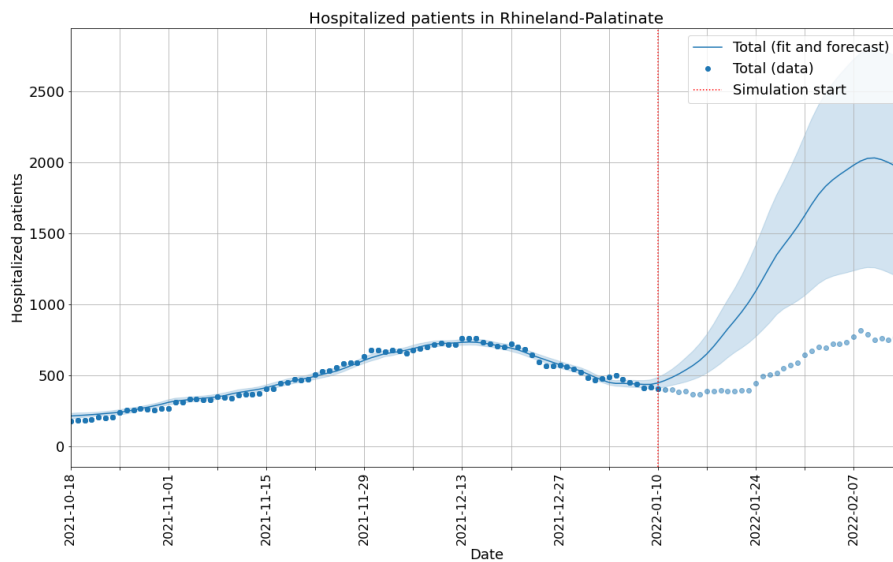

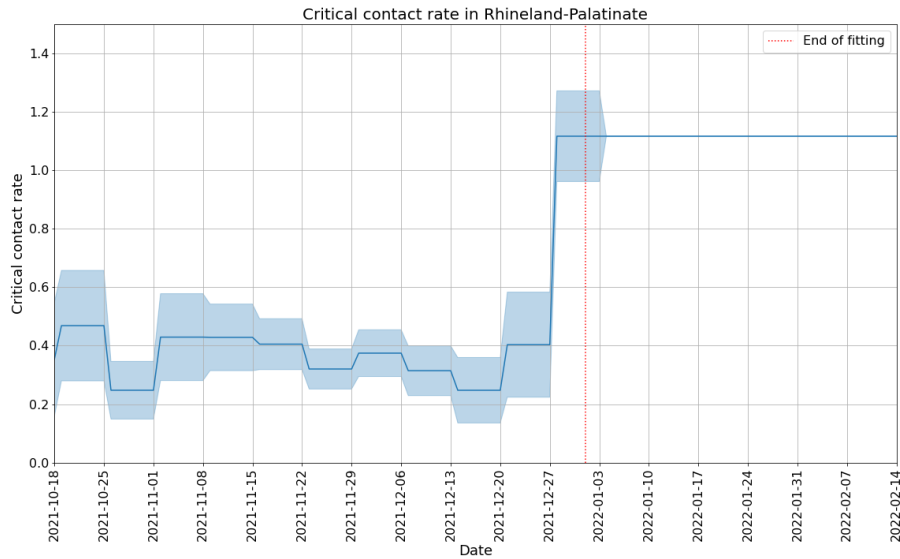Figure 5.17: Forecast of the hospitalized patients using the one-variant model

Figure 5.18: Critical contact rate using the one-variant model

overestimated both case incidences (Figure 5.20) and hospitalizations (Figure 5.21). Figure 5.19 shows that this is not the result of a wrong model to split the data. Soon, it became clear that the Omicron variant causes less severe infections than the Delta variant [49]. In particular, it is shown there that less severe infections cause a higher underreporting for the Omicron variant, i.e. the detection rates of the Omicron variant are lower than we assume because we fitted the detection rates to the Delta wave.

5.3.3 Results with the two-variant model with adapted parameters

If we would have known that Omicron causes less severe infections, we could have adapted the assumption that the detection rates of the one-variant model (displayed in Figure 5.22) can be set for both variants. As these are mainly fitted to cases caused by Delta, we will now set the detection rate for the Omicron variant to half the detection rate of the Delta variant, in the range of the findings in [49]. We also set the hospitalization rate of Omicron to one fifth of the Delta hospitalization rate as the initial value in our optimization, see Table 5.3.

Using this additional information, we are able to give a much better estimate for the case incidences, displayed in Figure 5.23. Still, predictions for the hospitalized (Figure 5.24) are very unsecure and significantly too high. The reasons for this have been discussed in Section 5.1.2. We also see in Figure 5.25 that in contrast to the one-variant case (Figure 5.18) there is not a huge jump in the critical contact rate at the end of the fit. Instead, the rise of cases at the end of the fit is now explained by the new Omicron variant with inherent higher transmissibility (see Table 5.3) and only a slight change in the contact behavior. The optimal value of the increased transmissibility is very close to the value 2.14 for non-household transmission found
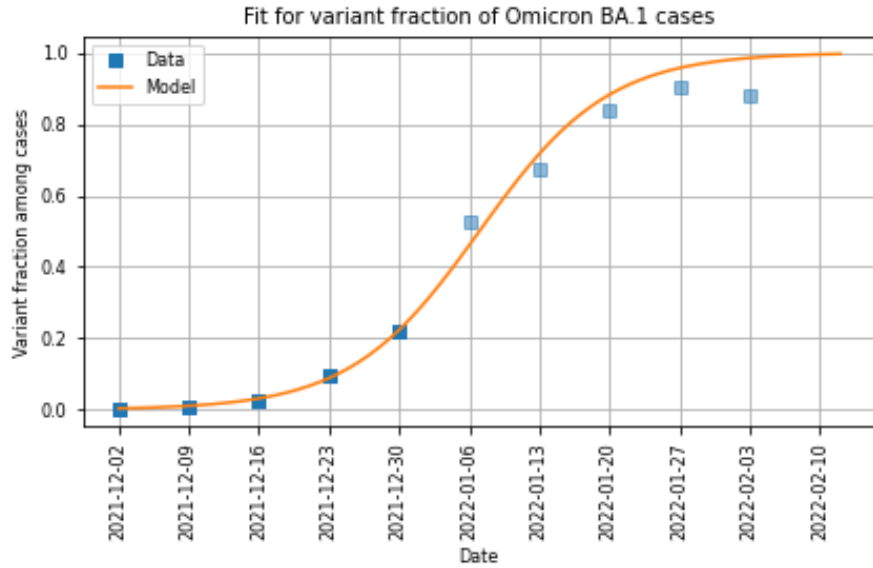
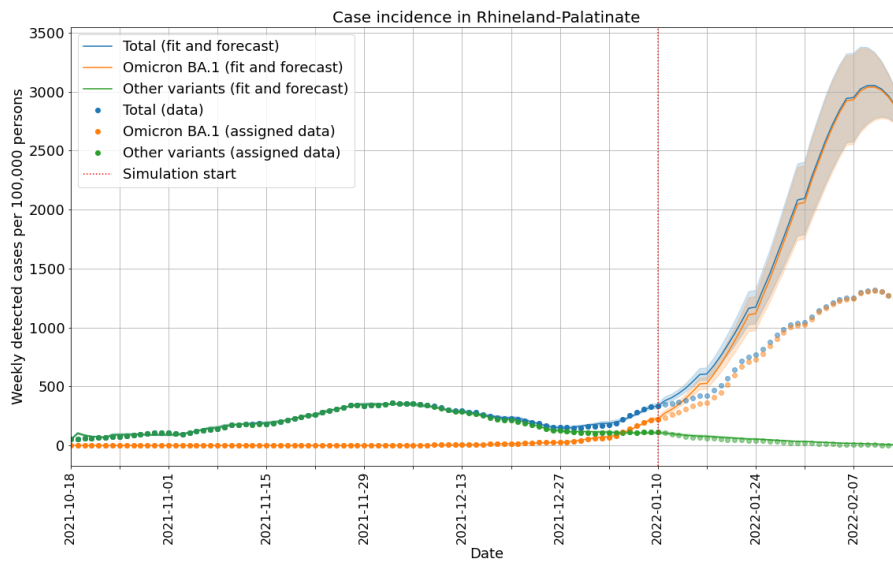Figure 5.19: Fit of variant fraction among cases

Figure 5.20: Forecast of the case incidence using the unadapted two-variant model
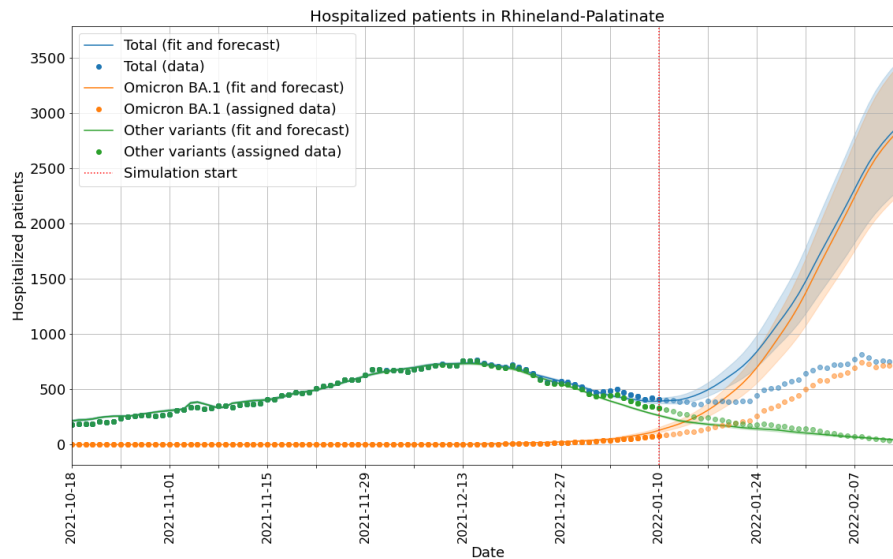
Figure 5.21: Forecast of the hospitalized patients using the unadapted two-variant model

in a case-study in England [1].

In comparison to the two previously discussed transitions, our forecast of the case incidence is still worse. Apart from the transition itself, it should be noted that it happened during a holiday period, which always makes predictions harder because of special effects, like increased travel or different testing [37] during this period.

For the forecasts, one has to note that if severity and/or detectability are very different for the new variant compared to the old one, care has to be taken about the assumption that the same detection rate can be set for both variants. We got much better results when taking this into account. However, it was not possible to detect this by unnatural behavior of the epidemic curves in the forecast. This strengthens the need of some early estimates on possible changes in underreporting, e.g. by experiences in other countries with an earlier transition to the new variant. For the model itself, one could question the assumption that immunity against both variants is lost at the same time, i.e. that the waning immunity transition is from $p_{0,1}(t)$ to $s(t)$. Data shows that immunity against Omicron wanes much faster than against Delta [4] [14]. In our forecast and the assigned data, we can, however, see that Omicron cases supersede Delta cases in a few weeks. Immunity even against Omicron typically lasts significantly longer than this transition period, i.e. the assumption can be justified in our experiment.
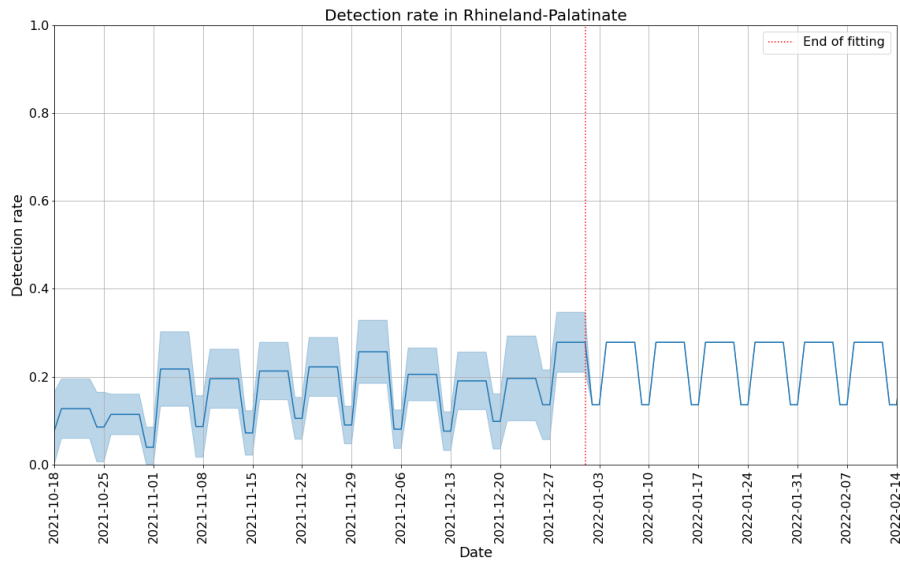
Figure 5.22: Detection rate using the one-variant model

Parameter	Initial value	Optimal value	standard deviation
ω_1	1	2.11	0.046
β_0	0.0030	0.0031	1.1e-05
β_1	0.00061	0.00099	6.0e-05
π_0	0.65 [14]	-	-
π_1	0.9 [14]	-	-
ε_0	0.7 [4]	-	-
ε_1	0.9 [4]	-	-

Table 5.3: Adapted initial and optimal values of two-variant model parameters
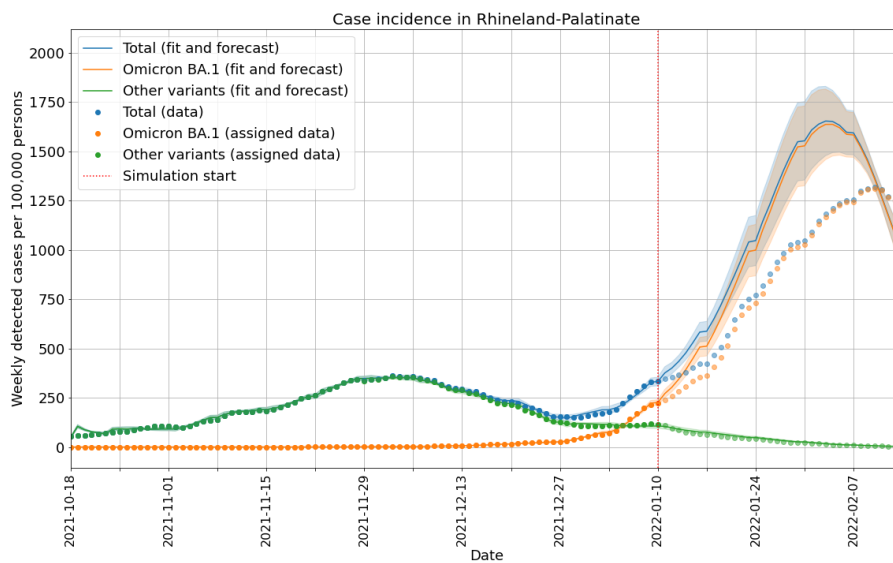

Figure 5.23: Forecast of the case incidence using the adapted two-variant model
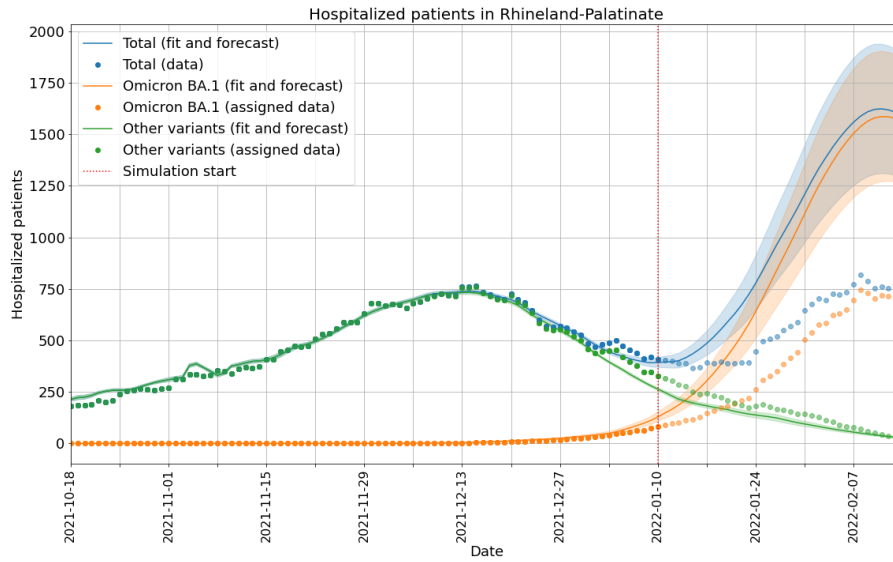
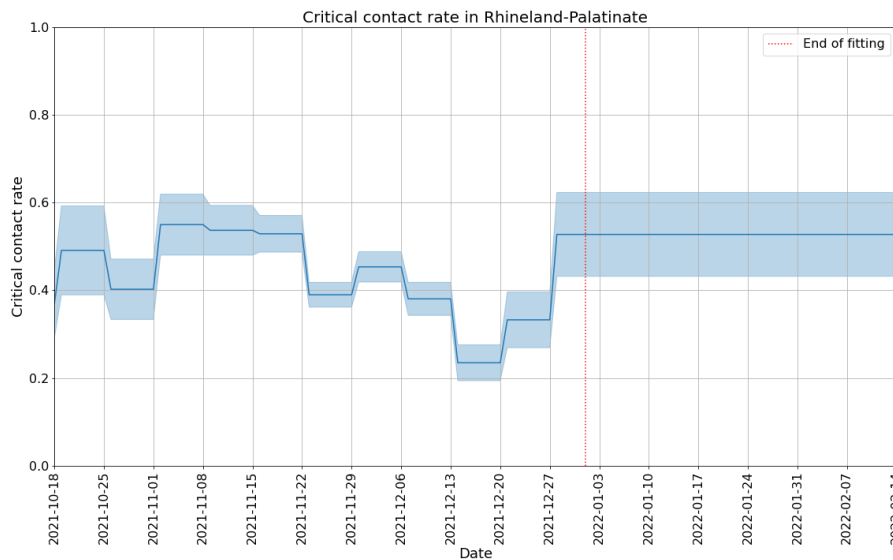Figure 5.24: Forecast of the hospitalized patients using the adapted two-variant model

Figure 5.25: Critical contact rate using the adapted two-variant model

Chapter 6

Outlook

In this chapter, we want to discuss further work that could be done subsequent to this thesis.

Chapter 2 dealt with the modeling itself. While the model seems complete with respect to modeling multiple virus variants, there are some further aspects which might be considered. First, the partial loss of immunity, i.e. only against some of the variants one is protected against, might be considered. For typical forecasts simulating a few weeks forward in time and transitions from one dominant variant to another, this effect can be neglected. If one wants to consider long-term scenarios with multiple endemic variants, however, this effect could play a crucial role if waning immunity against different variants occurs on different timescales. A more sophisticated model could also be developed regarding vaccination and its influence on the infection-related quantities like deaths and hospitalized patients. It is e.g. known that vaccinations have higher effectiveness averting severe cases than averting infection. This is only implicitly reflected in our model by adapting the respective hospitalization and dying rates. The necessity is again mostly given for long-term scenarios.

Other interesting adaptions of the model could be if the disease spread is not well described by deterministic approaches because of low incidences. Then, stochastic effects should be taken into account, possibly leading to stochastic delay differential equations. If the spatial spread of the disease should be modeled, a system of delay partial differential equations can be developed. The model can also be applied to an agent-based model. Each agent could be in a protection state equivalent to the groups of our model and changes occur according to the transition rates. This would be another way of dealing with stochasticity in case of low incidences. One should note that increasing model complexity and hence the number of paramters while not increasing data sources will make it harder or even impossible to fit model parameters.

In Chapter 3, we analyzed the model theoretically. An open question is to characterize the stability of the equilibrium points of the multi-variant model. It furthermore remains open if one can find algebraic expressions for all equilibria of the multi-variant model. Another interesting area of reasearch would be to quantify the effects of the parameters on the solution, e.g. by a sensitivity and uncertainty

analysis.

The results of the application of our model to real data were shown in Chapter 5. We mentioned that the contact rate is not adapted in the forward simulation. Behavioral changes, either mandatory by NPIs or voluntary, are hence not reflected in the prediction. To quantify these behavioral changes, especially voluntary ones, and use them in epidemiological models will be the main focus of BMBF-funded project *SEMSAI* [15], in which this model will be used. Another important topic is the handling of limited surveillance data. The model will then rely on coarser data like wastewater samples [24] where additional effects have to be taken into account. A first model using wastewater samples in Rhineland-Palatinate as a data source has already been coupled with our model in ongoing work. Handling of limited surveillance will also be crucial for the interesting aspect of applying the model to other infectious diseases, e.g. different virus strains of influenza, with much less surveillance data available than for COVID-19.

Overall, we can say that there are many open research and modeling questions regarding epidemiology and we hope that also in non-pandemic times reasonable attention will be given to this topic.

Chapter 7

Conclusion

In this thesis, we have developed an epidemiological model that covers the effects of multiple virus variants causing partial immunity against each other. The application of this model to SARS-CoV-2 transitions in Chapter 5 showed that we could improve the existing model significantly. It was shown that case incidences can be predicted with good accuracy during early transition phases. Having good data splitting detected cases and other measured quantities to the respective variants as well as some early estimates on model parameters, is essential for a good prediction. Related quantities that occur later in the course of infection, in this thesis we focused on hospitalizations, are harder to predict at early stages because of the additional delay in the quantities.

From a mathematical perspective, it was shown in Chapter 3 that the model possesses a solution for all future times if the initial history is feasible. This solution also stays feasible, i.e. the variables can be interpreted in a meaningful way, for all times. The equilibria of the system have in general been determined, together with a condition for being in the feasible region. An algebraic expression for all of them and a theoretical result on their stability remain open questions for the multi-variant model. It was shown for the one-variant model that a bifurcation occurs if the basic reproduction number $R^0 = 1$, which is the expected behavior for epidemiological models.

The development of the model and its implementation into ongoing simulations allow us to improve the predictions of future variant transitions, provided proper surveillance is maintained. Furthermore, it can be used for retrospective modeling studies, e.g. to examine the effects of non-pharmaceutical interventions and voluntary contact reductions. The model is valuable for this because it disentangles the effects of multiple variants from the specific effects to be analyzed. It can also be applied to future (local or global) pandemics and epidemics, possibly caused by other pathogens, as well as modeling endemic diseases.

In conclusion, this thesis has successfully achieved the goal of developing a model that improves the accuracy of forecasts during early transition periods between predominant virus variants.

Bibliography

[1] ALLEN, H., TESSIER, E., TURNER, C., ANDERSON, C., BLOMQUIST, P., SIMONS, D., LØCHEN, A., JARVIS, C. I., GROVES, N., CAPELASTEGUI, F., ET AL. Comparative transmission of sars-cov-2 omicron (b. 1.1. 529) and delta (b. 1.617. 2) variants and the impact of vaccination: national cohort study, england. *Epidemiology & Infection* (2022), 1–20.

[2] ALTARAWNEH, H. N., CHEMAITELLY, H., AYOUB, H., HASAN, M. R., COYLE, P., YASSINE, H. M., AL KHATIB, H. A., BENSLIMANE, F., AL-KANAANI, Z., AL KUWARI, E., ET AL. Protection of sars-cov-2 natural infection against reinfection with the ba. 4 or ba. 5 omicron subvariants. *MedRxiv* (2022), 2022–07.

[3] ALTARAWNEH, H. N., CHEMAITELLY, H., HASAN, M. R., AYOUB, H. H., QASSIM, S., ALMUKDAD, S., COYLE, P., YASSINE, H. M., AL-KHATIB, H. A., BENSLIMANE, F. M., ET AL. Protection against the omicron variant from previous sars-cov-2 infection. *New England Journal of Medicine 386*, 13 (2022), 1288–1290.

[4] ANDREWS, N., STOWE, J., KIRSEBOM, F., TOFFA, S., RICKEARD, T., GALLAGHER, E., GOWER, C., KALL, M., GROVES, N., O'CONNELL, A.-M., SIMONS, D., BLOMQUIST, P. B., ZAIDI, A., NASH, S., IWANI BINTI ABDUL AZIZ, N., THELWALL, S., DABRERA, G., MYERS, R., AMIRTHALINGAM, G., GHARBIA, S., BARRETT, J. C., ELSON, R., LADHANI, S. N., FERGUSON, N., ZAMBON, M., CAMPBELL, C. N., BROWN, K., HOPKINS, S., CHAND, M., RAMSAY, M., AND LOPEZ BERNAL, J. Covid-19 vaccine effectiveness against the omicron (b.1.1.529) variant. *New England Journal of Medicine 386*, 16 (2022), 1532–1546. PMID: 35249272.

[5] ANDREWS, N., TESSIER, E., STOWE, J., GOWER, C., KIRSEBOM, F., SIMMONS, R., GALLAGHER, E., THELWALL, S., GROVES, N., DABRERA, G., MYERS, R., CAMPBELL, C. N., AMIRTHALINGAM, G., EDMUNDS, M., ZAMBON, M., BROWN, K., HOPKINS, S., CHAND, M., LADHANI, S. N., RAMSAY, M., AND LOPEZ BERNAL, J. Duration of protection against mild and severe disease by covid-19 vaccines. *New England Journal of Medicine 386*, 4 (2022), 340–350. PMID: 35021002.

[6] AURANEN, K., SHUBIN, M., ERRA, E., ISOSOMPPI, S., KONTTO, J., LEINO, T., AND LUKKARINEN, T. Efficacy and effectiveness of case isolation and

quarantine during a growing phase of the covid-19 epidemic in finland. *Scientific Reports 13*, 1 (2023), 298.

[7] BAGHERI, G., THIEDE, B., HEJAZI, B., SCHLENCZEK, O., AND BODEN-SCHATZ, E. An upper bound on one-to-one exposure to infectious human respiratory particles. *Proceedings of the National Academy of Sciences 118*, 49 (2021), e2110117118.

[8] BELLMAN, R. E., AND COOKE, K. L. *Differential-Difference Equations*. RAND Corporation, Santa Monica, CA, 1963.

[9] BRAUER, F. The kermack–mckendrick epidemic model revisited. *Mathematical Biosciences 198*, 2 (2005), 119–131.

[10] BRAUER, F., CASTILLO-CHAVEZ, C., AND FENG, Z. *Mathematical Models in Epidemiology*. Texts in Applied Mathematics. Springer New York, 2019.

[11] BRAUER, F., VAN DEN DRIESSCHE, P., WU, J., AND ALLEN, L. J. *Mathematical epidemiology*, vol. 1945. Springer, 2008.

[12] CAMPBELL, S. A. Calculating centre manifolds for delay differential equations using maple™. *Delay Differential Equations: Recent Advances and New Directions* (2009), 1–24.

[13] CHEMAITELLY, H., AYOUB, H. H., COYLE, P., TANG, P., YASSINE, H. M., AL-KHATIB, H. A., SMATTI, M. K., HASAN, M. R., AL-KANAANI, Z., AL-KUWARI, E., ET AL. Protection of omicron sub-lineage infection against reinfection with another omicron sub-lineage. *Nature Communications 13*, 1 (2022), 4675.

[14] CHEMAITELLY, H., NAGELKERKE, N., AYOUB, H. H., COYLE, P., TANG, P., YASSINE, H. M., AL-KHATIB, H. A., SMATTI, M. K., HASAN, M. R., AL-KANAANI, Z., AL-KUWARI, E., JEREMIJENKO, A., KALEECKAL, A. H., LATIF, A. N., SHAIK, R. M., ABDUL-RAHIM, H. F., NASRALLAH, G. K., AL-KUWARI, M. G., BUTT, A. A., AL-ROMAIHI, H. E., AL-THANI, M. H., AL-KHAL, A., BERTOLLINI, R., AND ABU-RADDAD, L. J. Duration of immune protection of SARS-CoV-2 natural infection against reinfection. *Journal of Travel Medicine 29*, 8 (09 2022). taac109.

[15] DEUTSCHES FORSCHUNGSZENTRUM FÜR KÜNSTLICHE INTELLIGENZ GMBH. Semsai website. `https://semsai.dfki.de/`. Accessed: 2022-03-29.

[16] DRIVER, R. *Ordinary and Delay Differential Equations*. Applied Mathematical Sciences. Springer New York, 2012.

[17] EUROPEAN MEDICINES AGENCY. EMA recommends first COVID-19 vaccine for authorisation in the EU, Dec 2020.

[18] FORSTER, O. *Analysis 1: Differential-und Integralrechnung einer Veränderlichen.* Springer-Verlag, 2016.

[19] FORSTER, O. *Analysis 2: Differentialrechnung im IRn, gewöhnliche Differentialgleichungen.* Springer-Verlag, 2017.

[20] GRIEWANK, A. On automatic differentiation. *Mathematical Programming: recent developments and applications 6*, 6 (1989), 83–107.

[21] HAAS, E. J., MCLAUGHLIN, J. M., KHAN, F., ANGULO, F. J., ANIS, E., LIPSITCH, M., SINGER, S. R., MIRCUS, G., BROOKS, N., SMAJA, M., PAN, K., SOUTHERN, J., SWERDLOW, D. L., JODAR, L., LEVY, Y., AND ALROY-PREIS, S. Infections, hospitalisations, and deaths averted via a nationwide vaccination campaign using the pfizer–biontech bnt162b2 mrna covid-19 vaccine in israel: a retrospective surveillance study. *The Lancet Infectious Diseases 22*, 3 (2022), 357–366.

[22] HAKKI, S., ZHOU, J., JONNERBY, J., SINGANAYAGAM, A., BARNETT, J. L., MADON, K. J., KOYCHEVA, A., KELLY, C., HOUSTON, H., NEVIN, S., FENN, J., KUNDU, R., CRONE, M. A., PILLAY, T. D., AHMAD, S., DERQUI-FERNANDEZ, N., CONIBEAR, E., FREEMONT, P. S., TAYLOR, G. P., FERGUSON, N., ZAMBON, M., BARCLAY, W. S., DUNNING, J., LALVANI, A., BADHAN, A., VARRO, R., LUCA, C., QUINN, V., CUTAJAR, J., NICHOLS, N., RUSSELL, J., GREY, H., KETKAR, A., MISEROCCHI, G., TEJPAL, C., CATCHPOLE, H., NIXON, K., DI BIASE, B., HOPEWELL, T., NAREAN, J. S., SAMUEL, J., TIMCANG, K., MCDERMOTT, E., BREMANG, S., HAMMETT, S., EVETTS, S., AND KONDRATIUK, A. Onset and window of sars-cov-2 infectiousness and temporal correlation with symptom onset: a prospective, longitudinal, community cohort study. *The Lancet Respiratory Medicine 10*, 11 (2022), 1061–1073.

[23] HELLEWELL, J., ABBOTT, S., GIMMA, A., BOSSE, N. I., JARVIS, C. I., RUSSELL, T. W., MUNDAY, J. D., KUCHARSKI, A. J., EDMUNDS, W. J., SUN, F., FLASCHE, S., QUILTY, B. J., DAVIES, N., LIU, Y., CLIFFORD, S., KLEPAC, P., JIT, M., DIAMOND, C., GIBBS, H., VAN ZANDVOORT, K., FUNK, S., AND EGGO, R. M. Feasibility of controlling covid-19 outbreaks by isolation of cases and contacts. *The Lancet Global Health 8*, 4 (2020), e488–e496.

[24] HILLARY, L. S., MALHAM, S. K., MCDONALD, J. E., AND JONES, D. L. Wastewater and public health: the potential of wastewater surveillance for monitoring covid-19. *Current Opinion in Environmental Science & Health 17* (2020), 14–20.

[25] HUNTER, E., MAC NAMEE, B., AND KELLEHER, J. D. A comparison of agent-based models and equation based models for infectious disease epidemiology. In *AICS* (2018), pp. 33–44.

[26] Jones, T. C., Biele, G., Mühlemann, B., Veith, T., Schneider, J., Beheim-Schwarzbach, J., Bleicker, T., Tesch, J., Schmidt, M. L., Sander, L. E., Kurth, F., Menzel, P., Schwarzer, R., Zuchowski, M., Hofmann, J., Krumholz, A., Stein, A., Edelmann, A., Corman, V. M., and Drosten, C. Estimating infectiousness throughout sars-cov-2 infection course. *Science 373*, 6551 (2021), eabi5273.

[27] Karim, S. S. A., and Karim, Q. A. Omicron sars-cov-2 variant: a new chapter in the covid-19 pandemic. *The lancet 398*, 10317 (2021), 2126–2128.

[28] Kermack, W. O., and McKendrick, A. G. A contribution to the mathematical theory of epidemics. *Proceedings of the royal society of london. Series A, Containing papers of a mathematical and physical character 115*, 772 (1927), 700–721.

[29] Kirsebom, F. C., Andrews, N., Stowe, J., Toffa, S., Sachdeva, R., Gallagher, E., Groves, N., O'Connell, A.-M., Chand, M., Ramsay, M., et al. Covid-19 vaccine effectiveness against the omicron (ba. 2) variant in england. *The Lancet Infectious Diseases 22*, 7 (2022), 931–933.

[30] Kislaya, I., Casaca, P., Borges, V., Sousa, C., Ferreira, B. I., Fonte, A., Fernandes, E., Dias, C. M., Duarte, S., Almeida, J. P., et al. Comparative effectiveness of covid-19 vaccines in preventing infections and disease progression from sars-cov-2 omicron ba. 5 and ba. 2, portugal. *Emerging Infectious Diseases 29*, 3 (2023), 569.

[31] Kostova, D., Reed, C., Finelli, L., Cheng, P.-Y., Gargiullo, P. M., Shay, D. K., Singleton, J. A., Meltzer, M. I., Lu, P.-j., and Bresee, J. S. Influenza illness and hospitalizations averted by influenza vaccination in the united states, 2005–2011. *PloS one 8*, 6 (2013), e66312.

[32] Kupferschmidt, K., and Wadman, M. Delta variant triggers new phase in the pandemic, 2021.

[33] Lee, N., Chan, P. K. S., Hui, D. S. C., Rainer, T. H., Wong, E., Choi, K.-W., Lui, G. C. Y., Wong, B. C. K., Wong, R. Y. K., Lam, W.-Y., Chu, I. M. T., Lai, R. W. M., Cockram, C. S., and Sung, J. J. Y. Viral Loads and Duration of Viral Shedding in Adult Patients Hospitalized with Influenza. *The Journal of Infectious Diseases 200*, 4 (08 2009), 492–500.

[34] Lyngse, F. P., Kirkeby, C. T., Denwood, M., Christiansen, L. E., Mølbak, K., Møller, C. H., Skov, R. L., Krause, T. G., Rasmussen, M., Sieber, R. N., et al. Transmission of sars-cov-2 omicron voc subvariants ba. 1 and ba. 2: evidence from danish households. *MedRxiv* (2022), 2022–01.

[35] Meurer, A., Smith, C. P., Paprocki, M., Čertík, O., Kirpichev, S. B., Rocklin, M., Kumar, A., Ivanov, S., Moore, J. K., Singh, S., Rathnayake, T., Vig, S., Granger, B. E., Muller, R. P., Bonazzi, F.,

Gupta, H., Vats, S., Johansson, F., Pedregosa, F., Curry, M. J., Terrel, A. R., Roučka, v., Saboo, A., Fernando, I., Kulal, S., Cimrman, R., and Scopatz, A. Sympy: symbolic computing in python. *PeerJ Computer Science 3* (Jan. 2017), e103.

[36] Michlmayr, D., Hansen, C. H., Gubbels, S. M., Valentiner-Branth, P., Bager, P., Obel, N., Drewes, B., Møller, C. H., Møller, F. T., Legarth, R., et al. Observed protection against sars-cov-2 reinfection following a primary infection: A danish cohort study among unvaccinated using two years of nationwide pcr-test data. *The Lancet Regional Health-Europe 20* (2022), 100452.

[37] Mohring, J., Burger, M., Fessler, R., Fiedler, J., Leithäuser, N., Schneider, J., Speckert, M., and Wlazlo, J. Starker Effekt von Schnelltests (Strong effect of rapid tests). *arXiv* (2023).

[38] Polack, F. P., Thomas, S. J., Kitchin, N., Absalon, J., Gurtman, A., Lockhart, S., Perez, J. L., Pérez Marc, G., Moreira, E. D., Zerbini, C., Bailey, R., Swanson, K. A., Roychoudhury, S., Koury, K., Li, P., Kalina, W. V., Cooper, D., Frenck, R. W., Hammitt, L. L., Türeci, O., Nell, H., Schaefer, A., Ünal, S., Tresnan, D. B., Mather, S., Dormitzer, P. R., Şahin, U., Jansen, K. U., and Gruber, W. C. Safety and efficacy of the bnt162b2 mrna covid-19 vaccine. *New England Journal of Medicine 383*, 27 (2020), 2603–2615. PMID: 33301246.

[39] Postnikov, E. B. Estimation of covid-19 dynamics "on a back-of-envelope": Does the simplest sir model provide quantitative parameters and predictions? *Chaos, Solitons & Fractals 135* (2020), 109841.

[40] Robert Koch-Institut. Anzahl und Anteile von VOC und VOI in Deutschland. `https://www.rki.de/DE/Content/InfAZ/N/Neuartiges_Coronavirus/Daten/VOC_VOI_Tabelle.html`, Mar. 2023.

[41] Robert Koch-Institut. COVID-19-Hospitalisierungen in Deutschland. `https://doi.org/10.5281/zenodo.7762117`, Mar. 2023.

[42] Robert Koch-Institut. COVID-19-Todesfälle in Deutschland. `https://doi.org/10.5281/zenodo.7762170`, Mar. 2023.

[43] Robert Koch-Institut. Intensivkapazitäten und COVID-19-Intensivbettenbelegung in Deutschland. `https://doi.org/10.5281/zenodo.7760307`, Mar. 2023.

[44] Robert Koch-Institut. SARS-CoV-2 Infektionen in Deutschland. `https://doi.org/10.5281/zenodo.7754490`, Mar. 2023.

[45] Robert Koch-Institut. SARS-CoV-2 Sequenzdaten aus Deutschland. `https://doi.org/10.5281/zenodo.7761925`, Mar. 2023.

[46] ROBERT KOCH-INSTITUT, FACHGEBIET 33. COVID-19-Impfungen in Deutschland. https://doi.org/10.5281/zenodo.7762431, Mar. 2023.

[47] ROUSSEL, M. *Nonlinear Dynamics: A Hands-On Introductory Survey.* IOP Concise Physics. Morgan & Claypool Publishers, 2019.

[48] SHERRATT, K., GRUSON, H., GRAH, R., JOHNSON, H., NIEHUS, R., PRASSE, B., SANDMAN, F., DEUSCHEL, J., WOLFFRAM, D., ABBOTT, S., ULLRICH, A., GIBSON, G., RAY, E., REICH, N., SHELDON, D., WANG, Y., WATTANACHIT, N., WANG, L., TRNKA, J., OBOZINSKI, G., SUN, T., THANOU, D., POTTIER, L., KRYMOVA, E., BARBAROSSA, M., LEITHÄUSER, N., MOHRING, J., SCHNEIDER, J., WLAZLO, J., FUHRMANN, J., LANGE, B., RODIAH, I., BACCAM, P., GURUNG, H., STAGE, S., SUCHOSKI, B., BUDZINSKI, J., WALRAVEN, R., VILLANUEVA, I., TUCEK, V., ŠMÍD, M., ZAJÍCEK, M., PÉREZ ÁLVAREZ, C., REINA, B., BOSSE, N., MEAKIN, S., DI LORO, P. A., MARUOTTI, A., ECLEROVÁ, V., KRAUS, A., KRAUS, D., PRIBYLOVA, L., DIMITRIS, B., LI, M., SAKSHAM, S., DEHNING, J., MOHR, S., PRIESEMANN, V., REDLARSKI, G., BEJAR, B., ARDENGHI, G., PAROLINI, N., ZIARELLI, G., BOCK, W., HEYDER, S., HOTZ, T., E. SINGH, D., GUZMAN-MERINO, M., AZNARTE, J., MORIÑA, D., ALONSO, S., ÁLVAREZ, E., LÓPEZ, D., PRATS, C., BURGARD, J., RODLOFF, A., ZIMMERMANN, T., KUHLMANN, A., ZIBERT, J., PENNONI, F., DIVINO, F., CATALÀ, M., LOVISON, G., GIUDICI, P., TARANTINO, B., BARTOLUCCI, F., JONA LASINIO, G., MINGIONE, M., FARCOMENI, A., SRIVASTAVA, A., MONTERO-MANSO, P., ADIGA, A., HURT, B., LEWIS, B., MARATHE, M., POREBSKI, P., VENKATRAMANAN, S., BARTCZUK, R., DREGER, F., GAMBIN, A., GOGOLEWSKI, K., GRUZIEL-SLOMKA, M., KRUPA, B., MOSZYNSKI, A., NIEDZIELEWSKI, K., NOWOSIELSKI, J., RADWAN, M., RAKOWSKI, F., SEMENIUK, M., SZCZUREK, E., ZIELINSKI, J., KISIELEWSKI, J., PABJAN, B., HOLGER, K., KHEIFETZ, Y., SCHOLZ, M., BODYCH, M., FILINSKI, M., IDZIKOWSKI, R., KRUEGER, T., OZANSKI, T., BRACHER, J., AND FUNK, S. Predictive performance of multi-model ensemble forecasts of covid-19 across european nations. *medRxiv* (2022).

[49] SIGAL, A., MILO, R., AND JASSAT, W. Estimating disease severity of omicron and delta sars-cov-2 infections. *Nature Reviews Immunology 22*, 5 (2022), 267–269.

[50] STROGATZ, S. H. *Nonlinear dynamics and chaos with student solutions manual: With applications to physics, biology, chemistry, and engineering.* CRC press, 2018.

[51] TESCHL, G. *Ordinary Differential Equations and Dynamical Systems.* Graduate studies in mathematics. American Mathematical Society, 2012.

[52] THE NEW YORK TIMES. A timeline of the coronavirus pandemic. `https://www.nytimes.com/article/coronavirus-timeline.html`, 2021. Accessed: 2023-04-04.

[53] TIAN, D., SUN, Y., XU, H., AND YE, Q. The emergence and epidemic characteristics of the highly mutated sars-cov-2 omicron variant. *Journal of Medical Virology 94*, 6 (2022), 2376–2383.

[54] TURKYILMAZOGLU, M. An extended epidemic model with vaccination: Weak-immune sirvi. *Physica A: Statistical Mechanics and its Applications 598* (2022), 127429.

[55] VIRTANEN, P., GOMMERS, R., OLIPHANT, T. E., HABERLAND, M., REDDY, T., COURNAPEAU, D., BUROVSKI, E., PETERSON, P., WECKESSER, W., BRIGHT, J., VAN DER WALT, S. J., BRETT, M., WILSON, J., MILLMAN, K. J., MAYOROV, N., NELSON, A. R. J., JONES, E., KERN, R., LARSON, E., CAREY, C. J., POLAT, İ., FENG, Y., MOORE, E. W., VANDERPLAS, J., LAXALDE, D., PERKTOLD, J., CIMRMAN, R., HENRIKSEN, I., QUINTERO, E. A., HARRIS, C. R., ARCHIBALD, A. M., RIBEIRO, A. H., PEDREGOSA, F., VAN MULBREGT, P., AND SCIPY 1.0 CONTRIBUTORS. SciPy 1.0: Fundamental Algorithms for Scientific Computing in Python. *Nature Methods 17* (2020), 261–272.

[56] WERNER, D. *Funktionalanalysis*. Springer-Verlag, 2006.

[57] WORLD HEALTH ORGANIZATION. Who director-general's opening remarks at the media briefing on covid-19 - 11 march 2020. `https://www.who.int/director-general/speeches/detail/who-director-general-s-opening-remarks-at-the-media-briefing-on-covid-19---11-` 2020. Accessed: 2023-04-04.

[58] ZHANG, X., CHEN, L.-L., IP, J. D., CHAN, W.-M., HUNG, I. F.-N., YUEN, K.-Y., LI, X., AND TO, K. K.-W. Omicron sublineage recombinant xbb evades neutralising antibodies in recipients of bnt162b2 or coronavac vaccines. *The Lancet Microbe 4*, 3 (2023), e131.

[59] ZULKO. ddeint 0.2 - scipy-based delay differential equations solver. `https://pypi.org/project/ddeint/`. Accessed: 2022-03-29.